Dissertation

submitted to the

Combined Faculties for the Natural Sciences and for Mathematics

of the Ruperto-Carola University of Heidelberg, Germany

for the degree of

Doctor of Natural Sciences

presented by

Dipl. Biochem. Franziska Koser

born in: Zwickau

Oral examination:

Role of the ubiquitin-proteasome system in the pathogenesis of cardiac hypertrophy and aging

Referees: Prof. Dr. Markus Hecker

Prof. Dr. Thomas Wieland

Table of contents

Abbreviations

AAV	adeno-associated virus
AAV9	serotype 9 of the adeno-associated virus
AAV β1i	AAV9 CMV/MLC0.26 β1i
AAV Luci	AAV9 CMV/MLC0.26 luciferase
AIP	age induced protein
AMC	7-amino-4-methylcoumarin
ARP	age reduced protein
ATP	adenosine triphosphate
A value	active filling of ventricle
B-mode	brightness mode
bp	base pairs
BSA	bovine serum albumin
cAMP	cyclic adenosine monophosphate
cDNA	circular deoxyribonucleic acid
CMV	cytomegalovirus
CO	cardiac output
Da	Dalton
DAPI	4′,6-diamidin-2-phenylindol
DMEM	Dulbecco's modified eagle medium
DMSO	dimethyl sulfoxide
DNA	deoxyribonucleic acid
DTT	dithiothreitol
DUBs	deubiquitinating enzymes
E1	ubiquitin activating enzymes
E2	ubiquitin conjugating enzymes
E3	ubiquitin ligases
ECG	electrocardiogram
ECL	enhanced chemiluminescence
EDTA	ethylenediaminetetraacetic acid
EF	ejection fraction
EGFP	enhanced green fluorescent protein
E value	passive filling of the ventricle
FBS / FCS	fetal bovine serum / fetal calf serum
FS	fractional shortening
$G\alpha_i$	inhibitory G protein
$G\alpha_s$	stimulatory G protein
GE	gel electrophoresis
HBSS	Hanks balanced salt solution
HE	hematoxylin and eosin
HEK-293	human embryonic kidney cells
HEPES	4-(2-hydroxyethyl)piperazine-1-ethanesulfonic acid
HRP	horseradish peroxidase
HW	heart weight

HW/BW ratio	heart weight to body weight ratio
IGF-1	insulin-like growth factor 1
IgG	immunglobulin G
IPG	immobilized pH gradient
ITR	inverted terminal repeat
i.v.	intravenous
LB	Luria-Bertani
LiW/BW ratio	liver weight to body weight ratio
LVID;d / LVID;s	left ventricular internal diameter in diastole / systole
LVPWT;d / LVPWT;s	left ventricular posterior wall thickness in diastole / systole
LW/BW ratio	lung weight to body weight ratio
β-MHC	β-myosin heavy chain
MLC0.26	0.26 kb myosin light chain promoter
MLC2v	ventricular myosin light chain 2
MLC3	myosin light chain 3
M-MLV	Moloney murine leukemia virus
M-mode	motion mode
MOI	multiplicity of infection
mRNA	messenger ribonucleic acid
NBCS	new born calf serum
NRCMs	neonatal rat cardiomyocytes
OD	optical density
PAGE	polyacrylamide gel electrophoresis
PBS	phosphate buffered saline
PCR	polymerase chain reaction
PKA	protein kinase A
PLAX view	parasternal long axis view
PSAX view	parasternal short axis view
PW	pulse wave
Rpn10	regulatory particle non-ATPase 10
RNA	ribonucleic acid
rRNA	ribosomal ribonucleic acid
RT	room temperature
SD	standard deviation
SDS	dodecyl sodium sulfate
SV	stroke volume
TAC	transverse aortic constriction
TBE	TRIS-borate-EDTA
TBS	TRIS buffered saline
TBST	TRIS buffered saline containing Tween-20
TE	TRIS-EDTA
TRIS	tris(hydroxymethyl)aminomethane
UPS	ubiquitin-proteasome system
WT	wild type

Zusammenfassung

Kardiovaskuläre Erkrankungen gehören zu den häufigsten Erkrankungen und stellen die Haupttodesursache weltweit dar. Dabei nimmt die Prävalenz der an kardialer Hypertrophie mit Übergang in die Herzinsuffizienz erkrankten Personen, v.a. Frauen, mit dem Alter dramatisch zu. Es wird davon ausgegangen, dass der im Alterungsprozess auftretende Funktionsverlust des Ubiquitin-Proteasom-Systems (UPS) ein Schlüsselelement in der Verstärkung dieses Prozesses darstellt. Weiterhin wird angenommen, dass das UPS in die Entwicklung von kardialen Erkrankungen involviert ist, da es durch den zielgerichteten Abbau von Struktur-, Funktions- und Signalproteinen sowohl die Struktur, als auch Funktion der Kardiomyozyten aufrechterhält. Dennoch ist die Anzahl systematischer Studien, welche die Mechanismen der Proteasomregulation im Herzen und deren Rolle in der Pathogenese struktureller Herzerkrankungen bzw. beim Alterungsprozess untersuchen, derzeit begrenzt.

Laufende Untersuchungen unserer Arbeitsgruppe weisen auf eine Verstärkung der durch anhaltende Stimulierung kardialer β-Adrenozeptoren verursachten Herzhypertrophie im Mausmodell durch Knockout der induzierbaren Proteasomuntereinheit β1i hin. Daher beschäftigte sich die vorliegende Arbeit damit, ob vorrangig der fehlende Einbau von β1i in aktive kardiale Proteasomkomplexe oder der systemische Verlust von β1i *per se* für die verstärkte Herzhypertrophie in den β1i-defizienten Mäusen nach Isoprenalinbehandlung verantwortlich ist. Der Wiedereinbau von β1i in kardiale Proteasomkomplexe von β1i-defizienten Mäusen durch Reexpression der Proteasomuntereinheit mit Hilfe herzspezifischer (Serotyp 9) adeno-assoziierter Viren führte zu einer Abschwächung der Isoprenalin-induzierten Herzhypertrophie in diesen Tieren auf das Niveau Isoprenalin-behandelter Wildtyp-Mäuse und verhinderte das Auftreten einer systolischen ebenso wie einer diastolischen Dysfunktion. Die verstärkte, durch β-adrenerge Überstimulation verursachte Hypertrophieentwicklung in den β1i-defizienten Mäusen ist vermutlich nicht auf eine Störung der Sarkomerstruktur bzw. einen dysregulierten Abbau kontraktiler Proteine zurückzuführen. Allerdings scheint der Einbau von β1i in aktive Proteasomkomplexe des Herzen mit einer erhöhten Menge von intrazellulärem Troponin I als in der Kontrollgruppe assoziiert zu sein, was zur Aufrechterhaltung der kardialen Funktion beitragen könnte.

Im Gegensatz zu vorhergehenden Studien konnten im Zusammenhang mit dem Alterungsprozess deutliche Änderungen des kardialen Proteoms, welche mit einer starken Zunahme der 26S-Proteasomaktivitäten assoziiert waren, festgestellt werden. Des Weiteren scheint die Zunahme der 26S-Proteasomaktivitäten adaptiv zu Änderungen im kardialen Proteom zu erfolgen und mit einer altersbedingten Verschlechterung des Allgemeinzustands

der Tiere assoziiert zu sein. Sie dient damit höchstwahrscheinlich der Aufrechterhaltung der Proteinhomöostase und der Herzfunktion im Alterungsprozess.

Zusammenfassend wurde in der vorliegenden Studie erstmals gezeigt, dass der erhöhte Einbau von β1i in kardiale Proteasomkomplexe nach Hypertrophieinduktion ein wichtiger Schutzmechanismus bei diesem kardialen Umbauprozess zu sein scheint. Weiterhin könnte die Regulation der kardialen Proteasomfunktion im Alterungsprozess wesentlich komplexer sein als eingangs vermutet. Daher verdeutlichen die vorliegenden Ergebnisse wie wichtig es ist die mutmaßlich wichtige Rolle der Regulation der Proteasomfunktion sowohl beim Altern, als auch bei der Entwicklung von Herzmuskelerkrankungen besser zu verstehen.

Summary

Cardiovascular disease causes the highest morbidity and mortality worldwide. Moreover, the prevalence of cardiac hypertrophy and failure dramatically increases with aging, most notably in women. In this context, impairment of the ubiquitin-proteasome system (UPS) is supposed to be a pivotal element in the reinforcement of aging. Moreover, an involvement of the UPS, which accounts for the preservation of cardiomyocyte structure and function by the targeted degradation of structural, functional as well as signaling proteins, in the development of cardiac hypertrophy has been suggested. However, the number of systematic studies with regard to mechanisms underlying proteasome regulation in the heart and their role in cardiac remodeling, especially in the aging heart, is currently limited.

Ongoing studies in our group reveal that cardiac hypertrophy due to continuous β-adrenergic stimulation in the mouse is exaggerated by knockout of the proteasome subunit β1i. The present study therefore addresses the question whether it is the absence of β1i incorporation into active cardiac proteasome complexes or its deficiency *per se*, which augments cardiac hypertrophy in β1i-deficient mice upon treatment with isoprenaline. Reintroduction of β1i into cardiac proteasome complexes of β1i-deficient mice by way of cardiac-specific (serotype 9) adeno-associated viral gene transfer resulted in reduced hypertrophy development, comparable to the level in isoprenaline-treated wild type mice, and prevention of a manifest systolic and diastolic dysfunction. Presumably, the augmented hypertrophy development in the isoprenaline-treated β1i-deficient mice is not related to a disturbance of the sarcomeric structure or a dysregulated degradation of contractile proteins. However, reassembly of β1i into active cardiac proteasome complexes seems to be associated with higher intracellular troponin I levels compared to the control group, which may contribute to the maintenance of cardiac function.

In contrast to previous studies, marked alterations of the cardiac proteome associated with strongly increased 26S proteasome activities were detected in aging mouse hearts. Moreover, this increase in 26S proteasome activities seemed adaptive with respect to the extent of the alterations in the cardiac proteome, which may be associated with the age-related deterioration of the general health status of these animals. This increase in 26S proteasome activities may thus serve to maintain protein homeostasis and cardiac function during aging.

In conclusion, the present study revealed for the first time that increased incorporation of β1i into active cardiac proteasome complexes following induction of hypertrophy seems to be an important protective mechanism in maladaptive cardiac remodeling. Moreover, regulation of cardiac proteasome function during aging seems more complex than expected. Collectively, the current findings highlight how important it is to gain a better insight into mechanisms that regulate proteasome function in the context of aging and the pathogenesis of heart disease.

1 Introduction

1.1 The cardiovascular system and cardiac hypertrophy

The cardiovascular system consists of the blood, the heart, the blood vessels and the lymphatic system. The heart is an electromechanical pump with a primary function to circulate blood through the body via the blood vessels. Blood serves as central transport (e.g. O_2, CO_2, nutrients, hormones), regulatory (e.g. pH, temperature, osmotic pressure) and protection system (e.g. against pathogens). The right side of the heart delivers blood to the lungs via the pulmonary circuit. Accordingly, venous blood returns from the body to the right atrium through the superior and inferior venae cavae. The blood then passes through the tricuspid valve into the right ventricle (Figure 1). After entering the pulmonary artery through the pulmonary valve, the blood is delivered to the lungs (Figure 1) (Iaizzo 2007). The oxygenated blood returns from the lungs to the left atrium through the pulmonary veins and enters the left ventricle through the mitral valve (Figure 1). It leaves the left ventricle through the aortic valve into the aorta from where it is delivered to the body via the systemic circuit (Figure 1) (Iaizzo 2007). The cardiac cycle consist of two phases, the systole and the diastole. The ventricles contract and eject the blood into the systemic circulation during systole (Fernandis et al. 2002). In diastole, relaxation and passive filling of the ventricles occurs (Iaizzo 2007).

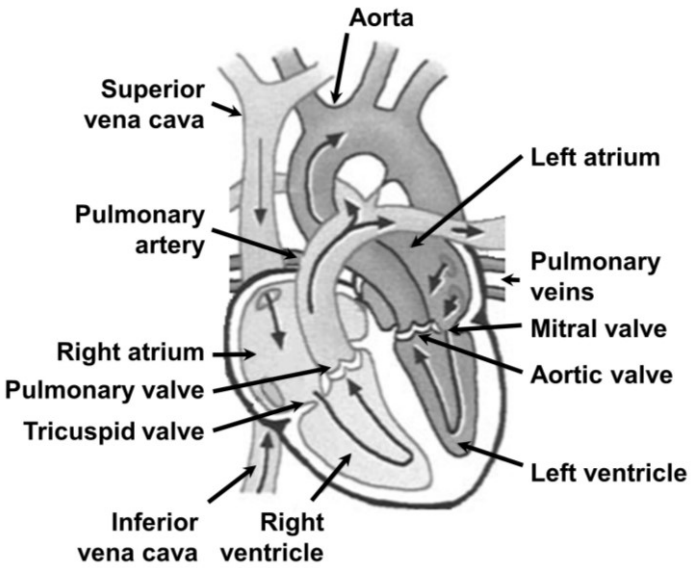

Figure 1. Functional anatomy of the heart.
Pathway of blood flow through the heart is visualized by arrows. The left side of the heart delivers blood via the systemic circuit to the entire body, whereas the right side of the heart delivers blood to the lungs via the pulmonary circuit.
Adapted from reference (Iaizzo 2007).

The pivotal role of the cardiovascular system for all vital functions may be derived from the fact that cardiovascular disease is the leading cause of morbidity and mortality worldwide. The term cardiovascular disease defines diseases of the heart as well as the blood vessels. Notably, heart failure is the most common cardiovascular disease, namely in the elderly and especially in women aged 65 years or older. It is defined as a deficiency in the heart's capability to deliver blood to the periphery in response to systemic demands (Heineke et al. 2006). Characteristic

symptoms of heart failure include premature fatigue, dyspnoea, and/or edema. Heart failure is commonly considered as the end stage of a number of heart-related diseases such as long-term hypertension, myocardial infarction or ischemia associated with coronary heart disease, valvular insufficiency and stenosis, familial hypertrophic and dilated cardiomyopathies, and arrhythmias (Klein et al. 2003, Lips et al. 2003). Most of these diseases result in maladaptive (pathophysiological) cardiac hypertrophy in response to cardiac stress (volume or pressure overload) as well as loss of contractile mass due to prior infarction, neurohumoral activation, and/or mutations of sarcomeric proteins (Berenji et al. 2005). Thus, maladaptive cardiac hypertrophy is a common preliminary stage of heart failure, which predisposes individuals to heart failure in the long-term. Accordingly, pathological cardiac hypertrophy may be considered as a risk factor for cardiovascular morbidity and mortality (Levy et al. 1990, Haider et al. 1998, Sundstrom et al. 2001).

In contrast, cardiac function is preserved in the long-term in adaptive (physiological) cardiac hypertrophy, which is associated with pregnancy or endurance training. The increase in the circulatory blood volume to supply the fast growing fetus or the mass of skeletal muscle under high burden in case of endurance training is the predominant stimulus for the development of physiological cardiac hypertrophy. In addition, development of maladaptive cardiac hypertrophy is associated with gender, obesity and diabetes mellitus. Moreover, a quantitative study demonstrated that the prevalence of cardiac hypertrophy increases in the context of aging (reviewed in (Lakatta et al. 2003)). At 60 years of age or older approximately 15% of men and approximately 20% of women were found to be affected by cardiac hypertrophy despite having a normal blood pressure (Lakatta et al. 2003). Thus, the prevalence of cardiac hypertrophy increases 2-fold and 4-fold in aged men and women, respectively, as compared to people 40 years of age or younger (Lakatta et al. 2003).

Cardiac hypertrophy is characterized by remodeling of the cardiomyocytes and extracellular matrix as well as coordinated neovascularization or angiogenesis. The common classification of cardiac hypertrophy is based on modification of the heart's shape and ventricular volume. This is commonly due to an alteration in the distribution of the muscle mass, which can be symmetrical (concentric) or asymmetrical (eccentric) (reviewed in (Heineke et al. 2006, Maillet et al. 2013)) (Figure 2). The alteration in cardiac muscle mass distribution is the pivotal element of hypertrophic growth of the heart. It results from an increase in cardiomyocyte size due to the addition of sarcomeres either in parallel or in series, which is induced by differing signaling pathways in physiological or pathophysiological cardiac hypertrophy. Eccentric hypertrophy is characterized by the relatively uniform addition of sarcomeres in parallel to increase the cardiomyocyte cell width as well as in series to lengthen the cardiomyocytes. These alterations of the geometry of the individual cardiomyoctes result in a uniform increase of the thickness of the ventricular wall and the septum along with a coordinated increase in ventricular volume

(outward remodeling) (Figure 2). In concentric hypertrophy, sarcomeres are typically added in parallel more than in series thus resulting in a non-uniform increase of the thickness of the ventricular wall. The ventricular volume may be reduced (inward remodeling) or maintained depending on the underlying remodeling processes (Figure 2). Physiological cardiac hypertrophy is predominantly eccentric, however concentric hypertrophy may be also induced by strength training in a milder form (Pluim et al. 2000). On the contrary, pathological hypertrophy is commonly associated with concentric cardiac hypertrophy and a reduction in ventricular volume, for example due to prolonged hypertension or aortic stenosis. Pathological hypertrophy may also result in what looks like eccentric cardiac growth as a consequence of (recurrent) myocardial infarction or dilated cardiomyopathy. However, in these cases remodeling of the extracellular matrix has gone wrong (scar tissue formation) so that the connective tissue skeleton of the ventricles has become less tear-resistant. If there still exists a volume or pressure overload situation for the heart, the hypertrophied ventricles will eventually dilate (the extracellular matrix ruptures) and their volume permanently increased above the norm. Consequently, the definition of eccentric or concentric cardiac hypertrophy cannot be clearly attributed to physiological or pathophysiological hypertrophy as such.

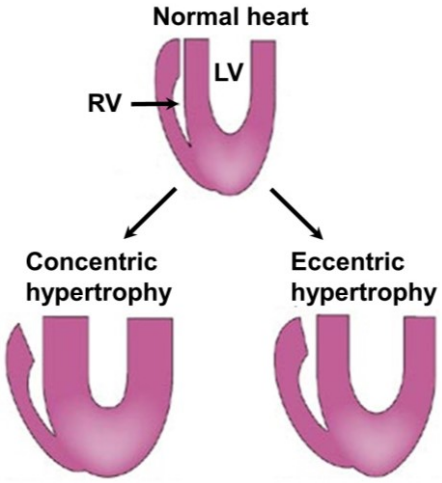

Figure 2. Types of cardiac hypertrophy.
A hypertrophic stimulus results in the alteration of the heart's shape. Symmetric remodeling, i.e. distribution of the muscle mass, and the accompanying increase in ventricular volume characterize adaptive, mostly physiological eccentric hypertrophy. On the contrary, concentric hypertrophy is characterized by asymmetric remodeling and the maintenance or decrease in ventricular volume. RV and LV indicates the right and the left ventricle, respectively.
Adapted from reference (Heineke et al. 2006).

Non-pathological cardiac hypertrophy is distinguished from pathological cardiac hypertrophy by several characteristics (reviewed in (Maillet et al. 2013)). One characteristic feature of physiological cardiac hypertrophy is the balanced growth of cardiomyocytes and capillaries (angiogenesis). In contrast, disruption of the coordinated increase in cardiac muscle mass and angiogenesis contributes to the transition of pathophysiological cardiac hypertrophy to heart failure due to the inadequate blood supply to the heart tissue (Shiojima et al. 2005). Moreover, one crucial characteristic of physiological cardiac hypertrophy due to pregnancy (Schannwell et al. 2002) or exercise (Ehsani et al. 1978, Maron et al. 1993, Pluim et al. 2000) is its complete reversibility. Non-pathological cardiac hypertrophy is not significantly associated with

remodeling of the extracellular matrix (reactive fibrosis) given that collagen I content is not altered in hearts of endurance trained rats (Burgess et al. 1996, Jin et al. 2000) and the absence of replacement fibrosis which would normally ensue due to cardiomyocyte apoptosis or necrosis (reviewed in (Krenning et al. 2010)). Thus, exessive remodeling of the extracellular matrix and/or replacement fibrosis is a pivotal element of maladaptive cardiac hypertrophy resulting in increased stiffness of the ventricular wall and diastolic dysfunction. The likewise reduced contractility, due to lost cardiomyocytes replaced by scar tissue, predisposes the affected individuals to systolic dysfunction and subsequent transition to heart failure.

Currently, the available drug treatment aims at delaying maladaptive cardiac hypertrophy transition into heart failure rather than regressing the hypertrophy as such, because these drugs usually inhibit the signaling pathways of the cardiac stress stimuli. In this context, neurohumoral signaling for example, which is induced by long-term hypertension, is inhibited by drugs such as angiotensin-converting enzyme inhibitors, angiotensin II receptor blockers, and/or β-adrenergic receptor blockers (Bisping et al. 2014). Novel therapeutic strategies for the treatment of pathological hypertrophy and heart failure include activation of physiological hypertrophic signaling cascades (reviewed in (Bernardo et al. 2010)). However, knowledge regarding the divergent mechanisms in pathological as compared to physiological cardiac hypertrophy is still rather limited. Thus, further investigation will identify new potential target molecules and mechanisms for therapeutic intervention.

1.2 Echocardiography – a non-invasive analysis of cardiac function and morphology

Echocardiography is a non-invasive and reliable method for the analysis of cardiac function and morphology. Thus, it is a standard procedure for the diagnosis of heart disease in humans. Improvement of the echocardiography instrumentation regarding spatial and temporal resolution via high-frequency ultrasound enabled the application of this method also in small animals, such as the mouse for which a range of cardiovascular disease models mimicking the human condition has been established (reviewed in (Gao et al. 2011)).

The echocardiographic analysis of the morphology of the heart enables calculation of left ventricular size. In humans, augmentation of left ventricular size is commonly used as an indicator of cardiac hypertrophy (Levy et al. 1987, Ghali et al. 1992) as well as a prognostic marker of heart failure (Lee et al. 1993, Wong et al. 1993). Moreover, the systolic function of the heart is analyzed by echocardiography. Currently, stroke volume and cardiac output are not commonly used as prognostic values of heart failure in humans. The former is defined as the ejected blood volume during systole while the latter is defined as the ejected blood volume per minute. Nevertheless, a recent study revealed the prognostic relevance of a decrease in stroke volume and cardiac output as predictors of a more severe outcome of heart failure (Agha

et al. 2009). In addition, the decrease in ejection fraction, defined as the ratio of stroke volume to end-diastolic volume of the ventricle, is commonly used as prognostic marker in patients with heart failure (Wong et al. 2004, Grayburn et al. 2005, Hobbs et al. 2007). Thus, patients presenting with an ejection fraction of below 0.35 or 35% are commonly considered to have established heart failure.

Moreover, passive filling of the ventricle (E value) and active filling of the ventricle (A value) are commonly analyzed to evaluate the diastolic function of the heart. In humans, the E/A ratio as well as transmitral inflow patterns are further used as indicators of diastolic function (Galderisi 2005, Nagueh et al. 2009). Four different transmitral inflow patterns are associated with the progression of normal towards severe diastolic dysfunction in humans. These patterns include normal filling (E>A), impaired left ventricular relaxation (E<A), pseudonormal filling (E>A) and restrictive filling (E>>A) (Nagueh et al. 2009). Analyzing diastolic function in patients with heart failure is of particular interest given that heart failure can be demonstrated in patients with preserved systolic function (Vasan et al. 1999, Zile et al. 2001, Hogg et al. 2004).

1.3 Murine models of cardiac hypertrophy

Various genetic and experimental mouse models of pathological cardiac hypertrophy are used to analyze the underlying mechanisms and the effectiveness of pharmacologic interventions (reviewed in (Hasenfuss 1998, Gomes et al. 2013)). Most of the commonly utilized murine models of maladaptive cardiac hypertrophy mimic the chronic pressure overload commonly associated with hypertension. A typical model of pharmacologically induced hypertension is the deoxycorticosterone acetate (DOCA) salt-induced model. In this model, the rise in blood pressure is mainly brought about by an increased salt and water retention by the kidneys, which in turn causes an increase in the circulating blood volume and hence hypertension. In addition, neurohumoral compensatory mechanisms such as a disinhibition of the sympathetic nervous system play a role (reviewed in (Gomes et al. 2013)). One limitation of this pressure overload model is the rather moderate left ventricular hypertrophy while there is a heavy burden inflicted onto the kidneys, which may result in deleterious side effects. Another model is the transverse aortic constriction (TAC) model, a well-established surgical model in which the aortic arch is partially narrowed resulting in an increased resistance in the outflow tract of the left ventricle comparable to that of a partially stenosed aortic valve. As a result, the left ventricle has to generate significantly more pressure to eject a normal stroke volume, which in turn leads to left ventricular hypertrophy and eventually failure. A drawback of this model is its low reproducibility, given the variation in time and extent of the ensuing cardiac hypertrophy and failure that is dependent upon the level of aortic constriction achieved (reviewed in (Gomes et al. 2013). However, when controlled by high-resolution ultrasound imaging of, e.g. blood flow and lumen size in the aortic arch, reproducibility of this model can be much improved.

The use of catecholamines in model organisms, namely small rodents, revealed a pivotal role of neurohumoral signaling in cardiac hypertrophy and progression towards heart failure. In this context, the β-adrenoceptor agonist isoprenaline, which has been widely utilized in rats and mice, is of particular interest since it induces a pathological concentric cardiac hypertrophy when chronically administered, e.g. by osmotic mini-pumps, at a dose of 30 mg * kg^{-1} * d^{-1} for 7 days (reviewed in (Osadchii 2007)). Application for 14 days in susceptible mice, for example, may lead to heart failure. The resulting pronounced cardiac hypertrophy in mice after 7 days treatment with isoprenaline is commonly analyzed by an increased heart weight to body weight (HW/BW) ratio (Saadane et al. 1999, Drews et al. 2010, Lukowski et al. 2010). When analyzed by echocardiography, one important parameter is the increased left ventricular posterior wall thickness in diastole (LVPWT;d) (Freund et al. 2005, Galindo et al. 2009, Li et al. 2013). However, continuous stimulation of β-adrenergic signaling for 7 days typically results in an increased systolic function (Drews et al. 2010, Lukowski et al. 2010, Shan et al. 2010) which, however, turns into systolic and diastolic dysfunction when continued, presumably due to β-adrenoceptor internalization and desensitization (reviewed in (Osadchii 2007)). This progression of cardiac hypertrophy towards heart failure likely is associated with changes in the extracellular matrix composition as well as myocardial replacement fibrosis due to apoptosis or necrosis of the cardiomyocytes (reviewed in (Osadchii 2007)).

1.4 Molecular regulation of cardiac hypertrophy – focus on β-adrenergic signaling

As mentioned before, pathological cardiac hypertrophy is induced, for instance, due to an increased work load for the heart. Hemodynamic overload induces multiple signaling pathways in cardiomyocytes such as mechanical stretch-induced signaling as well as that elicited by autocrine and paracrine humoral factors such as angiotensin II or transforming growth factor β (reviewed in (Heineke et al. 2006)). Moreover, disinhibition of the sympathetic nervous system and thus enhanced, namely β-adrenergic signaling serves as a key element in the development of cardiac hypertrophy and hear failure (Hunter et al. 1999, Ritter et al. 2003, Osadchii 2007).

Adrenergic signaling is induced and regulated through activation of different subclasses of adrenoceptors, including the α_1, α_2 as well as the β_1 and β_2-adrenoceptors. The human heart predominantly contains β-adrenoceptors (reviewed in (Barki-Harrington et al. 2004)), namely β_1-adrenoceptors (Rockman et al. 2002). In addition, the human heart contains β_2 and β_3-adrenoceptors, which are largely inactive under physiological conditions (reviewed in (Feldman et al. 2005)). In general, cardiac function is attenuated by the parasympathetic nervous system and its transmitter acetylcholine which is a direct (atria) or indirect (ventricles) antagonist of norepinephrine, the transmitter of the sympathetic nervous system (reviewed in (Triposkiadis et al. 2009)).

Beta-adrenergic signaling is G-protein coupled and regulates cardiac function via stimulatory ($G\alpha_s$) and inhibitory ($G\alpha_i$) G-protein signaling. The β_1-adrenoceptors signal through $G\alpha_s$, whereas β_2-adrenoceptors activate $G\alpha_s$ as well as $G\alpha_i$ proteins albeit to a lesser degree (reviewed in (Lohse et al. 2003, Feldman et al. 2005)). Signaling through $G\alpha_i$ inhibits while signaling through $G\alpha_s$ stimulates adenylyl cyclase, resulting in formation of the second messenger cyclic adenosine monophosphate (cAMP) and subsequent activation of protein kinase A (PKA). PKA in turn modulates the activity of several target proteins, which are essential for cardiac function (reviewed in (Lohse et al. 2003)). Beta-adrenergic, i.e. predominantly β_1-adrenergic signaling in the heart of both mice and men increases its contractility (positive inotropic effect), elevates heart rate (positive chronotropic effect), accelerates relaxation of the myocardium during diastole (lusitropic effect) as well as the rate of conduction through the atrioventricular node (positive dromotropic effect) (reviewed in (Triposkiadis et al. 2009)). Consequently, cardiac function is markedly enhanced through $G\alpha_s$ protein signaling.

On the contrary, cardiac β_3-adrenoceptors seem to be activated during acute β-adrenergic stimulation and are supposed to exert a negative ionotropic effect (Gauthier et al. 1998, Rozec et al. 2009). In vascular smooth muscle cells, activation of the predominant adrenoceptor subclass here, i.e. β_2, results in dilation of the coronary arteries and increased coronary blood flow (Schutzer et al. 2003). The development of cardiac hypertrophy is thought to be associated with activation of $G\beta\gamma$ signaling and activation of the extracellular regulated kinase pathway upon continuous β-adrenergic stimulation, resulting in the hypertrophic growth of the cardiomyocytes (Lorenz et al. 2009a, Lorenz et al. 2009b, Vidal et al. 2012).

The progression of cardiac hypertrophy towards heart failure (reviewed in (Barki-Harrington et al. 2004)) is commonly associated with desensitization of β-adrenoceptors, predominantly β_1-adrenoceptors. The β-adrenergic receptors are desensitized by phosphorylation or binding of β-arrestin impairing $G\alpha_s$ signaling (reviewed in (Ferguson 2001)). A further mechanism is up-regulation of $G\alpha_i$ signaling and internalization of the β-adrenergic receptors (reviewed in (Ferguson 2001)). Consequently, β-adrenergic signaling is decreased resulting in a decreased contractility and relaxation of the heart (systolic and diastolic dysfunction).

1.5 Cardiac function and the UPS – ubiquitin-proteasome system

Cardiac function is predominantly based on the integrity and functionality of the cardiomyocytes. Thus, preservation of cardiomyocytes is essential given the low rate of proliferation of these end-differentiated cells in adult mammalians. In adult mice and humans, the rate of cardiomyocyte turnover is approximately 1% or less per year (Bergmann et al. 2009, Mollova et al. 2013, Senyo et al. 2013). In this context, maintenance of protein homeostasis in

cardiomyocytes is crucial due to its pivotal role in the preservation of cellular integrity and viability. Predominantly, the ubiquitin-proteasome system (UPS) and autophagy systems account for the maintenance of protein homeostasis in the heart (reviewed in (Wang et al. 2015)).

However, it seems that the UPS mainly preserves cardiomyocyte structure and function through the targeted degradation of structural, functional as well as signaling proteins accounting for the control of vital signaling pathways (reviewed in (Drews et al. 2014)). The UPS consists of the ubiquitination machinery that encompasses four different enzyme classes (E1-E4), the proteasome complexes that degrade the polyubiquitin-tagged substrate proteins as well as the deubiquitination machinery comprising various deubiquitinating enzymes (DUBs) (Drews et al. 2014). The initial step of substrate poly-ubiquitination is the adenosine triphosphate (ATP) dependent activation of ubiquitin by the ubiquitin-activating enzymes (E1 class) (Haas et al. 1982). Subsequently, the activated ubiquitin is further transferred to the ubiquitin-conjugating enzymes (E2 class) (Pickart et al. 1985). Finally, the ubiquitin is ligated to the target protein via ubiquitin ligases (E3 class), which bind the E2 enzymes and their cargo (substrate proteins) and transfer the ubiquitin moiety onto the substrate proteins thus marking them for proteasomal degradation (Ciechanover et al. 1989, Reiss et al. 1989). In order to achieve this, target proteins normally have to be polyubiquitinated via the repetitive transfer of ubiquitin molecules to the already attached ubiquitin, and this ubiquitin chain elongation is also catalyzed by a concerted interaction of all three enzyme classes. Alternatively, an ubiquitin chain is transferred to the initially attached ubiquitin via E4 enzymes (Koegl et al. 1999). Currently, two different E1, approximately 30 E2 and more than 600 E3 class enzymes, conferring substrate specificity, are known in the human genome (Drews et al. 2014).

1.6 The proteasome – a proteolytic multiprotein complex

Proteasome complexes are a heterogeneous group of proteolytic multiprotein complexes with various functions (Gomes et al. 2006, Drews et al. 2007, Gomes et al. 2009). Notably, they are simultaneously present even under normal conditions. The core structure of the proteasome complexe is the 20S core complex further referred to as 20S proteasome. The 20S proteasome is composed of four heteroheptameric rings, two outer α-rings and two inner β-rings, forming a cylindrical particle (Murata et al. 2009). The proteolytic activities are assigned to the subunits β1, β2 and β5 and their corresponding inducible subunits β1i, β2i and β5i (Figure 3) (Bochtler et al. 1999, Voges et al. 1999). The proteolytic subunits cleave peptide bonds preferably after acidic (β1), alkaline (β2 and β2i), or hydrophobic residues (β5, β5i and β1i) and hence their activity is referred to as caspase-like (or peptidylglutamyl-peptide hydrolyzing activity), trypsin-like or chymotrypsin-like activity, respectively (Figure 3) (Bochtler et al. 1999, Voges et al. 1999, Groettrup et al. 2001).

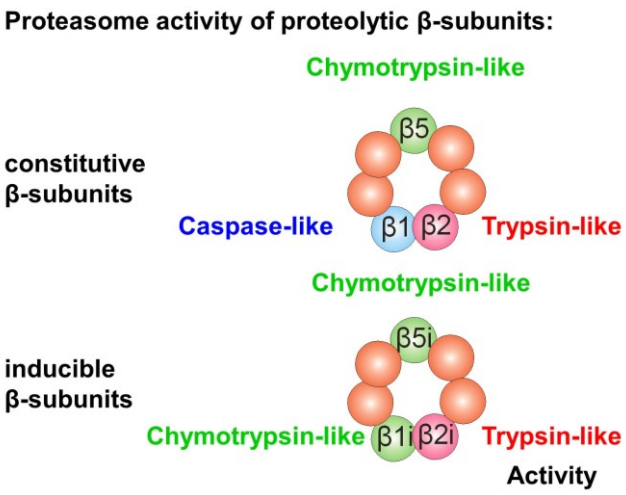

Figure 3. Proteasome activity of proteolytic β-subunits.
The β-ring of the 20S core complex is formed by 7 distinct β-subunits. The proteolytic activity is confined to the subunits β1, β2 and β5 and their corresponding inducible subunits β1i, β2i and β5i. The proteolytic activity is referred to as caspase-like, trypsin-like or chymotrypsin-like activity.

The assembly of the 20S proteasome is a complex process, requiring specific assembly factors (reviewed in (Murata et al. 2009)). First the α-ring is formed of seven distinct α-subunits (Figure 4) (Hirano et al. 2005, Hirano et al. 2006, Le Tallec et al. 2007). Subsequently, the α-ring serves as scaffold for the assembly of the β-ring starting with association of the subunit β2 (Figure 4) (Hirano et al. 2008). Then, the remaining six β-subunits are sequentially incorporated (Figure 4) (Hirano et al. 2008). Notably, proteolytic subunits and non-proteolytic subunits β6 and β7 are synthesized and attached to the α-ring with N-terminal propeptides (Figure 4). These propeptides are crucial for dimerization of the two half-proteasomes to form the 20S core complex (Figure 4) (Chen et al. 1996, Nandi et al. 1997). Moreover, removal of the propeptides at the final step of the assembly via autolysis is essential to expose the catalytic threonine residues of the proteolytic β-subunits and hence enable the proteolytic activity of the proteasome (Figure 4) (Chen et al. 1996, Schmidtke et al. 1996). Thus, undesirable proteolytic activity of synthesized β-subunits is blocked by the propeptides until they are incorporated into proteasome complexes. Consequently, proteasome subpopulations, containing constitutive or inducible proteolytic β-subunits or even a mixture of both, can only be generated through assembly, while subsequent exchange of proteolytic β-subunits within the mature 20S proteasome complex is impossible.

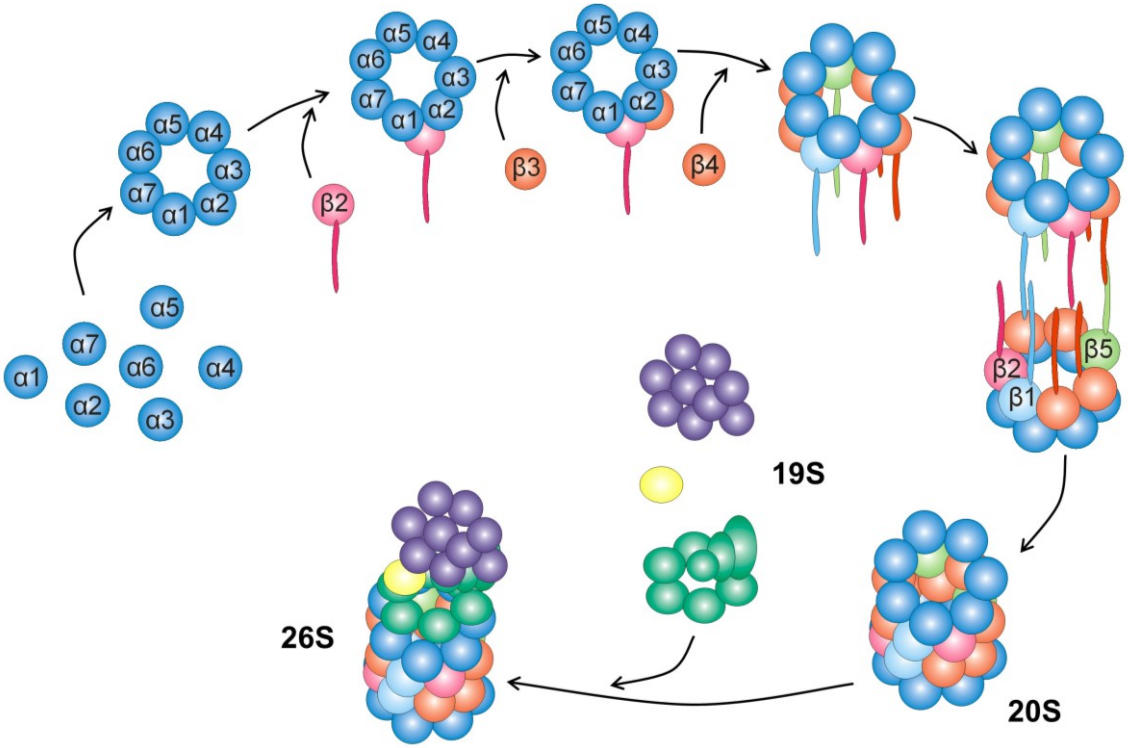

Figure 4. Model of proteasome assembly.

Assembly of the 20S core complex is initiated by formation of the α-ring. Subsequently, β-subunits are sequentially attached to the α-ring starting with the β2 subunit. The propeptides of the proteolytic β-subunits and the subunits β6 and β7 are cleaved via autolysis during maturation of the 20S core complex following association of the two half-proteasomes. The 20S core complex may associate with the 19S regulatory complex forming the 26S proteasome complex. The base (green) and the lid (purple) of the 19S regulatory complex are independently assembled. Subsequently these two subcomplexes and the subunit Rpn10 (yellow) are joined.

Adapted from reference (Murata et al. 2009).

Access to the proteolytic sites of the 20S proteasome is limited due to the conformation of the α-rings forming a pore (Groll et al. 2000). However, oxidized proteins, exposing hydrophobic patches on their surface, seem to be able to enter the 20S proteasome (reviewed in (Grune et al. 2003)). Thus, the 20S proteasome is supposed to be involved in the proteolytic degradation of oxidized proteins, which have not been ubiquitinated before (Shringarpure et al. 2001, Shringarpure et al. 2003). The entrance of proteins without exposed hydrophobic sites into the 20S core complex is gated through regulatory complexes, that associate with the 20S core complex (Adams et al. 1998). A common regulatory complex is the 19S particle consisting of two subcomplexes, designated as base and lid, as well as the regulatory particle non-ATPase 10 (Rpn10) (Figure 4). Assembly of the 19S regulatory particle is supposed to be associated with the 20S core complex, which potentially acts as an assembly factor (Figure 4) (Kusmierczyk et al. 2008). Notably, the proteasome complex consisting of the 20S core complex and the associated 19S regulatory complex is referred to as 26S proteasome

(Figure 4). The associated 19S regulatory complex enables enhanced substrate access to the 20S core complex via opening of the α-ring channel (Liu et al. 2006, Smith et al. 2007) and substrate unfolding (reviewed in (Bar-Nun et al. 2012)) in an ATP-dependent manner. The 19S regulatory particle further contains recognition sites for polyubiquitinated proteins (Deveraux et al. 1994, Husnjak et al. 2008). Thus, the 26S proteasome recognizes and degrades ubiquitin-tagged target proteins, which are subjected to degradation via the UPS. Consequently, the 26S proteasome is implicated in all cellular processes that are regulated through the UPS. Proteasomal degradation is further regulated via the association of other regulatory complexes, such as the 11S particle (Whitby et al. 2000) and PA200 particle (Ortega et al. 2005), which increase proteasomal activity, as well as the proteasome inhibitor 31 (PI31) (Zaiss et al. 1999) and the proline/arginine-rich 39-amino-acid peptide (PR39) (Gaczynska et al. 2003), which have inhibitory effects. In addition, the proteasomal activity is regulated by posttranslational modifications such as phosphorylation of the 20S core complexes (Scruggs et al. 2012).

1.7 The UPS and cardiovascular disease

Over the past decade a crucial role of the UPS in cardiovascular physiology and pathophysiology has been elucidated (Powell et al. 2012, Pagan et al. 2013, Drews et al. 2014). As mentioned before, targeted degradation of structural, functional, as well as signaling proteins and thus the control of vital signaling pathways is supposed to be responsible for the pivotal role of the UPS in maintaining cardiomyocyte structure and function.

In experimental mouse models of cardiac hypertrophy, 26S proteasome activity is commonly increased in hypertrophied hearts (Depre et al. 2006, Hedhli et al. 2008, Drews et al. 2010). Notably, proteasome inhibition results in a reduction of cardiac hypertrophy upon exposure to a pro-hypertrophic stimulus (Depre et al. 2006, Hedhli et al. 2008, Stansfield et al. 2008). However, the duration of proteasome inhibition as well as the submaximal inhibition of increased proteasome activities upon pro-hypertrophic stimulation is thought to be crucial for the positive effect of proteasome inhibition in relation to the development of cardiac hypertrophy (reviewed in (Drews et al. 2014)). Consequently, interfering with proteasomal regulation through utilization of proteasome inhibitors potentially reduces or prevents early cardiac remodeling upon exposure to a pro-hypertrophic stimulus. Notably, regulation of the proteasomal activity in heart failure is different from that in early cardiac hypertrophy, given the association of heart failure in humans with a markedly reduced proteasome function (Drews et al. 2014). Thus, a systematic and detailed analysis of proteasomal regulation is critical for targeted interventions in cardiac disease (reviewed in (Drews et al. 2014)). However, systematic studies concerning the mechanisms of proteasome regulation and their role in maladaptive cardiac remodeling are currently limited.

Previous research elucidated that at least three mechanisms contribute to proteasome regulation during the development of cardiac hypertrophy induced by β-adrenergic overstimulation (Drews et al. 2010). In hypertrophic hearts, incorporation of inducible β-subunits is increased, 20S core sensitivity to PKA activation is enhanced and the assembly of the 26S proteasome is up-regulated (Drews et al. 2010). Inducible β-subunits are incorporated into cardiac proteasomes without previous stimulation (Drews et al. 2007). However, this increased incorporation is commonly associated with stress responses (Angeles et al. 2012). In the context of the development of cardiac hypertrophy, such an enhanced incorporation of inducible β-subunits into active cardiac proteasome complexes might be adaptive or maladaptive. Ongoing studies in our group revealed an augmentation of cardiac hypertrophy in β1i-deficient mice upon continuous β-adrenergic stimulation.

1.8 Proteasome regulation in the heart in the context of aging

As mentioned before, the prevalence of cardiac hypertrophy dramatically increases with age. Moreover, analyses of cardiac function reveal alterations in relation to aging as a consequence of structural and functional changes of the cardiomyocytes (reviewed in (Lakatta 2003)). These changes in the cardiomyocytes may be associated with alterations of the cardiomyocyte proteome with increasing age. Previously, differential abundancies of proteins involved in cell signaling, metabolism and immune response as well as structural proteins and proteins mediating responses to oxidative stress have been demonstrated in the murine and rat heart in young as compared to old animals (Dai et al. 2008, Richardson et al. 2008, Grant et al. 2009). As the UPS potentially plays a pivotal role in maintaining cardiomyocyte structure and function as well as protein homeostasis, its impairment during aging may give rise to the accumulation and aggregation of damaged proteins that have been shown to be cytotoxic (reviewed in (Kevei et al. 2014)). On the other hand, targeted degradation of crucial regulators of aging-related pathways, such as insulin or insulin-like growth factor 1 (IGF-1) signaling, through an altered function and/or activity of the UPS may further account for the aging process (reviewed in (Kenyon 2010)). Although an essential role of the UPS with regard to aging seems self-explanatory, the number of studies on the functional or dysfunctional regulation of proteasome function, namely in the heart, in the context of aging are rather limited.

1.9 Research objectives

Global β1i knockout mice show an impaired cardiac function upon exposure to a pro-hypertrophic stimulus (β-adrenergic overstimulation) as compared to wild type (WT) mice. However, the question remains whether it is the absence of β1i incorporation into cardiac proteasome complexes in particular or its deficiency *per se*, which augments cardiac hypertrophy in β1i knockout mice upon treatment with isoprenaline. Thus, cardiac-specific reintroduction of β1i in β1i-deficient mice may elucidate the essential role of β1i incorporation into cardiac proteasome complexes upon exposure to a pro-hypertrophic stimulus.

Non-viral vector systems are rather inefficient for gene transfer *in vivo* due to the generally low transfection efficiency, lack of cell specificity requiring topical administration routes and potential cytotoxicity (reviewed in (Müller et al. 2007)). Moreover, commonly used viral vector systems such as retroviruses or adenoviruses lack the necessary tropism for the heart (Lyon et al. 2008). Currently, serotype 9 of the adeno-associated virus (AAV) is commonly used for the heart-specific reintroduction of transgenes, given that the serotype 9 has the highest tropism for the heart (Prasad et al. 2011). In addition, cardiac-specific transgene expression is further improved by using a genetically engineered promoter consisting of a fragment of the cardiomyocyte-specific myosin light chain promoter (MLC0.26) in combination with parts of the viral cytomegalovirus (CMV) immediate-early promoter (Kaya et al. 2011, Pleger et al. 2011, Schinkel et al. 2012). The latter acts as an enhancer to ensure constitutive expression in adult mice.

With the aforesaid in mind, three specific aims were pursued in the present work:

1) To determine through AAV9-based heart-specific reintroduction of the proteasome subunit β1i (rescue approach) whether the exaggerated cardiac hypertrophy in β1i-deficient mice upon β-adrenergic overstimulation can be abolished or prevented.

2) To investigate whether the expression and/or organization of sarcomeric proteins in the heart of β1i-deficient mice receiving AAV9 harboring β1i is different from that of β1i-deficient mice expressing an unrelated transgene following continuous treatment with isoprenaline.

3) To analyze in detail proteasome regulation in the heart of old versus young mice to confirm the presumed impairment of proteasome function and to discern on which level – proteasome composition, assembly and/or activity – this impairment takes place.

2 Materials

2.1 Chemicals

Chemicals used in general were obtained from Roth (Karlsruhe), Sigma-Aldirch (Steinheim), Roche (Mannheim), Merck (Darmstadt).

2.2 Consumable supplies

Consumable supplies used in cell culture or for molecular biological analysis were obtained from Sarstedt (Nürnbrecht), Eppendorf (Hamburg), TPP (Trasadingen, CH), Greiner (Frickenhausen), BD Biosciences (Heidelberg), Nunc (Thermo Scientific) (Dreieich).

2.3 Cell culture

Devices	Distributor	Model
Centrifuge	Hettich, Tuttlingen	Universal 320 R
Cell strainer (100µM nylon filter, sterile)	BD Biosciences (Corning), Heidelberg	352360
Coverslips	Marienfeld GmbH, Lauda-Königshofen	01 115 00
Forceps, scissors, tweezers	b.i.t. Chirurgiemechanik, Bammental	
Incubator	Thermo Scientific, Dreieich	Hera Cell 150
Laminar flow cabinet	Kojair Tech Oy, AD Vught, NL	Biowizard
Microscope	Olympus, Hamburg	CKX41
Microscope slides	Thermo Scientific, Dreieich	J1800AMNZ
Steritop GP sterilization bottle top vacuum filter (150 ml, 22µm)	Millipore, Schwalbach	SCGPS01RE
Water bath	Memmert, Schwabach	WNB 7-45

2.3.1 Human embryonic kidney cells (HEK-293)

Materials	Distributor	Catalogue number
DMEM (low glucose, GlutaMAX supplement, pyruvate)	GIBCO (Life Technologies), Darmstadt	21885-025
Fetal bovine serum (FBS)	GIBCO (Life Technologies), Darmstadt	105000064
Fungizon	GIBCO (Life Technologies), Darmstadt	15290026
Hanks balanced salt solution (HBSS) (- calcium, - magnesium)	GIBCO (Life Technologies), Darmstadt	14175095
Penicillin/streptomycin	GIBCO (Life Technologies), Darmstadt	15070063
Trypsin/ethylenediaminetetraacetic acid (EDTA)	GIBCO (Life Technologies), Darmstadt	25300054

2.3.2 Neonatal rat cardiomyocytes (NRCMs)

Materials	Distributor	Catalogue number
Collagenase type2	Worthington (Cell Systems Biotechnologie Vertrieb), Troisdorf	LS004176
Collagen solution (Collagen A)	Biochrom (Millipore), Berlin	L7220
Disodium hydrogenphosphate x H_2O	Grüssing, Filsum	12295
D(+)-glucose	Merck, Darmstadt	1.083.371.000
DMEM medium (high glucose 4.5g/l, 11g/l sodium pyruvate, no glutamine)	GIBCO (Life Technologies), Darmstadt	21969-035
Fetal calf serum (FCS) Gold	PAA-Laboratories (GE Healthcare), Cölbe	A15-151
HEPES (> 99.5%)	Roth, Karlsruhe	9105.2
L-glutamine (200 mM)	GIBCO (Life Technologies), Darmstadt	25030-024
Magnesium sulfate heptahydrate	Merck, Darmstadt	1.058.861.000
New born calf serum (NBCS)	GIBCO (Life Technologies) Darmstadt	26010-074
Pancreatin	Sigma-Aldrich, Steinheim	P3292
Penicillin/streptomycin	GIBCO (Life Technologies), Darmstadt	15140-122
Percoll	GE Healthcare, Freiburg	17-0891-01
Potassium chloride	Applichem, Darmstadt	A3582.1000
Sodium chloride	Sigma-Aldrich, Steinheim	31424
Trypan blue solution (0.4%)	Sigma-Aldrich, Steinheim	T8154

2.4 *In vivo* studies – OP and echocardiography

Devices	Distributor	Model
Anaesthesia device	Groppler, Deggendorf	UniVet Prota
Animal trimmer	Braun,Kronberg	GT 420
Echocardiography	Visualsonics, Amsterdam, NL	Vevo 2100 imaging system (transducer: MS-550D)
Hot plate	Labotect, Rosdorf	Hot Plate 062
Mirco-osmotic pumps	Alzet, Cupertino, CA	model 1002
Oxygenizer	Respironics (GE Healthcare), Freiburg	EverFlo
Moscito hemostat, forceps, scissors, tweezers	b.i.t. Chirurgiemechanik, Bammental	

Materials	Distributor	Catalogue number
Analgesic (carbostesin luerfit ampoule 0.25% / 5 ml)	AstraZeneca, Wedel	PZN: 1177870
Eye creme (Bepanten)	Bayer, Leverkusen	PZN: 2182442
Foliodrape OP-tape	Hartmann, Heidenheim	250 5 2418
Hair removal creme (Snä-Epil Sensitive)	Axisis, Düsseldorf	PZN: 2186115
Isoflurane	Baxter, Unterschleißheim	HDG9623
Isoprenaline hydrochloride	Sigma-Aldrich, Steinheim	I5627-25g (Lot #BcBk9694V)
Iodine ointment (10%) (Braunovidon)	B. Braun, Melsungen	PZN: 03188955
NEG 50	Richard-Allan Scientific (Thermo Scientific), Dreieich	6502
Sodium metabisulfite	Sigma-Aldrich, Steinheim	S-1516
Surgical sutures	Ethicon (Johnson & Johnson Medical), Norderstedt	EH 7800 H
Transpore surgical tape	3M, Neuss	S6 1527-1

2.5 Molecular biological methods

Kits	Distributor	Catalogue number
EndoFree plasmid megaprep kit	Qiagen, Hilden	12381
PeqGOLD total RNA kit	Peqlab, Erlangen	12-6634-02
QIAquick gel extraction kit	Qiagen, Hilden	28706
QIAprep spin miniprep kit	Qiagen, Hilden	27104
RNeasy mini kit	Qiagen, Hilden	74104
Transcriptor high fidelity cDNA synthesis kit	Roche, Mannheim	05081955001

Devices	Distributor	Model
Agarose gel chamber (length 11 cm)	Peqlab, Erlangen	40-0911
Centrifuge (small volumes: up to 2 ml)	Thermo Scientific, Dreieich	Heraeus Pico 21
Centrifuge (small volumes: up to 2 ml; refrigerated)	Hettich, Tuttlingen	Micro 22 R
Centrifuge (large volumes: 2-50 ml)	Hermle, Gosheim	Z 323 K
Gel documentation (RNA, DNA)	BioRad, München	Gel Doc XR
Incubator (bacteria)	New Brunswick Scientific (Eppendorf), Hamburg	Innova 4230
pH meter	WTW, Weilheim	inoLab
Thermocycler	Eppendorf, Hamburg	Mastercycler Personal
Scales	Sartorius, Göttingen	BP 121 S

Scales	Kern, Balingen	EW 820
Spectrophotometer	Thermo Scientific, Dreieich	Nanodrop ND-1000

Materials	Distributor	Catalogue number
AAV CMV/MLC0.26 EGFP vector	provided by Dr. O. Müller	
AAV CMV/MLC0.26 *Renilla* luciferase vector	provided by Dr. O. Müller	
Agarose	Sigma-Aldrich, Steinheim	A9539
Ampicillin	Sigma-Aldrich, Steinheim	A9518
100 bp DNA Ladder	New England BioLabs, Frankfurt/Main	N3231S
E. coli DH1	ATTC, Wesel	33849
E. coli Sure cells	Agilent Technologies (Stratagene), Santa Clara, USA	200238
Ethidium bromide (1%=10 mg/ml))	Roth, Karlsruhe	2218
FastAP thermosensitive alkaline phosphatase	Thermo Scientific, Dreieich	#EF0651
GeneRuler 1 kb DNA Ladder	Thermo Scientific, Dreieich	# SM0311
LB medium	Roth, Karlsruhe	X964.2
LB agar	Roth, Karlsruhe	X965.2
M-MLV reverse transcriptase	Promega, Mannheim	M170B
pBlueScript II SK(+)	Agilent Technologies (Stratagene), Santa Clara, USA	#212205
Phusion high fidelity polymerase	New England BioLabs, Frankfurt/Main	M0531S
Proteinase K (20 mg/ml)	Thermo Scientific, Dreieich	EO-0491
pSP72	Promega, Mannheim	P2191
Restriction enzymes AgeI BamHI BsrGI HindIII SmaI	New England BioLabs, Frankfurt/Main	 R0552S R0104S R0575S R0136S R0141S
T4 polynucleotide kinase	Thermo Scientific, Dreieich	#EK0031
T4 DNA ligase	New England BioLabs, Frankfurt/Main	M0202S

2.6 Protein biochemical methods

Kits	Distributor	Catalogue number
Renilla-Glo luciferase assay system	Promega, Mannheim	E2710

Devices	Distributor	Model
Fluorescence reader	Thermo Scientific, Dreieich	Fluoroskan Ascent
Luminescence reader	Berthold, Bad Wildbad	MicroLumat LB 96 P
Microplate spectrophotometer	BioTek; Bad Friedrichshall	Powerwave Xs
Molecular imager	Bio-Rad; München	Pharos FXTM Plus
Isoelectric focusing 2D GE	Pharmacia Biotech (GE Healthcare), Freiburg	IPGphor
Power supply (Western blot)	Bio-Rad; München	PowerPac basic
Power supply (2D GE)	Consort, Turnhout, BE	E833
Semidry blotting	Bio-Rad; München	TransBlot turbo transfer system
Hand-held homogenizer for 1.5 ml tubes	Sigma-Aldrich, Steinheim	Z359947
Tenbroeck hand-held homogenizer	VWR, Bruchsal	432-1276
Ultracentrifuge	Beckmann Coulter, Krefeld	TL-100 ultracentrifuge
Western blot documentation system	GE Healthcare, Freiburg	QuantLAS 4000 mini
Westen blot gel chamber	Bio-Rad; München	Mini Protean
2D GE chamber	GE Healthcare, Freiburg	Ettan Daltsix

Materials	Distributor	Catalogue number
7-Amino-4-methylcoumarin (AMC)	Sigma-Aldrich, Steinheim	257370
Bradford assay solution	BioRad, München	500-0006
ECL prime (Western blot detection reagent)	GE Healthcare, Freiburg	RPN2232
IPG strips	GE Healthcare, Freiburg	17-6002-45
Microfluor black plate, flat bottom	Fisher Scientific, Schwerte	1058-8885
Milk powder	Roth, Karlsruhe	T145.2
Ponceau S solution	Sigma-Aldrich, Steinheim	P7170
Phosphatase inhibitor cocktail II	Sigma-Aldrich, Steinheim	P5726
Phosphatase inhibitor cocktail III	Sigma-Aldrich, Steinheim	P0044
Protease inhibitor cocktail	Roche, Mannheim	04 693 132 001
Precision plus protein dual color standard	BioRad, München	161-0374
Ruthenium(II)-tris (bathophenanthroline-disulphonate) (RuBP) [Fluo-R]	Serva Electrophoresis, Heidelberg	35091.01
Sea sand	Grüssing, Filsum	13137
Transfer membrane (nitrocellulose)	VWR(BioTrace), Bruchsal	732-3031
Ultracentrifuge tubes	Beranek, Weinheim	343778
Unstained protein marker (2-212 kDa)	New England BioLabs, Frankfurt/Main	P7702S

2.7 Immunochemical methods

Devices	Distributor	Model
Fluorescence microscope (Xcellence RT software)	Olympus, Hamburg	IX 81 filters (FITC/TRITC/DAPI) FITC λex 460-480nm, λem 495-540nm, 484 beamfilter TRITC λex 535-550nm, λem 610-675nm, 565 LP beamfilter DAPI λex 360-370 nm, λem 420-485nm, 400 beamfilter
Microscope	Olympus, Hamburg	CX31
Microtome cryostat	Thermo Scientific, Dreieich	HM 500 O

Materials	Distributor	Catalogue number
Bovine serum albumin (BSA)	Sigma-Aldrich, Steinheim	A2153
Casein	Sigma-Aldrich, Steinheim	C5890
1,4-Diazabicyclo[2.2.2]octane solution (DABCO)	Sigma-Aldrich, Steinheim	290734
4′,6-Diamidin-2-phenylindol (DAPI)	Life Technologies, Darmstadt	D1306
Eukitt	O. Kindler (Sigma-Aldrich), Steinheim	03989
Mayer's hematoxylin solution	Roth, Karlsruhe	T865.2
Mowiol 4-88	Calbiochem (Millipore), Schwalbach	475904

2.8 Buffers and solutions

Buffer/solution	Ingredients
PBS (pH 7.4)	140 mM sodium chloride 2.7 mM potassium chloride 8 mM disodium hydrogenphosphate 1.5 mM potassium dihydrogenphosphate
TBE (pH 7.5)	90 mM TRIS 73 mM boric acid 3 mM EDTA
TBS (pH 7.4)	20 mM TRIS 0.9% (w/v) sodium chloride
TBST	0.1% (w/v) Tween-20 in TBS buffer

2.8.1 HEK-293 cells

Buffer/solution	Ingredients
DMEM medium (HEK-293)	10% FBS 1% penicillin/streptomycin 1% fungizon

2.8.2 NRCMs

Buffer/solution	Ingredients
10x ADS (pH 7.4) (sterile)	1163.6 mM sodium chloride 197.2 mM HEPES 94.2 mM disodium hydrogenphosphate x H_2O 55.5 mM glucose 53.6 mM potassium chloride 8.3 mM magnesium sulfate heptahydrate
Digestion solution (NRCMs) (sterile)	0.6 mg/ml pancreatin 0.5 mg/ml collagenase type 2 in ADS buffer
DMEM medium including FCS (NRCMs)	10% FCS Gold 1% penicillin/streptomycin 2 mM L-glutamine
DMEM medium without FCS (NRCMs)	1% penicillin/streptomycin 2 mM L-glutamine
Percoll gradient	7 ml bottom-layer 3 ml top-layer
Percoll stock solution	90% (v/v) Percoll in 10x ADS buffer
Bottom-layer Percoll gradient	65% (v/v) Percoll stock solution 35% (v/v) 1x ADS buffer
Top-layer Percoll gradient	45% (v/v) Percoll stock solution 55% (v/v) 1x ADS buffer with phenol red

2.8.3 Molecular biological methods

Extraction of genomic DNA from mice tail biopsies

Buffer/solution	Ingredients
Tail biopsy digestion buffer (pH 8.8)	67 mM TRIS 16.6 mM ammonium sulfate 6.5 mM magnesium chloride 1% (v/v) 2-mercaptoethanol 0.5% (w/v) TritonX-100 1 µg/µl proteinase K

Agarose gel electrophoresis

Buffer/solution	Ingredients
Agarose gel	1% (w/v) agarose 0.3 pg/ml ethidium bromide in TBE buffer
5x RNA/DNA loading buffer	75% (w/v) glycerine 180 mM TRIS 146 mM boric acid 6 mM EDTA 0.01% (w/v) xylene cyanol 0.01% (w/v) bromphenol blue

Preparation of plasmid DNA by alkaline lysis

Buffer/solution	Ingredients
Alkaline lysis solution I (pH 8.0)	50 mM glucose 25 mM TRIS 10 mM EDTA
Alkaline lysis solution II	0.2 M sodium hydroxide 1% (w/v) SDS
Alkaline lysis solution III	5 M potassium acetate 4.3% (v/v) acetic acid
TE	10 mM TRIS 1 mM EDTA

2.8.4 Protein biochemical methods

Proteasome activity assay and active site labeling

Buffer/solution	Ingredients
Homogenization buffer (pH 7.5)	20 mM HEPES (500 mM stock solution) 150 mM sodium chloride (5 M stock solution) 1 mM magnesium chloride (100 mM stock solution) 0.5 mM EDTA (50 mM stock solution)
10x Caspase- and trypsin-like activity buffer (pH 7.5)	250 mM HEPES 5 mM EDTA 0.5% (w/v) NP-40 0.01% (w/v) SDS
10x Chymotrypsin-like activity buffer (pH 7.5)	250 mM HEPES 5 mM EDTA 0.3% (w/v) SDS

Western blot analysis and total protein staining

Buffer/solution	Ingredients
Acrylamide gel Stacking gel (6% acrylamide)	 1.25 ml stacking gel buffer 0.75 ml 40% (w/v) acrylamide (37.5:1) 0.32 g glycerin 2.75 ml water 100 µl 10% (w/v) ammonium persulfate 100 µl N, N, N', N'-tetramethylethylenediamine
Resolving gel (13% acrylamide)	2.5 ml resolving gel buffer 3.25 ml 40% (w/v) acrylamide (37.5:1) 0.63 g glycerin 3.78 ml water 50 µl 10% (w/v) ammonium persulfate 50 µl N, N, N', N'-tetramethylethylenediamine
Fixation solution	40% (w/v) ethanol 10% (w/v) acetic acid
5x Protein loading buffer (pH 6.8)	310 mM TRIS 50% (v/v) glycerin 170 mM SDS 5% (v/v) 2-mercaptoethanol
Resolving gel buffer (pH 8.8)	1.5 M TRIS 0.4% (w/v) SDS
10x Running buffer	240 mM TRIS 2 M glycin 1% (w/v) SDS
Ruthenium staining solution	1 µM RuBP
Semi-dry transfer buffer	48 mM TRIS 39 mM glycin 0.02% (w/v) SDS 20% (v/v) methanol
Stacking gel buffer (pH 6.8)	0.5 M TRIS 0.4% (w/v) SDS

2.8.5 Immunochemical methods

Buffer/solution	Ingredients
Aniline blue solution	2.5% (w/v) aniline blue 2% (v/v) acetic acid
Biebrich Scarlet acid fuchsin solution	90 ml 1% Biebrich scarlet solution 10 ml 1% acid fuchsin solution 1 ml 37% acetic acid

Isofix (pH 7.3)	0.3% (w/v) paraformaldehyde 1% (w/v) glutaraldehyde 0.07 M cacodylate
Phosphotungstic-phosphomolybic acid solution	25 ml 5% phosphotungstic acid solution 25 ml 5% phosphomolybic acid solution
Weigert's hematoxylin solution	0.5% (w/v) hematoxylin 50% (v/v) ethnol 0.6% (v/v) iron trichloride 0.2% (v/v) hydrochloride acid
Mowiol (pH 8.5)	10% (w/v) mowiol 4-88 25% (v/v) glycerine 0.1 M TRIS 2.5% (v/v) DABCO

2.9 Primer

Primer	Sequence	Reference
AAV ITR forward	5' GCG ACT CTA GAT CAT AAT CAG CC 3'	
AAV ITR reverse	5' GGC TAT GAA CTA ATG ACC CCG 3'	
AAV sequencing forward	5' AGG CTA GCC TCG ACG GTA CC 3'	
AAV sequencing reverse	5' GGC TGA TTA TGA TCT AGA GTC GC 3'	
β1i_2 forward	5' CCCGTGTCCCTCCGAGATAC 3'	(Van Kaer et al. 1994)
β1i_4 reverse	5' GGGATCCAGGACCAGGAAAG 3'	(Van Kaer et al. 1994)
β1i_3 forward	5' AGGGTGTCAGCTCCCCTGGA 3'	(Van Kaer et al. 1994)
neo_A reverse	5' CTTGGGTGGAGAGGCTATTC 3'	(Van Kaer et al. 1994)
β1i direct forward	5' ATG CTG CGG GCA GGA GCA C 3'	
β1i direct reverse	5' TCA CTC ATC GTA GAA TTT TGG CAG C 3'	
β1i overhang forward	5' TT ACC GGT GCC ACC ATG CTG CGG GCA GGA GCA C 3'	
β1i overhang reverse	5' GGG CCC TGT ACA TCA CTC ATC GTA GAA TTT TGG CAG C 3'	

2.10 Fluorescently tagged substrates

Substrate	Distributor	Catalogue number
Z-LLE-AMC	Calbiochem (Millipore), Schwalbach	53914
Boc-LSTR-AMC	Bachem, Bubendorf, CH	I-1940
Suc-LLVY-AMC	Bachem, Bubendorf, CH	I-1395

2.11 Proteasome inhibitors

Inhibitor	Distributor	Catalogue number
Z-Pro-Nle-Asp-H	Enzo Life Sciences, Lörrach	BML-ZW9490
Epoxomicin	Boston Biochem, Cambridge, USA	I-112
Bortezomib	LC Laboratories, Woburn, USA	B-1408

2.12 Antibodies

WB: Western blot; IHC: Immunohistochemistry

2.12.1 Primary antibodies

Antibody	Distributor (Catalogue number)	Dilution	Application
Mouse anti-α7	Enzo Life Sciences, Lörrach (PW8110)	1:2500	WB
Mouse anti-β1	Abcam, Cambridge, UK (ab58081)	1:1666 1:400	WB IHC
Mouse anti-β1i	Enzo Life Sciences, Lörrach (PW8840)	1:800 1:200	WB IHC
Mouse anti-β2	Enzo Life Sciences, Lörrach (PW9300)	1:2500	WB
Rabbit anti-β5	Enzo Life Sciences, Lörrach (PW88959	1:1666	WB
Mouse anti-β5i	Enzo Life Sciences, Lörrach (PW8845)	1:1666	WB
Rabbit anti-actin	Sigma-Aldrich, Steinheim (A2066)	1:3000	WB
Mouse anti-α-actinin	Sigma-Aldrich, Steinheim (A7811)	1:2000 1:1500	WB IHC
Rabbit anti-desmin	Dianova, Hamburg (DLN-13734)	1:4000 1:400	WB IHC
Rabbit anit-MLC2v (cardiac)	Abcam, Cambridge, UK (ab79935)	1:4000	WB
Mouse anti-β-MHC	Millipore, Schwalbach (MAB1628)	1:1500	WB
Mouse anti-troponin I (cardiac)	Abcam, Cambridge, UK (ab19615)	1:4000	WB
Mouse anti-α-tubulin	Sigma-Aldrich, Steinheim (T5168)	1:6000	WB

2.12.2 Secondary antibodies

Antibody	Distributor (Catalogue number)	Dilution	Application
Goat anti-mouse IgG (Fab fragment)	Dianova, Hamburg (115-007-003)	1:13	IHC
Rat anti-mouse IgG HRP	Rockland (Biomol), Hamburg (18-8817-33)	1:5000-1:10000	WB
Goat anti-rabbit IgG HRP	Sigma-Aldrich, Steinheim (A-6154)	1:10000	WB

Goat anti-mouse IgG biotin-SP-conjugated	Dianova, Hamburg (115-067-003)	1:500	IHC
Donkey anti-mouse IgG Cy3	Dianova, Hamburg (715-166-150)	1:1000	IHC
Goat anti-rabbit IgG Alexa Fluor 647	Dianova, Hamburg (111-495-006)	1:1000	IHC
Streptavidin Cy3	Dianova, Hamburg (016-160-084)	1:500	IHC

2.13 AAVs

AAV	Concentration
AAV2-β1i	$3.9 * 10^{10}$ vg/ml
AAV6-β1i	$1.87 * 10^{11}$ vg/ml
AAV6-EGFP	$2.56 * 10^{11}$ vg/ml
AAV9-β1i	$1.2 * 10^{12}$ vg/ml
AAV9-*Renilla* Luciferase	$1.0 * 10^{12}$ vg/ml

The packaging of DNA in different serotypes of AAV for this project was kindly performed by the research group of Dr. O. Müller (Dept. of Internal Medicine III, University Clinic Heidelberg).

3 Methods

3.1 Cell culture

In general, sterile materials and solutions were used, all solutions were pre-warmed to 37°C in a water bath. All cell culture related work was carried out under a laminar flow cabinet. The cells were cultured in the incubator at 37°C and 5% carbon dioxide.

3.1.1 HEK-293 cells

Thawing of HEK-293 cells

The cells (passage 15) stored in cryotubes in liquid nitrogen were quickly thawed in 37°C water bath and transferred to DMEM medium . The cell suspension was carefully mixed by inverting, pelleted by centrifugation for 5 min at 500 x *g* and the supernatant fraction removed by aspiration. The cells were resuspended in 5 ml of DMEM medium and transferred in a T25 filter flask.

Maintenance of HEK-293 cells

The cells were periodically checked under the microscope. The medium was changed every second day or earlier in cases where the cell confluence was lower than 80% and/or upon a noticeable color change of the media from red to orange as indicative of a pH shift and nutrient deficiency. For this purpose, the medium was aspirated and 5 ml of fresh DMEM medium was added after washing the cells with 2 ml of HBSS.

Passaging of HEK-293 cells

The cells were passaged at approximately 80% confluency. For this purpose, the cells were detached from the culture vessel by adding 1 ml of 0.05% trypsin EDTA solution per T25 flask and incubated for 1-3 min at room temperature (RT) after washing the cells with 2 ml of HBSS. The detachment was microscopically monitored and stopped by the addition of 2 ml of DMEM medium. The cells were pelleted by centrifugation for 5 min at 500 x *g* to remove all traces of the trypsin EDTA solution. Finally, the cell suspension was passaged at a ratio of 1:3 to 1:5 and was transferred in a new T25 filter flask after gently resuspending the cell pellet in DMEM medium.

Sub-culturing of HEK-293 cells

HEK-293 cells were sub-cultured for 12 to 16 hours before starting the AAV2 infection. After detachment, the cells were counted using a Neubauer chamber (Harrison et al. 1997). For this

purpose, the cells were 1:100 diluted in HBSS and 20 µl of this suspension was transferred in the prepared Neubauer chamber. The cells within the corner squares were counted and the number was divided by four to get the mean cell number of one corner square. Then, the cell number was calculated according to the formula outlined below.

$$\frac{cells}{ml} = \frac{cells}{corner\,square} \times dilution \times 10^4$$

The cell suspension was diluted according to the necessary cell amount and total volume.

	cells / well	medium / well
6-well plate	5 x 10^5	2 ml

3.1.2 Preparation of NRCMs

The preparation of neonatal rat cardiomyocytes (NRCMs) was performed with the approval (T-05/13) of the sanctioning authority (Regierungspräsidium Karlsruhe) and according to the German animal protection code.

Primary NRCMs were prepared from the hearts of neonatal rats on the postnatal day one to three according to previously published protocol (Frank et al. 2008). The preparation of NRCMs was established with support of Susann Werkmeister (Dept. of Internal Medicine III, University Clinic Heidelberg). One day before preparation of NRCMs (at least 2 h before plating the cells), the cell culture dishes and plates were coated using collagen stock solution diluted 1:10 in ADS buffer. In addition, sterile coverslips were placed into 48-well plates prior to coating for the immunofluorescence analysis.

The neonatal rats were decapitated using sterile large scissors. Then, the heart was excised and transferred to the ice-cold ADS buffer. After removing the atria and other remaining tissue pieces, the ventricles were transferred to the fresh, ice-cold ADS solution. Subsequently, the tissue was digested under sterile conditions using a digestion solution containing pancreatin and collagenase type 2 to isolate the cells. For this purpose, the ADS buffer was carefully removed by pipetting and the ventricles were cut into small pieces. The tissue pieces were then transferred to a T75 flask containing the digestion solution and shaken for 20 min at 37°C in a water bath.

- standard volumes of digestion solution:

  24 neonatal rats = 18-20 ml digestion solution = 1x T75

  36 neonatal rats = 27-30 ml digestion solution = 1x T75

The supernatant solution from the first digestion step was discarded. On the contrary, cell suspensions from the following digestion steps were collected and stored in 50 ml tubes at 37°C with loosened cap. The collected solution was passed through a cell strainer in a 50 ml

tube containing 5 ml of NBCS and the cell strainer was washed with additional 2-3ml of NBCS. After adding new digestion solution to the tissue pieces, the cell suspension was centrifuged for 5 min at ~500 x *g* in the meantime. The cell pellet was resuspended in 5 ml of NBCS after aspiration of the supernatant. The digestion was repeated up to 6 times until the tissue was almost entirely digested. Next, the cell suspensions, stored at 37°C, were pooled and pelleted by centrifugation for 5 min at ~500 x *g*. The cell pellet was then carefully resuspended in 1x ADS buffer. Then, the cell suspension was added drop-wise onto the Percoll gradient (7 ml bottom-layer + 3 ml top-layer) in 2 ml increments.

- standard: 2 pregnant rats = 4 Percoll gradients
  3 pregnant rats = 6 Percoll gradients
  4 pregnant rats = 8 Percoll gradients

The cardiomyocytes were separated from fibroblasts using a Percoll gradient centrifugation step for 30 min at 1000 x *g* at 4°C (turn off brake). After centrifugation, the upper, colorless phase and the interphase containing fibroblasts as well as the first half of the top, red layer phase was removed and discarded. The second half of the top-layer phase and the colorless bottom-layer phase containing cardiomyocytes were pooled in 2x 50 ml tubes. Next, ice-cold 1x ADS buffer was added up to 50 ml to each cell suspension. After centrifugation for 5 min at ~500 x *g*, the supernatant was discarded and the cells were pooled and resuspended in 50 ml of ice-cold 1x ADS buffer, centrifuged as before and carefully resuspended in 40 ml of medium containing 10% FCS. The cell suspension was 1:2 diluted in 0.4% trypan blue solution to determine the cell concentration using a Neubauer chamber as described previously (see 3.1.1) (Harrison et al. 1997). Living, unstained cells within all corner squares were counted (dead cells = blue). Following this, the cell suspension was diluted according to the necessary cell amount and total volume and plated onto the previously prepared, collagen-coated culture vessels.

	cells / well	medium / well
60mm dish	3 x 10^6	4 ml
6-well plate	1.5 x 10^6	2 ml
12-well plate	500.000	1 ml
24-well plate	150.000	0.5 ml
48-well plate	90.000	0.3 ml

Two days after preparation, the cardiomyocytes were starved by changing the medium (0% FCS). The AAV6 infection was initiated three days after the preparation.

3.1.3 Infection of cells

The AAV CMV/MLC0.26 β1i or EGFP vector was packaged into AAV2 particles for HEK-293 or AAV6 particles for NRCMs infection. In HEK-293 cells, the infection was carried out 12 to 16 hours after sub-culturing. In contrast, the primary NRCMs were infected three days after preparation and one day after starvation. After the application of the virus, the medium was not changed in both *in vitro* systems. The infected cells were incubated at 37°C for 48 hour to 72 hours before they were harvested or fixed on coverslips for immunofluorescence staining.

The virus titer of each virus batch used was determined by quantitative real time PCR by our collaborators (O. Müller, Dept. of Internal Medicine III, University Clinic Heidelberg). Thus, a defined number of vector genomes instead of infectious virus particles per cell was used for infection of NRCMs or HEK-293 cells. In accordance, the number of infectious virus particles is assumed to be lower than the number of vector genomes. The number of vector genomes per cell is hereafter referred to as multiplicity of infection (MOI).

The infection experiment was started by the addition of fresh medium containing the appropriate vector amount after aspiration of the old medium. The vector amount, needed for a defined MOI, was calculated according to the formula outlined below.

- example: AAV6 CMV/MLC0.25 β1i
    - virus stock concentration = $1.87\times10^{11}\ \frac{vg}{ml}$ (vg = vector genomes)

      = 1.9×10^{8} vg in 1 µl

    - the MOI should be 10^4 using 7×10^{4} cells, thus 7×10^{8} vg are needed:

$$\frac{1.9\times10^{8}\ vg}{1\mu l}=\frac{7\times10^{8}vg}{x\mu l}$$

$$x=\frac{1\mu l\times7\times10^{8}\ vg}{1.9\times10^{8}vg}=3.7\mu l$$ virus stock solution

3.1.4 Harvesting cells

mRNA and protein analysis

The cells were harvested directly in the cell media using a cell scraper. After centrifugation for 5 min at ~500 x *g*, the supernatant was discarded and the cell pellet was resuspended in 1 ml of PBS to remove all traces of the medium. Then, the cells were pelleted again by centrifugation and were quick-frozen in liquid nitrogen and stored at -20°C after aspiration of the supernatant.

Immunfluorescence analysis

The cells, grown on coverslips, were fixed according to the scheme outlined below.

	fixative	incubation time
HEK-293 cells	isofix	30 min on ice
NRCMs	4% paraformaledhyde and 4% sucrose in PBS	10 min at RT on shaker

3.2 *In vivo* studies

3.2.1 *In vivo* hypertrophy model

The animal experiments were performed with the approval (35-9185.81/G-194/11) of the sanctioning authority (Regierungspräsidium Karlsruhe) and according to the German animal protection code.

The experimental setup used to investigate the influence of the reintroduction of β1i in β1i-deficient mice upon induction of hypertrophy is shown in figure 5.

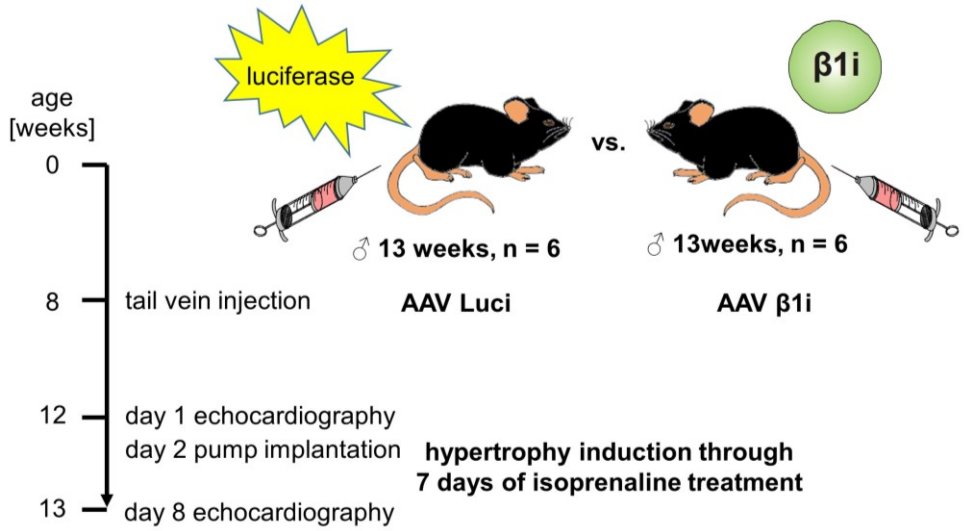

Figure 5. β1i-deficient mice received 10^{11} vector genome equivalents of the cardio-tropic serotype 9 of adeno-associated virus harboring β1i (AAV β1i) or *Renilla* luciferase (AAV Luci) 4 weeks prior to induction of hypertrophy via 7-day treatment using an infusion rate of 30 mg * kg^{-1} * day^{-1} of isoprenaline

Male β1i knockout mice were intravenously injected using 10^{11} vector genome equivalents of the cardio-tropic AAV9 CMV/MLC0.26 β1i at the age of 8 weeks. The *Renilla* luciferase gene packaged into AAV9 served as a control in β1i-deficient mice. The tail vein injection was kindly performed by Bianca Heil (Interfacultary Biomedical Faculty, University Heidelberg). After 4 weeks, cardiac function was analyzed by echocardiography prior to and post pharmacologic

induction of hypertrophy by isoprenaline treatment (Figure 5). Subsequently, the proteasome regulation was investigated in hypertrophic hearts.

Hypertrophy induction by treatment with isoprenaline

In accordance with previously utilized animal model, cardiac hypertrophy was induced by 7 days of isoprenaline treatment using micro-osmotic pumps, which release isoprenaline at a rate of 30 mg * kg^{-1} * day^{-1} (Drews et al. 2010).

The following parameters of the micro-osmotic pump (alzet, model 1002) and the experimental setup were used to calculate the necessary isoprenaline concentration.

- micro-osmotic pump = alzet model 1002 (length: 1.5 cm; diameter: 0.6 cm; weight: 400 mg):
  - pumping rate: 0.22 µl/h (± 0.05 µl/h)
  - duration: 14 d
  - reservoir volume: 100 µl
- experimental setup:
  - infusion rate isoprenaline: 30 mg/kg/d = 1.25 mg/kg/h
  - maximum body weight mouse: 35 g

$$c\ (isoprenaline\ solution) = \frac{1.25\frac{mg}{h} \times body\ weight[kg]}{0.00022\frac{ml}{h}}$$

$$c\ (isoprenaline\ solution) = \frac{1.25\frac{mg}{h} \times 0.035\ [kg]}{0.00022\frac{ml}{h}}$$

$$c\ (isoprenaline\ solution) = 198.86\ \frac{mg}{ml}$$

Accordingly, 20 ml solution was calculated to contain 3.977 g of isoprenaline. Thus, 4.663 g of isoprenaline hydrochloride was diluted in 20 ml of sterile PBS. Aliquots of the isoprenaline stock solution were prepared and stored at -20°C.

The loading of the micro-osmotic pumps with isoprenaline solution was kindly performed by Dr. O. Drews (Dept. of Cardiovascular Physiology, University Heidelberg) according to the manufacturer's instructions (Alzet, Cat. no. 0004317). The isoprenaline stock solution was diluted with PBS depending on the actual weight of the mice. The loaded pumps were primed overnight in sterile PBS.

Subsequently, the micro-osmotic pump was implanted under 1-3% isoflurane anesthesia. Initially, the fur was completely removed on the implant site on the back using an animal fur shaver and a hair removal creme. After disinfection with iodine ointment (braunovidion), the skin on the back was incised and a paravertebral pocket was created towards the head

between the subcutis and the fasciae of the back muscles. Next, the pump was washed thoroughly in sterile water and inserted in the paravertebral pocket. Finally, the wound was sutured using surgeon's knots and disinfected with iodine ointment. On the first two days the mice were monitored at least twice a day and thereafter at least once. The pump implantation was kindly performed by Felix Trogisch (Dept. of Cardiovascular Physiology, University Heidelberg).

Echocardiography

Cardiac function was investigated by echocardiography using the transducer MS-550D and the Vevo 2100 imaging system (Visualsonics) prior to and post induction of hypertrophy by 7 days treatment with isoprenaline (Gao et al. 2011).

The echocardiography was done under 1-3% isoflurane anesthesia. The morphology and the systolic function of the heart were analyzed in the parasternal long axis view (PLAX) (Figure 6A) as well as in the parasternal short axis view (PSAX) (Figure 6B). Anatomical structures are identified in the brightness mode (B-mode) (Figure 6A, B) displaying two-dimensional images of an area of interest. In the motion mode (M-mode) the movement of the sample volume (vertical line in B-mode) over time is displayed (Figure 6C). In the PLAX view, the aorta and the apex are on a horizontal line and only the left ventricle is displayed (Figure 6A). In the PSAX view, the cross section of the middle of the heart is shown, indicated by the presence of both papillary muscles (Figure 6B). Morphological parameter, such as left ventricular internal diameter (LVID) and left ventricular posterior wall thickness (LWPWT) in systole and diastole, are analyzed in M-mode in the PLAX and PSAX view (Figure 6C). Moreover, the left ventricular internal dimensions (LVID;d and LVID;s) are used to calculate the ejection fraction (EF) and the fractional shortening (FS), which are utilized to evaluate the contractility of the ventricle. In addition, parameters reflecting the systolic function of the heart are analyzed, such as stroke volume (SV) and cardiac output (CO). The former is defined as the ejected blood volume during systole while the latter is the ejected blood volume per minute.

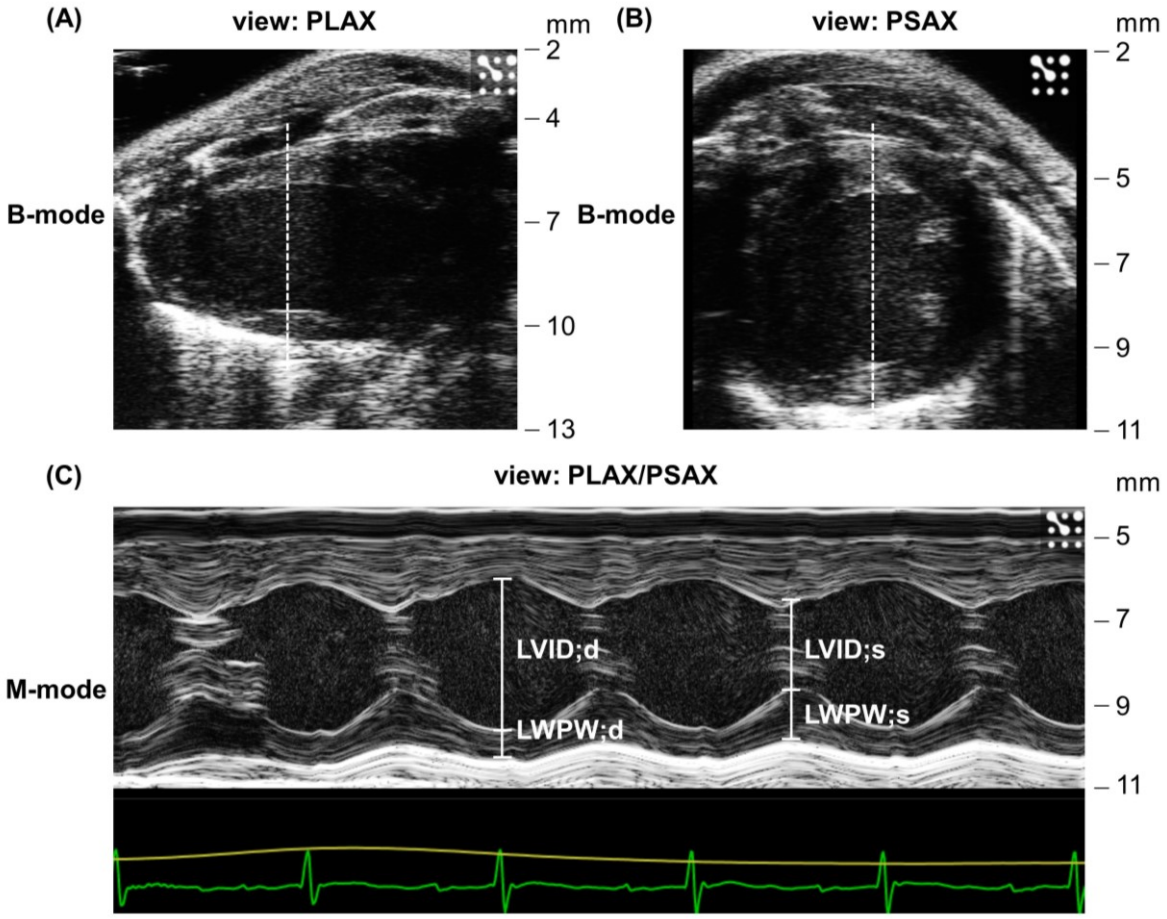

Figure 6. Representative echocardiographic images in mice.

Cardiac morphology and systolic function is analyzed in the parasternal long axis (PLAX) **(A)** and in the parasternal short axis (PSAX) **(B)** view in B-mode as well as in M-mode **(C)**. The movement of the line in B-mode is displayed over time in M-mode. The corresponding electrocardiogram (ECG) (green) and the respiration rate (yellow) is displayed below the M-mode image. In M-mode **(C)**, the left ventricular internal diameter (LVID) and left ventricular posterior wall thickness (LVPW) in diastole and systole were measured.

The diastolic function of the heart is analyzed in the apical four chamber view (Figure 7A) utilizing color and pulse wave (PW) Doppler mode (Figure 7B, C). Doppler mode imaging is utilized to analyze the velocity of the movement of blood or tissue. In color Doppler mode, the direction and the velocity of blood flow is visualized. Accordingly, blood flow towards and away from the transducer is gradually colored in blue to white and red to white, respectively. In PW Doppler mode, the values such as the velocity of blood flow, which is visualized in color Doppler mode imaging, are measured. For this purpose, the sample volume (square) is placed above the mitral valves and the blood flow is visualized using the color Doppler mode (Figure 7B). In the apical four chamber view, both ventricles and atria are visible (Figure 7A). Using the PW Doppler mode, the passive filling of the ventricle (E value) and the active filling

of ventricle (A value) is analyzed (Figure 7C). In addition, the E/A ratio, a common indicator of diastolic dysfunction is calculated.

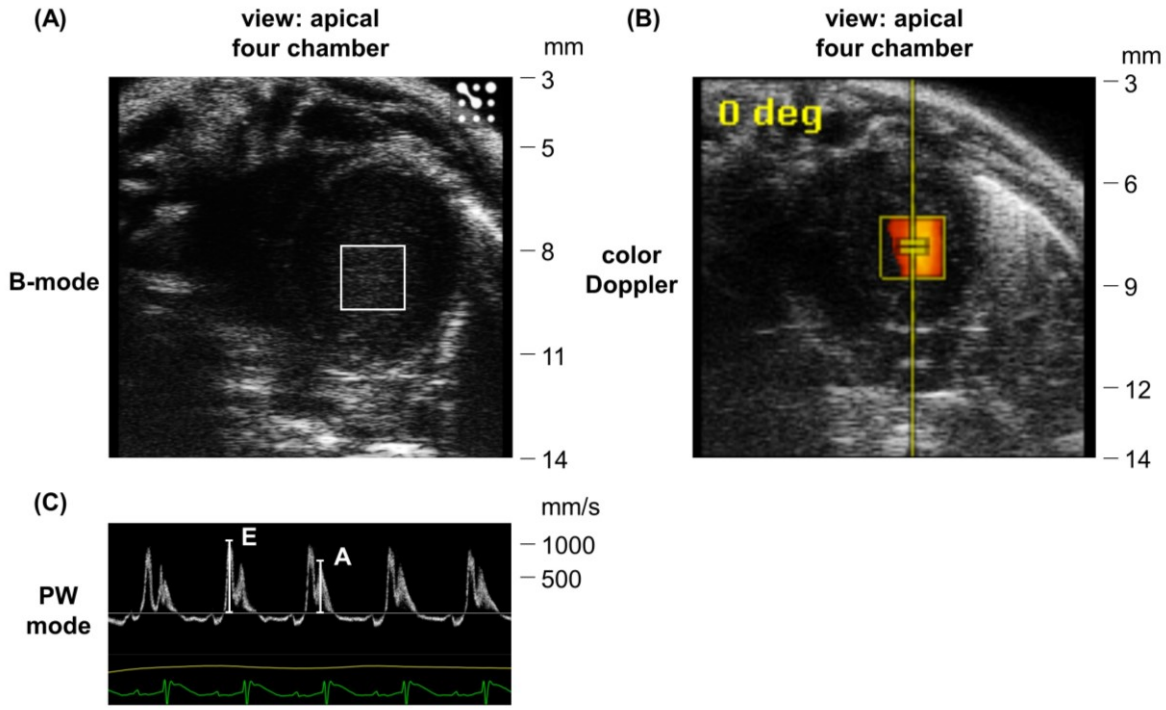

Figure 7. Representative echocardiographic images in mice.
Diastolic function is investigated in the apical four chamber view of the heart **(A)**. For this purpose, the sample volume (square) is placed above the mitral valves in color Doppler mode **(B)**. The E and A value is measured in the pulse wave (PW) Doppler mode **(C)**. The corresponding ECG (green) and the respiration rate (yellow) is displayed below the PW mode image.

The Vevo 2100 software (Visualsonics) was used for the analysis of the echocardiographic data. The analyzed morphological, systolic and diastolic parameter, as well as the formula used for calculations are outlined below.

- morphological parameter (PLAX, M-Mode):
  - LVID;s / LVID;d
  - LVPWT;s / LVPWT;d
- systolic function (PLAX, M-Mode):
  - $SV = \left(\frac{7.0}{2.4+LVID;d} * LVID;d^3\right) - \left(\frac{7.0}{2.4+LVID;s} * LVID;s^3\right)$
  - $CO = SV * \frac{heart\ rate}{1000}$
  - $EF = 100 * \left[\frac{\left(\frac{7.0}{2.4+LVID;d} * LVID;d^3\right) - \left(\frac{7.0}{2.4+LVID;s} * LVID;s^3\right)}{\frac{7.0}{2.4+LVID;d} * LVID;d^3}\right]$
  - $FS = 100 * \frac{LVID;d - LVID;s}{LVID;d}$

- diastolic function (apical four chamber, PW Doppler):
    - E value
    - A value
    - E/A

Euthanasia and organ removal

The mice were euthanized by cervical dislocation under 1-3% isoflurane anesthesia. The organs were removed in following order: heart, lungs and liver. All organs were washed in ice-cold PBS and dried on tissue wrap to remove all traces of liquid. In addition, the heart was carefully and manually pumped in PBS on ice to remove blood from the ventricles. This step is important given that the blood contamination would interfere with the downstream analysis. Then, the organ weight was measured prior to quick-freezing in liquid nitrogen and long-term storage at -80°C.

In addition, the basis of the heart of animals utilized for histological analyses were embedded in NEG 50 to enable the preparation of cryosections (Bancroft et al. 2008c). For this purpose, the heart was horizontally cut using a scalpel and the apex was quick-frozen in liquid nitrogen and stored at -80°C for biochemical analysis. The basis was transferred in 30mM 2,3-butanedionemonoxime in PBS to relax the cardiac muscle. After incubation for 3 min on ice, the basis was washed in ice-cold PBS and dried on tissue wrap to remove all traces of liquid. Subsequently, the basis was transferred in a cup made of aluminum foil covered with NEG 50 (cross section down). After ensuring that the heart basis was covered completely in NEG 50 and the samples were frozen in liquid nitrogen using pre-cooled isopentane as a freezing agent and stored at -80°C.

3.2.2 *In vivo* aging model

In collaboration with Dr. Kleinbongard (Dept. of Pathophysiology, University Hospital Essen), the proteasome regulation in cardiac aging was investigated in two blinded studies using 4 versus 26 months old male mice and 3, 9 and 30 months old male mice (Figure 8). It should be noted that animals of the former study (4 versus 26 months old mice) were sacrificed due to visible signs of distress, suggesting a very poor overall health condition, thus accounting for the variability in their age upon analysis (communicated by Dr. Kleinbongard, Dept. of Pathophysiology, University Hospital Essen). Analysis of the cardiac function of 3, 9 and 30 months old mice via echocardiography by our collaborators (data not shown) did not show pathological abnormalities. Thus, these mice appeared healthy.

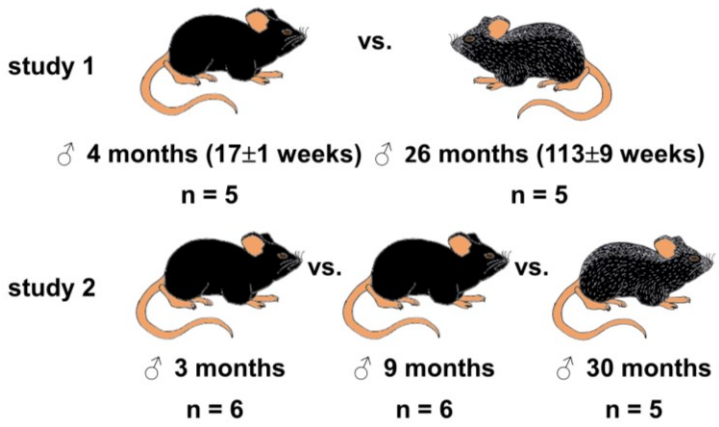

Figure 8. Scheme of different age groups compared in two blinded studies.

3.3 Molecular biological methods

3.3.1 Extraction of nucleic acids

RNA extraction from mouse tissue

Total RNA was purified from the tissues of C57BL/6J WT mice utilizing the RNeasy mini kit according to manufacturer's recommendations. Notably, the excised tissue was stabilized in RNA*later* RNA stabilization reagent before disruption in 2 ml of RLT buffer utilizing a handheld homogenizer on ice. In addition, the integrity of total RNA was assessed via agarose gel electrophoresis (see 3.3.5.) with intact total RNA resulting in clear 28S and 18S rRNA bands.

RNA extraction from cell pellets

The total RNA was purified from cell pellets using the peqGOLD total RNA kit according to manufacturer's instructions.

Extraction of genomic DNA from mice tail biopsies

The genomic DNA was extracted from mice tail biopsies stored at -20°C (Malumbres et al. 1997, Wang et al. 2006). For this purpose, the tail biopsy (~1 cm) was digested in 150 µl of tail biopsy digestion buffer at 55°C overnight. On the next day, the proteinase K was heat inactivated for 10 min at 95°C. Next, cell debris were removed by centrifugation for 10 min at ~20.000 x *g*. Subsequently, the genomic DNA in the supernatant was precipitated to remove components which inhibit the PCR reaction (Malumbres et al. 1997, Wang et al. 2006). For this purpose, 5 µl of 3 M actetate solution (pH 5.2) and 125 µl of ice-cold 100% ethanol were added to 50 µl of the supernatant. After incubation at -20°C overnight, the DNA was pelleted by centrifugation for 15 min at ~20.000 x *g* at 4°C. Then, the DNA pellet was washed with 1 ml of 70% ethanol. After centrifugation for 5 min at ~20.000 x *g* at 4°C, the supernatant was

carefully decanted and the DNA pellet was air-dried for 5-10 min at room temperature (RT). Finally, the DNA was dissolved in 50 µl of 10 mM TRIS buffer (pH 8.5).

The genomic DNA was used to analyze the genotype of the mice via PCR (see 3.3.4) and subsequent agarose gel electrophoresis (see 3.3.5).

3.3.2 Determination of RNA and DNA concentration

The RNA, cDNA or DNA concentration was determined using the Nanodrop ND-1000 spectrophotometer. According to Lambert-Beer law, the RNA, cDNA or DNA concentration was calculated by measuring the ultraviolet light absorption (OD_{260nm} = 1 corresponds to a concentration of 40 ng of RNA, 33 ng of cDNA or 50 ng of DNA per µl solution) (Buckingham 2011). In addition, the purity of the RNA or DNA solution was assessed using the ratio of the absorption at 260 nm to 280 nm. An A260/A280 ratio of 2.0 indicated a highly purified RNA. Values below 2.0 may indicate DNA contamination, whereas values above 2.0 suggest potential protein or other aromatic compound contamination. In contrast, an A260/A280 ratio of 1.8 is indicative of highly purified DNA. Values above 1.8 may indicate RNA, protein or contamination with aromatic compounds (Buckingham 2011).

3.3.3 Reverse transcription

Reverse transcription using total RNA extracted from mouse tissue

The cDNA was synthesized from total RNA via reverse transcriptase reaction using the Transcriptor high fidelity cDNA synthesis kit according to manufacturer's instructions. First, the pre-annealing mixture was prepared according to the scheme outlined below. After 10 min denaturation at 65°C and cooling on ice, the components of the reaction mixture were added to the pre-annealing mixture and the reverse transcription was performed for 30 min at 55°C. Finally, the reverse transcriptase was heat inactivated by incubation at 85°C for 5 min.

pre-annealing mixture (1x):

water (PCR-grade)	10.4 µl - x µl
anchored-oligo$(dT)_{18}$ primer [50 pmol/µl]	1 µl
total RNA (5 µg in total)	x µl
total volume	11.4 µl

reaction mixture (1x):

5x reaction buffer	4 µl
desoxynucleotide mix [10 mM each]	2 µl
DTT [100 nM]	1 µl
pre-annealing mix	11.4 µl
protector RNase inhibitor [40 U/µl]	0.5 µl
reverse transcriptase [180 U/µl]	1.1 µl
total volume	20 µl

Notably, the Transcriptor high fidelity cDNA synthesis kit provides a markedly higher fidelity than the M-MLV reverse transcriptase used for the reverse transcription of total RNA from cell pellets. Thus, the cDNA, which was synthesized via reverse transcriptase reaction using the

Transcriptor high fidelity cDNA synthesis kit, was used for plasmid construction due to the higher accuracy of the reaction.

Reverse transcription using total RNA isolated from cell pellets

The cDNA was synthesized from total RNA, isolated from cell pellets, via reverse transcriptase reaction using the moloney murine leukemia virus (M-MLV) reverse transcriptase according to manufacturer's recommendations. First, the pre-annealing mixture was prepared according to the scheme outlined below and denatured for 5 min at 70°C. After cooling on ice, the components of the reaction mixture were added and the reverse transcription was performed for 60 min at 42°C. Then, the reaction mix was incubated for 5 min at 85°C to heat inactivate the reverse transcriptase.

pre-annealing mixture (1x):

water (PCR-grade)	13 µl - x µl
anchored-oligo(dT)$_{15}$ primer [0.5 µg/µl]	2 µl
total RNA (2 µg in total)	x µl
total volume	15 µl

reaction mixture (1x):

water (PCR-grade)	17.75 µl
5x M-MLV reaction buffer	5 µl
desoxynucleotide mix [10 mM each]	1.25 µl
pre-annealing mix	15 µl
reverse transcriptase [200 U/µl]	1 µl
total volume	40 µl

3.3.4 Polymerase chain reaction (PCR)

PCR – amplification of gene of interest for cloning

The gene of interest was amplified via polymerase chain reaction (PCR) using Phusion high fidelity polymerase according to manufacture's recommendations. The 'β1i direct primers' or 'β1i overhang primers' were used for the amplification of the β1i gene or the insertion of the Kozak consensus sequence, as well as the restriction sites, needed for subcloning, respectively.

- PCR master mix (1x):

nuclease-free water	21 µl – x µl
forward primer [10 µM]	2 µl
reverse primer [10 µM]	2 µl
template cDNA (200 ng per reaction)	x µl
2x phusion master mix	25 µl
total volume	50 µl

- thermocycler protocol:

step	**time**	**temperature**
preheat cycler		98°C
initial denaturation	2min	98°C
35 cycles:		
denaturation	1min	98°C
annealing	1min	60°C
extension	1min	72°C
final extension	10min	72°C
store		4°C

Semiquantitative PCR

The β1i mRNA expression was analyzed after AAV2 CMV/MLC0.26 β1i infection in HEK-293 cells.

First, total RNA was purified from cell pellets (6-well; 5 x 10^5 cell / well sub-cultured; 48 hours after AAV infection) using the peqGOLD total RNA kit (see 3.3.1.). Subsequently, cDNA was synthesized from 2µg of total RNA via reverse transcriptase reaction using the M-MLV reverse transcriptase (see 3.3.3). Then, the β1i gene was amplified using 250 ng of cDNA via polymerase chain reaction (PCR) utilizing Phusion high fidelity polymerase according to manufacture's recommendations. Finally, the mRNA expression of β1i (660 bp) in HEK-293 cells was analyzed by agarose gel electrophoresis (see 3.3.5).

- PCR master mix (1x):

nuclease-free water	8.4 µl – x µl
β1i direct primer forward [10 µM]	0.8 µl
β1i direct primer reverse [10 µM]	0.8 µl
template cDNA (250 ng per reaction)	x µl
2x phusion master mix	10 µl
total volume	20 µl

- thermocycler protocol:

step	**time**	**temperature**
preheat cycler		98°C
initial denaturation	2min	98°C
35 cycles:		
denaturation	1min	98°C
annealing	1min	60°C
extension	1min	72°C
final extension	10min	72°C
store		4°C

PCR - genotyping

Heterozygous β1i-deficient mice were mated and genotyped. Male homozygous β1i knockout mice were then subsequently used for the *in vivo* hypertrophy model.

The DNA was assessed for the presence of the β1i gene (primer pair: β1i-2 and β1i-4; 550 bp) and the neomycin cassette (primer pair: β1i-3 and neoA; 1500 bp) via PCR using the Phusion high-fidelity DNA polymerase according to manufacturer's recommendations. Subsequently, the PCR products were analyzed by agarose gel electrophoresis (see 3.3.5) using a 1.5% (w/v) agarose gel, which was commonly run at 80 V for approximately 90 min. Accordingly, homozygous β1i-deficient mice were negative for the β1i gene (550 bp) and positive for the neomycin cassette (1500 bp) PCR product.

- PCR master mix (1x):

nuclease-free water	18.8 µl
5x phusion HF buffer	4 µl
dNTPs [each 10mM]	0.2 µl
forward primer [10 µM] = β1i-2 or β1i-3	0.2 µl
reverse primer [10 µM] = β1i-4 or neoA	0.2 µl
Phusion polymerase [2 U/µl]	0.2 µl
precipitated genomic DNA	1.2 µl
total volume	20 µl

- thermocycler protocol:

primer pair		**β1i-2 & β1i-4**	**β1i-3 & neoA**
step	**time**	**temperature**	
preheat cycler		94°C	94°C
initial denaturation	2min	94°C	94°C
35 cycles:			
denaturation	1min	94°C	94°C
annealing	1min	**55°C**	**65°C**
extension	3min	72°C	72°C
final extension	10min	72°C	72°C
store		4°C	4°C

3.3.5 Agarose gel electrophoresis

In general, agarose gel electrophoresis of PCR products was used to analyze the mRNA expression of a gene of interest or for genotype determination. Moreover, the electrophoretic separation of digested plasmids or PCR products was used to purify the products or to assess the digestion or the successful gene of interest insertion into a plasmid (Sambrook et al. 1989).

After adding 5x loading buffer, the DNA fragments were commonly separated using a 1% (w/v) agarose gel. The gel was run at 100 V for approximately 90 min. Finally, the DNA fragments were visualized by ultraviolet light due to the intercalated ethidium bromide and recorded using the Gel Doc XR gel documentation system. The DNA fragment sizes were verified by utilizing DNA ladders. In addition, DNA bands were excised to purify the DNA utilized in subsequent procedures (e.g. construction of plasmid).

3.3.6 Purification of DNA after enzymatic reactions and agarose gel electrophoresis

Following enzymatic reactions such as PCR, dephosphorylation and restriction digestion, the DNA fragments used for cloning were purified due to presence of ions or other ingredients which would otherwise interfere with downstream reactions. The DNA fragments that were separated by agarose gel electrophoresis were thus purified using the QIAquick gel extraction kit according to manufacturer's instruction.

3.3.7 Cloning

Restriction digestion of cloning vectors

Restriction digestion of cloning vectors was used to insert specific DNA fragments as well as to verify the successful insertion of the gene of interest. The restriction digestion using different restriction enzymes was performed according to manufacturer's instructions regarding specific buffer conditions, incubation temperature and time. Subsequently, 1500-2000ng of plasmid were used for the preparative restriction digestions, subjected to gel electrophoresis (see 3.3.5) and later purified using the QIAquick gel extraction kit (see 3.3.6). The successful insertion of the specific DNA fragment (100 ng starting amount) was verified by agarose gel electrophoresis and visualization by ultraviolet light (see 3.3.5).

Dephosphorylation of blunt end digested cloning vectors

Blunt end digested cloning vectors (e. g. via restriction enzyme SmaI) were dephosphorylated using FastAP thermosensitive alkaline phosphatase according to manufacturer's recommendations to avoid re-ligation. One phosphatase unit was added per 1 µg of template. After incubation for 20 min at 37°C, the phosphatase was inactivated by incubation for 5 min at 75°C. Then, the digested and dephosphorylated cloning vector was purified using the QIAquick gel extraction kit (see 3.3.6) after agarose gel electrophoresis (see 3.3.5).

Phosphorylation of PCR products

At least one of the templates had to be phosphorylated to ligate a vector and an insert (Sambrook et al. 1989). Since the blunt end digested vectors were dephosphorylated to avoid re-ligation, the PCR products were thus phosphorylated using the T4 polynucleotide kinase. According to manufacturer's recommendations, the T4 DNA ligase buffer was used to optimize the reaction conditions for the subsequent ligation. First, the molarity of 5'-termini, which were phosphorylated in the reaction, was calculated using the following formula.

$$M\left(\frac{mol}{l}\right)=\left(template\frac{\mu g}{\mu l}\div\left[base\ pairs\times 650D\right]\right)\times 2\ ends$$

Accordingly, one T4 polynucleotide kinase unit was added per 1 nmol 5'-termini. The phosphorylation mix was incubated for 20 min at 37°C. After heat inactivation (10 min at 75°C) of the T4 polynucleotide kinase the phosphorylated PCR products were used for ligation of double-stranded DNA (dsDNA).

Ligation of dsDNA

Phosphorylated PCR products were ligated with dephosphorylated blunt end digested cloning vectors using the T4 DNA ligase according to manufacturer's instructions. In addition, the T4 DNA ligase was further utilized to ligate AgeI and BsrGI digested β1i insert and AAV CMV/MLC0.26 vector. The amount of insert, needed for specific vector to insert ratio, was calculated and the ligation mix was prepared and incubated at RT overnight using the formula and scheme outline below.

$$\frac{length\,of\ insert\,in\,kb}{length\,of\ vector\,in\,kb}\times ng\ of\ vector=ng\ of\ insert\,needed\ for\ a\,1:1\ ratio$$

- inserts: β1i direct PCR product = 660 bp
  β1i overhang PCR product = 686 bp
  AgeI and BsrGI restricted β1i insert = 666 bp
- vectors: pBlueScript II SK(+) = 2961 bp
  pSP72 = 2462 bp
  AAV CMV/MLC0.26 = 5312 bp

- ligation mix (1x):

water (PCR-grade)	10 µl - x µl - y µl
10x T4 DNA ligase buffer	1 µl
linear vector	x µl
insert	y µl
50% PEG 4000 solution	1 µl
T4 DNA ligase [400 CEU / µl]	1.25 µl
total volume	10 µl

3.3.8 Transformation

Preparation of competent *E.coli*

Competent E.coli (DH1 or Sure cells) derived from a chemical induction were prepared according to the published protocol by Joe Sambrook (Sambrook et al. 1989). Sterile materials were used, the working place was disinfected using 70% ethanol and procedures were performed next to the flame of a Bunsen burner in order to generate semi-sterile working conditions. First, an overnight culture was prepared. For this purpose, 10 µl of *E. coli* suspension of a glycerin stock was used to inoculate 10 ml of sterile LB medium in 13 ml round bottom tubes with push caps and the bacterial suspension was incubated at 37°C with vigorous shaking (150 rpm) over night. The next day, 100 µl of overnight culture were used to inoculate 100 ml of sterile LB medium in a 250 ml Erlenmeyer flask. The bacterial culture was incubated at 37°C with vigorous shaking (110 rpm) and the growth was monitored by measuring the absorbance at 600 nm (OD_{600}). When the OD_{600} reached 0.4-0.6, the bacterial culture was chilled for 10 min on ice in order to stop the growth of the culture in its exponential phase. The bacterial cells were then harvested by centrifugation for 10 min at 2700 x g at 4°C. The cell pellet was resuspended in 60 ml of ice-cold solution containing 80 mM $MgCl_2$ and 20 mM $CaCl_2$. After centrifugation for 10 min at 2700 x g at 4°C, the supernatant was decanted and the tube was inverted to remove all traces of the liquid. In a subsequent step, the cell pellet was resuspended in 4 ml of ice-cold 100 mM $CaCl_2$ solution. After adding 140 µl of sterile DMSO, the solution was immediately mixed by inverting and was placed for 15 min on ice. Finally, the suspension was dispensed in single-use aliquots and quick-frozen in liquid nitrogen. The chemically competent cells were placed at -80°C for long-term storage.

Transformation of competent *E. coli*

Competent *E. coli* were transformed using a ligation mix (see 3.3.7.) or plasmid DNA (Sambrook et al. 1989). Accordingly, 1 µl of ligation mix or approximately 20 ng of plasmid DNA was added to 50 µl of competent *E.coli*, which were thawed on ice. Notably, *E.coli* DH1 were utilized for the transformation with the ligation mix due to the higher transformation efficiency as compared to *E.coli* Sure cells which lack endonuclease. The latter cells were used for transformation of AAV CMV/MLC0.26 vectors to avoid recombination processes by the inverted terminal repeats (ITRs). After incubation of *E.coli* for 45 min on ice, the cells were subject to heat shock for exactly 2 min at 42°C and chilled on ice followed by the addition of 200 µl of pre-warmed sterile LB medium. Next, the solution was shaken (350 rpm) for 90 min at 37°C before plating on LB agar plates containing the selective antibiotic ampicillin (0.1 mg/ml). The cultures were incubated up-side down over night at 37°C

Propagation of positively transformed colonies

Distinct colonies which formed on agar plates (positively transformed bacteria containing ampicillin resistance gene) were singly selected to inoculate 9 ml of sterile LB medium containing 0.1 mg/ml ampicillin in 13 ml round bottom tubes with push caps. The cell suspension was incubated at 37°C with vigorous shaking (150 rpm) over night to propagate potentially positively transformed colonies (Sambrook et al. 1989).

Preparation of plasmid DNA by alkaline lysis according to Birnboim and Doly (1979)

The plasmid DNA, prepared according to the protocol of Birnboim and Doly (1979), was used for the verification of the insertion by restriction digestion (Birnboim et al. 1979). In contrast, the plasmid DNA was prepared utilizing specific kits for all other applications e.g. sequencing or subcloning.

For the purpose of preparing plasmid DNA by alkaline lysis, 1.5 ml of the overnight bacterial culture were harvested by centrifugation for 20 s at ~20.000 x *g* at 4°C. After decanting the supernatant, the cell pellet was resuspended in 100 µl of ice-cold alkaline lysis solution I. Then, 200 µl of alkaline lysis solution II and 150 µl of alkaline lysis solution III were added. The suspension was inverted after the addition of each solution and was incubated for 5 min on ice. After centrifugation for 5 min at ~20.000 x *g* at 4°C, the supernatant was transferred to a new 1.5 ml tube and the DNA was precipitated by the addition of 2 volumes of 100% ethanol followed by 2 min incubation on ice. The solution was then centrifuged for 5 min at ~20.000 x *g*. The DNA pellet was washed by adding 1 ml of 70% ethanol and centrifugation for 2 min at ~20.000 x *g*. After decanting the supernatant, the DNA pellet was air-dried for 5-10 min at RT and was dissolved in 30 µl of buffer TE.

Preparation of purified plasmid DNA

Purified plasmid DNA, subsequently used for sequencing and subcloning, was prepared using the QIAprep spin miniprep kit. For this purpose, 8 ml of overnight bacterial culture was harvested by centrifugation for 10 min at 6800 x *g* at 4°C. Subsequently, the plasmid DNA was purified according to manufacturer's instructions.

Preparation of glycerol stocks for long-term storage

Glycerol stocks of colonies harboring the desired insert were prepared for long-term storage. For this purpose, 520 µl of sterile 87% glycerol solution were added to 420 µl of overnight bacterial culture and carefully mixed by inverting. The glycerol stocks were stored at -80°C.

3.3.9 Sequencing

Sequencing was used to verify the inserted sequence ('AAV sequencing primers') as well as the integrity of the ITR's ('AAV ITR primers') of the AAV CMV/MLC0.26 vectors and was carried out by Seqlab - sequence laboratories Göttingen GmbH.

3.3.10 Preparation of AAV CMV/MLC0.26 β1i vector for packaging into AAV particles

AAV CMV/MLC0.26 β1i or *Renilla* Luciferase (provided by Dr. O. Müller, Dept. of Internal Medicine III, University Clinic Heidelberg) vector, used for packaging into AAV particles, were purified utilizing the EndoFree plasmid megaprep kit according to manufacturer's instructions. Large culture volumes were used due to the low copy number of the plasmid.

Initially, 2 ml of overnight culture of *E. coli* harboring AAV CMV/MLC0.26 β1i or *Renilla* Luciferase were used to inoculate pre-warmed 2 L of sterile LB medium containing the selective antibiotics ampicillin (0.1 mg/ml). The bacterial culture was incubated at 37°C with vigorous shaking (110 rpm) and the growth was monitored by measuring the absorbance at 600 nm. After approximately six to seven hours, the OD_{600} of 0.8-0.9 was reached revealing the end of the exponential phase of growth. Then, the bacterial culture was chilled on ice prior to harvesting by centrifugation at 12.000 *x g* for 10 min at 4°C. The procedure was repeated 4 times to harvest a sufficient amount of bacterial cells (= 11-12 g wet cell pellet) prior to plasmid DNA preparation using EndoFree plasmid megaprep kit in conjunction with the plasmid DNA isolation procedure according to the protocol of Birnboim and Doly (Birnboim et al. 1979).

Briefly, the plasmid DNA was isolated according to the protocol of Birnboim and Doly (Birnboim et al. 1979). For this purpose, the cell pellets were resuspended in 180 ml of ice-cold alkaline lysis solution I and were transferred to a 1 L bottle. In subsequent steps, 180 ml of alkaline lysis solution II and 180 ml of alkaline lysis solution III were added. The suspension was inverted after the addition of each solution and was incubated for 10 min on ice. The bacterial lysate was then centrifuged for 5 min at 9.000 x g at 4°C. After pooling the supernatant in a 2 L bottle, the DNA was precipitated by adding 2 volumes of 100% ethanol and incubated for 20 min on ice. Next, the precipitated DNA was pooled into one 50 ml tube by centrifugation for 5 min at 10.000 x g at 4°C. The DNA pellet was washed by adding 40 ml of 70% ethanol, centrifuged for 5 min at ~15.000 x g at 4 °C and air-dried overnight at RT. Finally, plasmid DNA was purified using the EndoFree plasmid megaprep kit according to manufacturer's recommendations.

The presence of the gene of interest as well as the integrity of the ITR's of the AAV CMV/MLC0.26 β1i or *Renilla* Luciferase vector, used for packaging in AAV particles, was checked by restriction digestion and sequencing prior to packaging in AAV particles.

3.4 Protein biochemical methods

3.4.1 Protein extraction

Protein extraction from cell pellets

The total protein extraction from cells was performed using a modified protocol for protein extraction from heart tissue (Drews et al. 2010). For this purpose, cell pellets (6-well; 5 x 10^5 cell / well sub-cultured; 48 hours after AAV infection) were thawed on ice and homogenized in 100 µl of freshly prepared homogenization buffer containing 1 mM DTT and a spatula tip of sea sand (higher shear force) using a hand-held homogenizer (1.5 ml tube specificity) by turning the pestle 20 times. The cell homogenate was then centrifuged for 30 min at ~20.000 x *g* at 4°C. The supernatant fraction containing the proteins was transferred to a new tube and stored at -20°C and the cell debris pellet was discarded.

Protein extraction from hearts

The total protein was extracted from mouse hearts in accordance with previously published protocols (Drews et al. 2010). Notably, all solutions and equipment were pre-cooled to 4°C.

First, the frozen heart was homogenized in 1.5 ml of freshly prepared homogenization buffer (containing 1mM DTT, 1% (v/v) phosphatase inhibitor cocktail II, 1% (v/v) phosphatase inhibitor cocktail III) using a Tenbroeck hand-held homogenizer by turning the pestle 20 times. The supernatant (= crude extract) was carefully removed after centrifugation for 1 min at 500 x *g* at 4°C to remove the cell debris. Following this, the crude extract was ultracentrifuged for 1 h at 100.000 x *g* at 4°C. Finally, the supernatant (= heart homogenate) was transferred to a new 1.5 ml tube. The solution amount necessary for 26S activity assays and active site labeling was kept on ice. Aliquots of the remaining homogenate were quick-frozen in liquid nitrogen and stored at -20°C. Notably, 1% (w/v) protease inhibitor cocktail was added to the homogenates which were not used for proteasome activity assays or active site labeling prior to freezing.

3.4.2 Determination of protein concentration – Bradford assay

The protein concentration was determined utilizing the Bradford reagent according to manufacturer's recommendations. This assay is based on the shift in the absorbance maximum to 595 nm when the *Coomassie* dye reacts with basic or aromatic amino acid

residues (solution turns blue). Moreover, the absorbance at 595 nm is proportional to the protein concentration over a broad dynamic range. A standard curve using 0, 20, 40, 60, 80, 100, 120, 140, 160,180 and 200 µg of BSA per ml was utilized to determine the protein concentration of the samples. The Bradford assay was performed in a 96-well plate. For this purpose, 100 µl of Bradford reagent was added to 10 µl of protein solution. After 5 min incubation at RT, the optical density (OD) was measured at 595 nm using the Powerwave Xs microplate spectrophotometer.

3.4.3 Proteasome activity assays

Proteasome activity was analyzed according to previously published protocols (Drews et al. 2010). The 26S proteasome activities were measured on the day of heart homogenization, given the remarkable decline of 26S proteasome activities due to freezing. In addition, the 20S proteasome activities were commonly analyzed up to one day following heart homogenization due to the decline of 20S proteasome activity with increasing storage time of the homogenate.

The 26S or 20S caspase-, trypsin- or chymotrypsin-like activities were analyzed using 0.1mM fluorescently tagged substrates Z-LLE-AMC, Boc-LSTR-AMC or Suc-LLVY-AMC, respectively, for 25 µg of total protein homogenate. All samples were measured in triplicates and the total reaction volume was 100 µl. In addition, all activities were analyzed in the absence and presence of a specific proteasome inhibitor. In accordance with the analyzed proteasome activity, 10 µM epoxomicin, 20 µM epoxomicin or 30 µM Z-Pro-Nle-Asp-H inhibitor was used to inhibit chymotrypsin-, trypsin- or caspase-like activity, respectively. The ATP-dependent 26S activities were analyzed in homogenization buffer after the addition of 50 µM ATP. In contrast, the 20S activity assays were performed in specific buffers containing low amounts of detergents. For this purpose, the 20S caspase- and trypsin-like activity buffer and the 20S chymotrypsin-like activity buffer were prepared as 10x stock solutions (stored at -20°C) in order to adjust the buffer conditions in the 20S activity assays. Moreover, a standard curve using 100, 275, 600, 1250 and 2500 nM free AMC was prepared to calculate the substrate turnover rate.

First, the required buffer conditions were created by applying 80 µl of buffer per well in a black 96-well plate. Then, 10 µl of 2.5µg/µl heart homogenate solution was added and incubated for 30 min at RT in the dark to facilitate inhibition of the specific proteasome activity in sample mixtures containing proteasome inhibitors for measuring non-proteasomal background activity. After pre-equilibration for 15 min on ice, 10µl of 1mM fluorescently tagged substrate was added using a multistep pipette. Finally, the release of AMC was measured at 37°C using the fluorometer Fluoroskan Ascent at an excitation wavelength of 390 nm and an emission

wavelength of 460 nm for up to 90 min using a measurement interval of 5 min. The measured signal was integrated over 20 ms.

The time was plotted against the emission values to evaluate the proteasomal activity. The substrate turnover rate (pmol/[mg*min]) was calculated from the linear phase of the curve for each sample using the AMC standard curve. Non-proteasomal activities measured in the presence of specific proteasome inhibitors were subtracted.

3.4.4 Active site labeling of proteolytic proteasome subunits

The incorporation of proteolytic β-subunits into active proteasome complexes was investigated using the activity based probes MV151 (Verdoes et al. 2006) or MVB003 (Florea et al. 2010). These proteasome-specific and fluorescently-tagged inhibitors label proteolytic β-subunits in native 26S and 20S proteasomes and were kindly provided by Dr. B. Florea and Prof. H. Overkleeft (Institute of Chemistry, University of Leiden, NL). Notably, the active site labeling was performed on the day of heart homogenization given the remarkable decrease of the 26S proteasome activity due to freezing. Proteolytic proteasome subunits were labeled using 25 µg of total protein and 1µM activity based probe MV151 or MVB003, respectively for the total reaction volume was 20 µl. The active site labeling was performed in homogenization buffer after the addition of 1 mM DTT and 50 µM ATP. In addition, the active site labeling was performed in the presence and absence of the specific proteasome inhibitor bortezomib to ensure that the detected bands correspond to the proteolytic β-subunits. For this purpose, 0.1 µM bortezomib was used to inhibit proteasomal activity. First, the required buffer conditions were established in a total volume of 6 µl. Then, 10 µl of 2.5 µg/µl heart homogenate solution was added and incubated for 1 h on ice to inhibit the specific proteasome activity. Finally, the proteolytic β-subunits were labeled by adding 2 µl of 10 µM MV151 or MVB003 solution and incubated for 1 h at 37°C. After polyacrylamide gel electrophoresis (PAGE) (see 3.4.4.), the β-subunits were visualized and documented using the Pharos FX™ Plus Molecular Imager at an excitation wavelength of 532 nm and an emission wavelength of 605 nm. The band intensities were analyzed using the QuantityOne software and normalized to the total protein staining using ruthenium.

3.4.5 Luciferase activity assay

The enzymatic activity of the *Renilla* luciferase in the β1i knockout mice injected with AAV9 CMV/MLC0.26 luciferase was analyzed in triplicates utilizing the *Renilla*-Glo luciferase assay system according to manufacturer's recommendations. For this purpose, the crude extracts of the hearts (without ultracentrifugation) were used, stabilized by the addition of 1% (w/v) protease inhibitor cocktail. In addition, all samples were diluted in homogenization buffer (1:20), incubated for 15 min on ice as well as pre-equilibrated for 15 min at RT before the

Renilla luciferase assay reagent was added. These additional steps were performed given that isoflurane, used for the anesthesia of the mice, inhibits the *Renilla* luciferase activity (Keyaerts et al. 2012). Accordingly, preliminary experiments revealed the increase in the *Renilla* luciferase activity due to the reduced effect of the inhibitor when the crude extracts were diluted and incubated for a prolonged time period. The luminescence was measured using the MicroLumat LB 96 P after the addition of 100 µl of *Renilla* luciferase assay reagent per 100 µl of 1:20 diluted sample in black 96-well plates and 10 min incubation at RT. The measured signal was integrated over 10 s. The AAV β1i treated samples were utilized for background correction of the AAV Luci treated samples. In addition, the *Renilla* luciferase activity was normalized to the total protein utilized in the assay.

3.4.6 Western blot analysis

The Western blot analysis is a routine technique to analyze the abundance of a protein in a sample (Hames 1998). First, the proteins are separated by their size using polyacrylamide gel electrophoresis (PAGE). For this purpose, 25 µg of total protein were denatured by adding 5x protein loading buffer and incubation for 5 min at 95°C. The lysates were loaded onto a polyacrylamide gel (in general 13% resolving and 6% stacking gel) that was subject to 100 V for 2-2.5 h. Notably, the precision plus protein dual color standard was used to estimate the molecular weight of the separated proteins. After electrophoresis, the proteins were blotted onto a nitrocellulose membrane using the semi dry TransBlot turbo transfer system for 1 h at 25V and 400 mA according to manufacturer's recommendations. Following this, the membrane was air-dried for 30 min. The membrane was then stained with Ponceau S solution for 5 min after rehydration to visualize the proteins. Subsequently, the membrane was scanned and documented. After destaining in water or TBST, the unspecific binding sites were blocked using 5% (w/v) milk solution for 1 h at RT or overnight at 4°C. Finally, the protein of interest was detected using a specific primary antibody (see 2.12.1.) in combination with a horseradish peroxidase (HRP) -conjugated secondary antibody (see 2.12.2.) according to manufacturer's recommendations. The primary and secondary antibodies were diluted in 5% (w/v) milk solution and applied for 4 h at RT or overnight at 4°C (primary antibody) or 1 h at RT (secondary antibody). After the application of ECL prime chemiluminescent substrate for 5 min at RT the emitted light was detected using the Image QuantLAS 4000 mini system. The band intensities were analyzed using the Image QuantLAS 4000 mini software and normalized to total protein staining using Ponceau S.

3.4.7 Proteome analysis

2D gel electrophoresis

The 2D gel electrophoresis (2D GE) was performed according to published protocols (Drews et al. 2007). First, the samples were isoelectric focused using the IPGphor. This was performed according to a modified protocol of Gorg et al. using 18 cm, pH 3-10 IPG strips (Gorg 2004). Accordingly, 200 µg of precipitated protein was resuspended in 350 µl buffer containing 8 M (w/v) urea, 0.1% (w/v) CHAPS, 0.2% (w/v) DTT and 0.5% (v/v) Pharmalytes 3-10 for in gel rehydration at 30 V for 11 h. The voltage was gradually increased from 150 V, 300 V to 600 V every 60 min. Subsequently, the voltage was increased to 3500 V within 30 min. The steady state of the isoelectric focusing was reached after 18 kV-h at 3500 V. The second dimension was facilitated on 12% acryl amide gels. Prior to loading, the samples were equilibrated according to previously published protocols (Gorg et al. 1988). Finally, the separated proteins were visualized by ruthenium staining. Precipitation, 2D GE, staining and laser densitometry were kindly performed by Dr. O. Drews, Anita Kühner and Mathilde Lorenz (Dept. of Cardiovascular Physiology, University Heidelberg). Spot volumes were quantified using the QuantityOne analysis software.

Proteins were compared to published reference gels of a cardiac proteome database (HP-2DPAGE: http://web.mpiib-berlin.mpg.de/hp-2dpage/heart1.html).

Total protein staining using ruthenium

After one or two-dimensional gel electrophoresis, proteins were stained using a ruthenium complex. First, the gels were fixed using fixation solution containing 40% (v/v) ethanol and 10% (v/v) acetic acid on a shaker for 6 h or overnight. Following this, the gels were washed two times in 20% ethanol on a shaker for 30 min. After complete removing of the washing solution, the proteins were stained using 1 µM ruthenium(II)-tris-(bathophenanthroline-disulphonate) (RuBP) in deionized water on a shaker in the dark for 6 h or overnight. The gels were then washed two times in deionized water in the dark for 15 min. Finally, the gels were destained in fixation solution on a shaker in the dark for 6 h or overnight. The Proteins were visualized and documented using Pharos FX^{TM} Plus Molecular Imager at an excitation wavelength of 488 nm and an emission wavelength of 605 nm. The band intensities were analyzed utilizing the QuantityOne analysis software and normalized to total protein staining. The molecular weight of the separated bands or spots were estimated by the utilization of the protein standard from the same gel.

3.5 Immunochemical methods

3.5.1 Immunofluorescence analysis

The localization as well as the abundance of various proteins was analyzed using immunofluorescence staining of cells or heart tissue cryosections (7 µm), which were prepared on glass slides using the microtome HM 500 O microtome cryostat and air-dried for 30 min at RT (Bancroft et al. 2008c). The preparation of the cryosections was kindly performed by Anita Kühner (Dept. of Cardiovascular Physiology, University Heidelberg). Endogenous mouse IgG were blocked using anti mouse F_{ab} fragments when primary mouse antibodies were used in NRCMs or mouse heart tissue to prevent unspecific staining of the fluorescent-labeled secondary antibodies.

First, the cells or 7µm heart tissue cryosections were fixed according to the scheme outlined below.

	fixative	incubation time
HEK-293 cells	isofix	30 min on ice
NRCMs	4% paraformaledhyde and 4% sucrose in PBS	10 min at RT on shaker
heart tissue cryosections	4% paraformaldehyde in PBS	30 min at RT

After washing the samples three times for 5 min in 1x PBS, the cells were permeabilized by adding 0.2% (w/v) TritionX-100 in PBS for 10 min at RT. Then, the unspecific binding sites and, if necessary, the endogenous moue IgG were blocked using the solutions listed below.

- unspecific binding sites:

	blocking solution	incubation time
cells	5% (w/v) BSA in PBS	30 min at RT on shaker
heart tissue cryosections	2% (v/v) goat serum in 0.1% (w/v) TritonX-100 in PBS	2h at RT

- endogenous mouse IgG:

	blocking solution	incubation time
cells	1:13 diluted F_{ab} goat anti-mouse in 0.1% (w/v) BSA / 0.25% (w/v) casein in PBS	1h at RT
heart tissue cryosections	1:13 diluted F_{ab} goat anti-mouse in 1% (v/v) goat serum in 0.05% (w/v) TritonX-100 in PBS	overnight at 4°C

Following this, the protein of interest was detected using a specific primary antibody (see 2.12.1.) in combination with a fluorescently tagged secondary antibody (see 2.12.2.) according to manufacturer's recommendations. In contrast, β1i and β1 was detected in cells

using a cascade of the β1i specific primary antibody, a biotin conjugated secondary antibody and Cy3 conjugated streptavidin binding to the biotin molecules to amplify the signal. The antibodies as well as the Cy3 conjugated streptavidin were diluted in the same solutions listed in the scheme above for blocking the endogenous mouse IgG and were applied for 20 min to 2h at RT in the dark. The samples were washed three times for 5 min in PBS after each incubation step. Next, the nuclei were stained by the application of 2 mg/ml DAPI stock solution diluted 1:5000 in PBS for 10 min at RT. Finally, the samples were mounted in mowiol and a coverslip was applied. The Olympus IX81 microscope and Exellence RT software was used for the analysis. Notably, EGFP expression and localization in NRCMs upon AAV6 CMV/MLC EGFP infection was analyzed on the Olympus IX81 microscope using the FITC filters (λex 460-480nm, λem 495-540nm, 484 beamfilter).

3.5.2 Histological staining of heart cryosections

Apart from immunofluorescence staining, histological staining of heart cryosections was used for the analysis of the cardiomyocyte size (HE staining) (Bancroft et al. 2008a) or fibrosis (Masson's trichrome staining) (Bancroft et al. 2008b).

Hematoxylin and eosin (HE) staining

For this purpose, 7 µm heart cryosections were prepared using the microtome HM 500 O microtome cryostat on glass slides and were air-dried for 30 min at RT. In the next step, the nuclei were stained by incubation in Mayer's hematoxylin solution for 8 min and rinsed in running tap water (= bluing) for 10 min. After rinsing in deionized water, the counterstaining was performed by applying 0.1% (w/v) eosin solution for 5 min. Subsequently, the cryosections were washed 3 times in deionized water for 1 min. Finally, the tissue was dehydrated through one-minute incubation in 70%, 85%, 96% ethanol and isopropanol respectively and two times incubation in xylol for 2 min. Following this, the cryosections were mounted in Eukitt and a coverslip was applied. The HE staining was kindly performed by Anita Kühner (Dept. of Cardiovascular Physiology, University Heidelberg).

The HE staining results in a dark blue stained nuclei and non-nuclear structures which are colored in various shades of red. The cross-sectional area was quantified using the ImageJ software.

Masson's trichrome staining

Similarly to the HE staining described previously, 7 µm heart cryosections were prepared using the microme HM 500 O microtome cryostat and were air-dried for 30 min at RT on glass slides. Then, the tissue was fixed via incubating in 4% paraformaldehyde in PBS for 1 h. After washing

3 times in deionized water for 1 min, the cryosections were incubated in Bouin's mordant overnight. On the next day, the tissue was rinsed in running tap water until the yellow color was removed. Following this, the cryosections were stained in Weigert's hematoxylin solution and Biebrich Scarlet acid fuchsin solution for 10min each. The tissue was then stained in aniline blue solution for 5 min after acidification in freshly prepared phosphotungstic-phosphomolybic acid solution for 10 min. Finally, the cryosections were transferred in 1% acetic acid solution for 2 to 5 min. In addition, the samples were washed in deionized water after each staining step. Next, the tissue was dehydrated in a one-minute incubation in 70%, 85%, 96% ethanol and isopropanol respectively and two times incubation in xylol for 2 min. Finally, the cryosections were mounted in Eukitt and a coverslip was applied. The Masson's trichrome staining was kindly performed by Anita Kühner (Dept. of Cardiovascular Physiology, University Heidelberg).

Following the Masson's trichrome staining the nuclei are stained in black, the collagen is stained in blue, the muscle fibers and the cytoplasm are dyed in red. The ImageJ software was used to measure the area of collagen.

3.6 Statistical analysis

A two-tailed student's t-test with unequal variance was used for the statistical analysis (Bonner et al. 2011). In this test, the probability of the occurrence of the null hypothesis is calculated. The null hypothesis implies the comparability of the data sets. A high p value ($p > 0.1$) confirms the null hypothesis. In contrast, a low p value ($p < 0.05$) refutes the null hypothesis. Thus, the data sets are considered to be significantly different ($p < 0.05$ = significant; $p < 0.01$ = highly significant).

4 Results

4.1 Cardiac-specific β1i reintroduction via adeno-associated virus

A cardiac tissue-specific expression vector harboring the β1i gene was constructed to reintroduce β1i into the heart of β1i knockout mice via serotype 9 of adeno-associated virus (Figure 9).

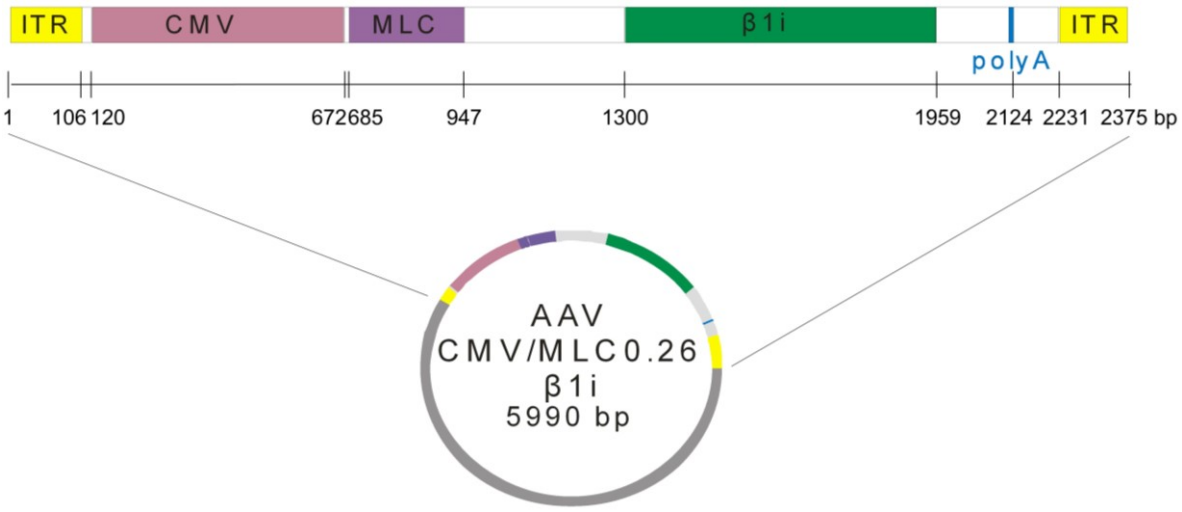

Figure 9. Scheme of AAV CMV/MLC0.26 β1i vector.

Schematic illustration of the β1i vector construct containing a genetically engineered promoter consisting of parts of the viral cytomegalovirus (CMV_{enh}) immediate-early gene promoter and a fragment of the tissue-specific myosin light chain promotor (MLC0.26) as well as the β1i gene within the inverted terminal repeats (ITR).

Given the absence of a commercially available β1i clone which exhibits perfect complementarity to the β1i gene of C57BL/6J wild type mice, the initial task within this project was to isolate and clone the β1i gene (660 bp) from *Mus musculus* (strain C57BL/6J). For this purpose, the total RNA was extracted from the liver of C57BL/6J mice and the β1i gene was amplified via PCR using the 'β1i direct primers' after reverse transcription (Figure 10A). Subsequently, the β1i gene was introduced into the pBlueScript II SK(+) vector after restriction digestion using SmaI via blunt end ligation (Figure 10B) in order to use one clone with verified β1i sequence for further processing. In a subsequent step, an AgeI restriction site as well as the Kozak sequence were inserted upstream and a BsrGI restriction site downstream of the β1i gene by PCR using 'β1i overhang primers' (Figure 10C).

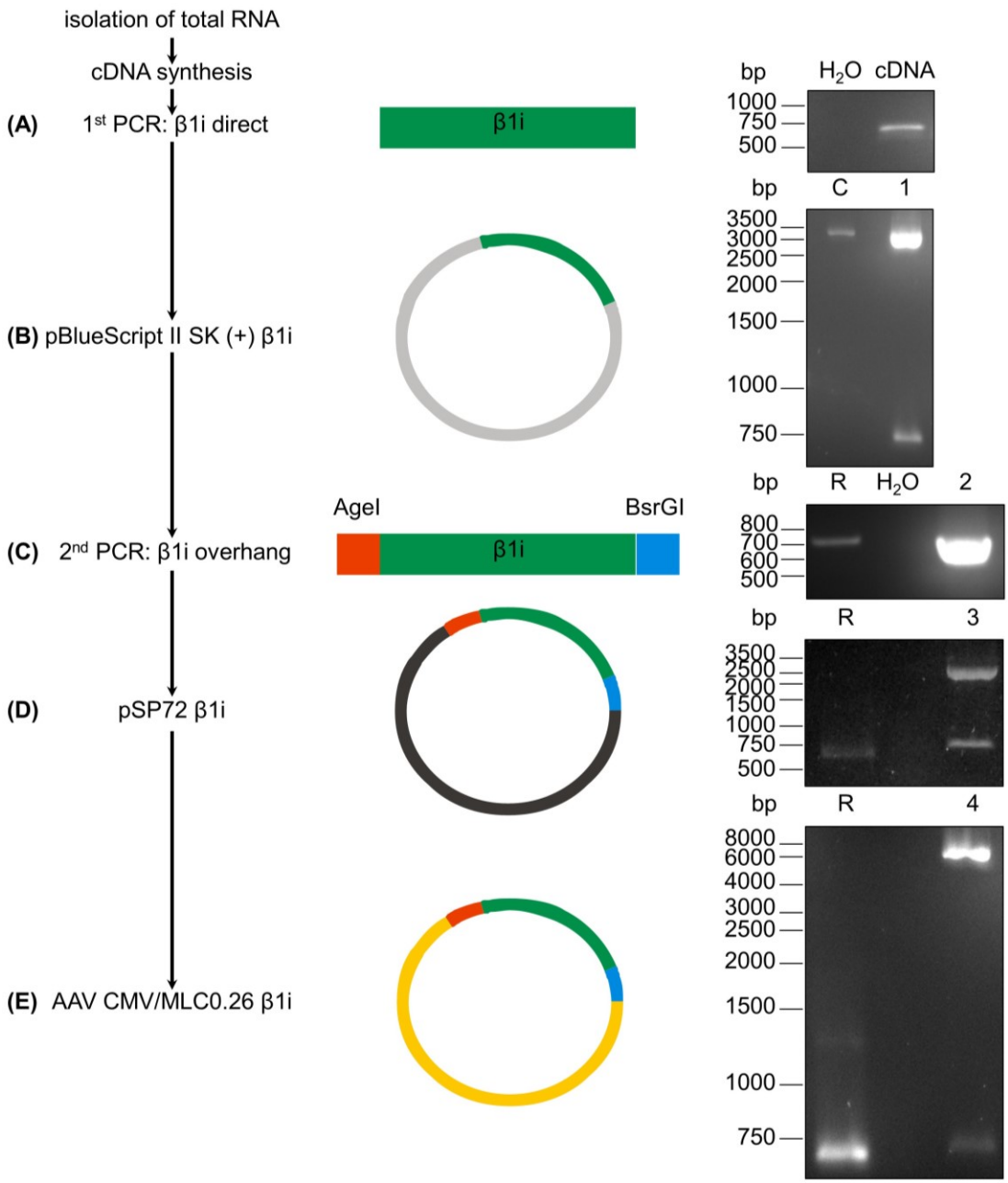

Figure 10. AAV CMV/MLC0.26 β1i vector construction.

(A) The β1i gene (660 bp) from C57BL/6J wild type mice was amplified via PCR after isolation of total RNA from the liver and cDNA synthesis. **(B)** The insertion of β1i in the pBlueScript II SK(+) vector via blunt end ligation was verified by HindIII (5' end) and BamHI (3' end) digestion indicating two distinct bands corresponding to β1i (684 bp) and the pBlueScript II SK(+) backbone (2925 bp) in lane 1 as compared to the empty vector (lane C). **(C)** Subsequently, the Kozak sequence and an AgeI and BsrGI restriction site was introduced by PCR using 'β1i overhang primers' (lane 2). **(D)** The successful insertion of the extended β1i sequence in the pSP72 vector via blunt end ligation was verified by AgeI (5' end) and BsrGI (3' end) digestion indicating two distinct bands corresponding to β1i (666 bp) and the pSP72 backbone (2462 bp) in lane 3. **(E)** In the last step, the β1i gene was subcloned into the AAV CMV/MLC0.26 vector via the AgeI and BsrGI restriction sites. Using these restriction enzymes, two distinct bands were revealed, corresponding to β1i (666 bp) and the AAV CMV/MLC0.26 backbone (5312 bp) in lane 4. (R = β1i direct PCR product)

The extended β1i gene was further introduced into a vector after restriction digestion using SmaI via blunt end ligation for sequence verification. For this purpose, the pSP72 vector was used in parallel to the pBlueScript II SK(+) vector, given the low transformation efficiency using the pBlueScript II SK(+) vector in the previous blunt end ligation. In accordance with this previous result, a clone containing the correct extended β1i sequence was obtained using the pSP72 vector. Initially, the insertion of the extended β1i sequence in the pSP72 vector was analyzed via BamHI digestion (Figure 11). The successful introduction of the insert resulted in an increase in size of the linearized vector (Figure 11). Subsequently, the insertion of the extended β1i sequence in the pSP72 vector was verified by AgeI (5' end) and BsrGI (3' end) digestion indicating two distinct bands corresponding to β1i and the pSP72 backbone (Figure 10D). Finally, the β1i gene was subcloned into the AAV CMV/MLC0.26 vector through the AgeI and BsrGI restriction sites (Figure 10E).

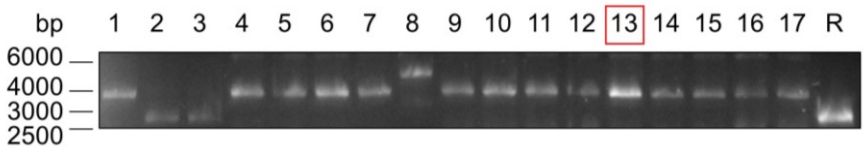

Figure 11. Representative image of BamHI digested clones.

The insertion of the extended β1i sequence in the pSP72 vector via blunt end ligation resulted in an increase in size of the linearized vector after BamHI digestion (R = empty pSP72 vector [2462 bp]). In accordance, clones 2 and 3 contained no insert, whereas clones 1, 4-7 and 9-17 contained the extended β1i sequence. In contrast, clone 8 potentially contained two inserts. After AgeI and BsrGI digestion, clone 13 was used for subcloning into the AAV CMV/MLC0.26 vector (Figure 10E).

4.2 Infection of HEK-293 cells using the AAV CMV/MLC0.26 β1i vector construct led to correct expression of β1i at an elevated level

The initial task was to verify the correct expression of β1i using the AAV CMV_{enh}/MLC0.26 β1i vector construct. For this purpose, the abundance of β1i was analyzed on the mRNA and protein levels in HEK-293 cells after AAV2 CMV/MLC0.26 β1i infection. The AAV CMV/MLC0.26 β1i vector was packaged into AAV2 instead of AAV9 virus particles due to the higher infection efficiency of the former (O. Müller, personal communication).

The mRNA and protein abundance of β1i was increased 2.6-fold and 1.6-fold, respectively, 48 hours after infection of the HEK-293 cells using AAV2 CMV/MLC0.26 β1i at a MOI of 10^3 (Figure 12A, C). The infection efficiency of AAV2 virus particles was not analyzed at this stage.

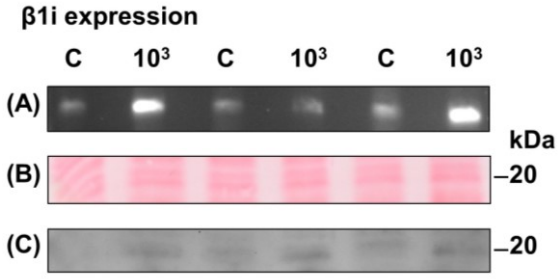

Figure 12. Analysis of β1i expression 48 hours post AAV2 CMV/MLC0.26 β1i infection of HEK-293 cells.

(A) Analysis of β1i mRNA expression 48 hours post infection of HEK-293 cells at a MOI of 10^3 as analyzed by semi-quantitative PCR. n=3.

(B) Ponceau S staining of the nitrocellulose membrane before Western blot shown in C.

(C) Analysis of β1i protein abundance 48 hours post infection of HEK-293 cells at a MOI of 10^3 as analyzed by β1i Western blot analysis. n=3.

4.3 Immunofluorescence analysis revealed increased β1i abundance in cardiomyocytes after AAV6 CMV/MLC0.26 β1i infection

Primary neonatal rat cardiomyocytes (NRCMs) were chosen to analyze β1i abundance in cardiomyocytes via immunofluorescence staining after AAV6 CMV/MLC0.26 β1i infection. The advantage of NRCMs as compared to HEK-293 cells was the higher degree of similarity to the *in vivo* conditions. The primary cells isolated from the hearts of neonatal rats were composed of cardiomyocytes and other cells (e.g. fibroblasts). Thus, the initial task was to identify the cardiomyocytes. Close to 80% of the cells were identified as cardiomyocytes according to α-actinin staining (Figure 13A). Infection efficiency was approximately 50% using AAV6 CMV/MLC0.26 EGFP at a MOI of 10^5 for 48 hours (Figure 13B). Moreover, the α-actinin staining of AAV6 CMV/MLC0.26 EGFP infected NRCMs revealed a rather specific infection of the cardiomyocytes using AAV6 virus particles (Figure 13B).

Due to the lower titer of vector genomes in the AAV6 CMV/MLC0.26 β1i batch, the MOI was lowered while the exposure time was simultaneously extended to 72 hours. Thus, β1i gene transfer was investigated by immunofluorescence analysis after infection of the NRCMs with AAV6 CMV/MLC0.26 β1i at a MOI of 10^4 for 72 hours. The number of β1i-positive cells was increased in AAV6 CMV/MLC0.26 β1i infected cells in relation to untreated cells. In the virus control, the number of β1i-positive cells was found to be increased after AAV6 CMV/MLC0.26 EGFP infection as compared to the untreated control cells (Figure 13C, E). This increase in β1i may be attributed to cellular stress due to strong EGFP overexpression suggesting that EGFP is an unsuitable control for *in vivo* gene transfer. AAV6 CMV/MLC0.26 β1i or EGFP infection did not influence expression of the proteasomal β1 subunit, the constitutive counterpart of β1i, in relation to the untreated cells (Figure 13D, E).

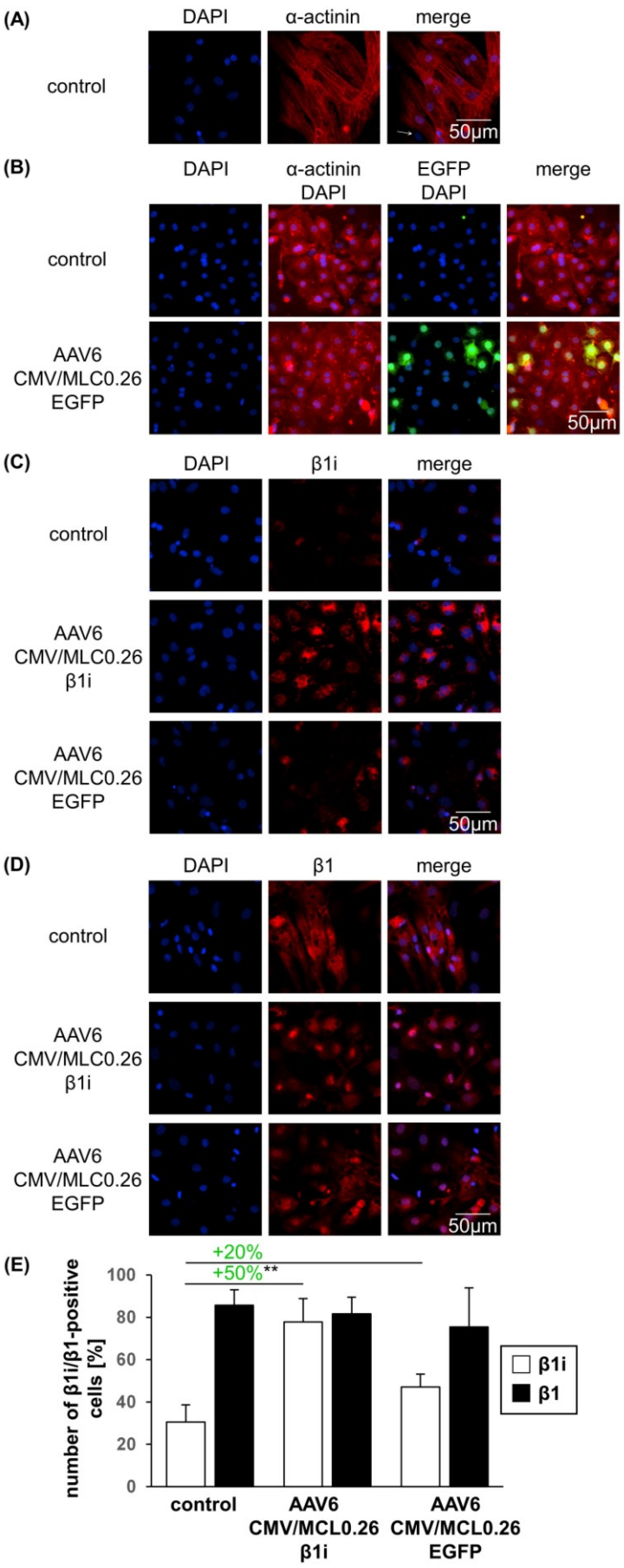

Figure 13. Increased β1i abundance in isolated cardiomyocytes after AAV6 CMV/MLC0.26 β1i infection of NRCMs.

(A) Representative image of NRCMs. Cardiomyocytes were stained by α-actinin staining. Other cells (e.g. fibroblast) are indicated by the arrow.

(B) Infection efficiency of the construct in cultured NRCMs was analyzed by using AAV6 CMV/MLC0.26 EGFP at a MOI of 10^5 for 48 hours. Cardiomyocytes were stained for α-actinin. n=3.

(C) Analysis of the number of β1i positive cells 72 hours after infection of NRCMs using AAV6 CMV/MLC0.26 β1i or EGFP at a MOI of 10^4. n=3.

(D) The number of β1-positive cells was analyzed 72 hours after infection of NRCMs using AAV6 CMV/MLC0.26 β1i or EGFP at a MOI of 10^4. n=3.

(E) Statistical analysis of the number of β1i (C) or β1 (D) positive cells 72 hours after infection of NRCMs using AAV6 CMV/MLC0.26 β1i or EGFP at a MOI of 10^4. Mean±SD. ** p<0.01 vs. control cells. n=3.

4.4 Reintroduction of β1i into β1i-deficient mice reduced cardiac remodeling and improved cardiac function following isoprenaline treatment

Initially, the correct expression of β1i after AAV9 CMV/MLC0.26 β1i (AAV β1i) injection (i.v.) into β1i knockout mice was analyzed in heart homogenates by Western blot analysis.

The proteasome subunit β1i was not detected in hearts of untreated β1i knockout mice (Figure 14). On the contrary, AAV9-based reintroduction of β1i into β1i-deficient animals was revealed by detection of β1i via Western blot analysis (Figure 14). In addition, two bands corresponding to β1i were observed in β1i knockout mice upon AAV β1i injection (Figure 14). The abundance of β1i in AAV β1i-injected β1i-deficient mice was similar as in untreated wild type animals (Figure 14). In contrast, abundance of β1i was increased following 7 days of isoprenaline treatment in AAV β1i-injected β1i knockout mice as compared to AAV β1i-treated β1i-deficient animals without exposure to a pro-hypertrophic stimulus (Figure 14).

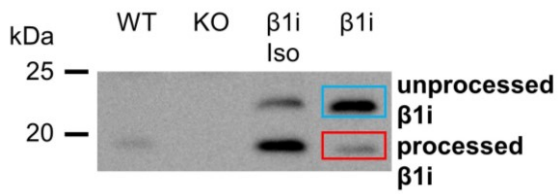

Figure 14. Successful β1i reintroduction into β1i knockout mice after AAV β1i injection.
The abundance of β1i (highlighted in blue and red) was analyzed by Western blot analysis in heart homogenates of untreated wild type (WT) or β1i knockout (KO) mice as well as in AAV β1i-injected β1i-deficient mice without (β1i) or with exposure to isoprenaline for 7 days (β1i Iso).

After demonstrating the functional expression of β1i using the AAV CMV_{enh}/MLC0.26 β1i vector construct, the effect of β1i reintroduction on the development of isoprenaline-induced cardiac hypertrophy was investigated in β1i-deficient mice. For this purpose, cardiac morphology and function was analyzed by echocardiography prior to and post induction of hypertrophy by isoprenaline treatment in AAV9 CMV/MLC0.26 β1i (AAV β1i) or AAV9 CMV/MLC0.26 luciferase (AAV Luci) injected β1i knockout mice.

Echocardiographic analysis of the cardiac morphology in the parasternal long axis view in M-mode indicated no significant differences between AAV β1i or AAV Luci-injected β1i-deficient mice prior to treatment with isoprenaline (Figure 15, 16; Table 1).

In contrast, echocardiographic analysis revealed an increase in left ventricular posterior wall thickness in diastole in AAV Luci and AAV β1i-injected mice indicating the development of cardiac hypertrophy in both groups after 7 days of isoprenaline treatment (Figure 16A). Notably, the increase in left ventricular posterior thickness in diastole was higher in AAV Luci

as compared to AAV β1i-injected β1i-deficient mice upon exposure to isoprenaline (Figure 16A).

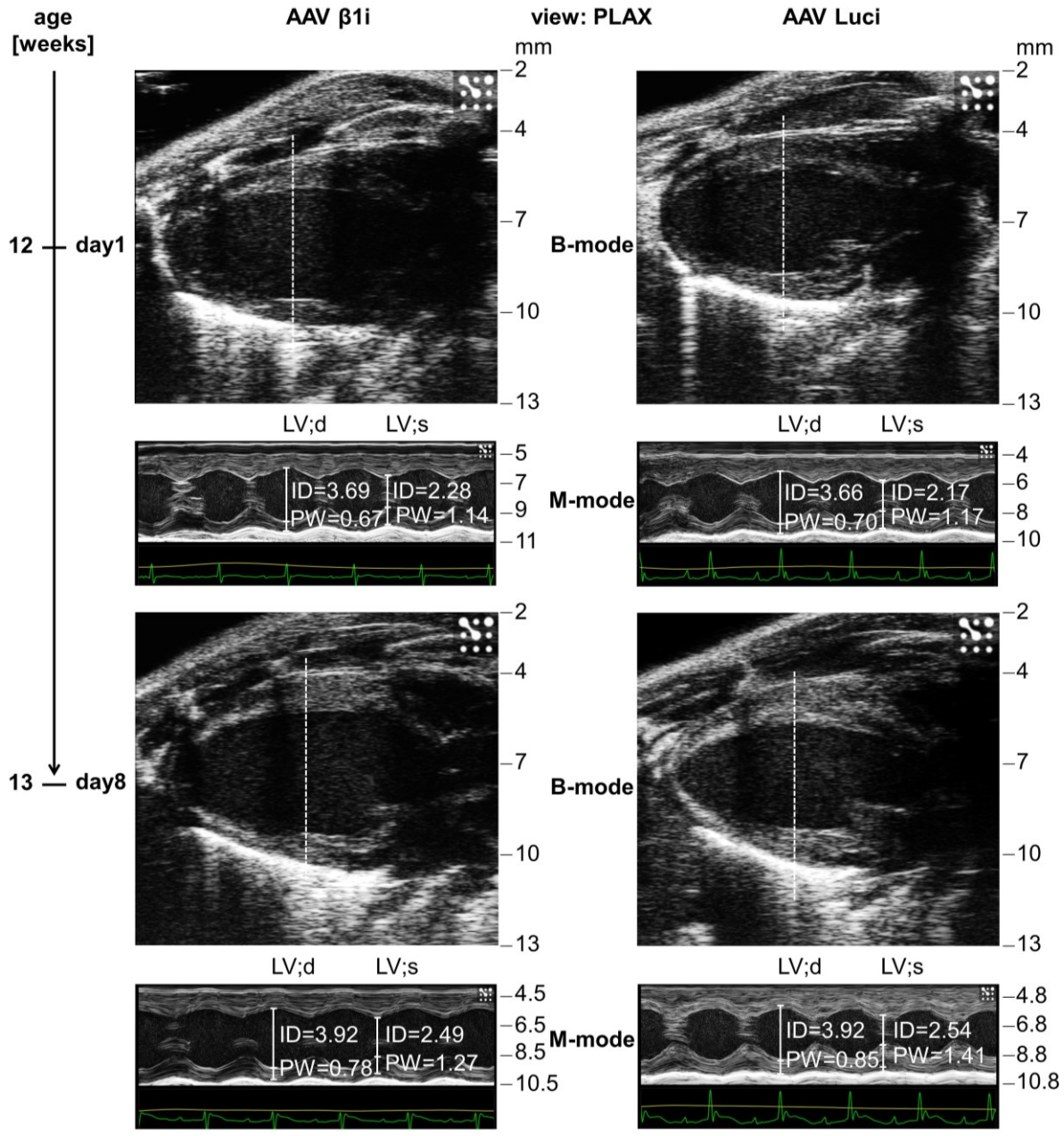

Figure 15. Representative echocardiographic images of the parasternal long axis (PLAX) view. Beta1i knockout mice treated with AAV β1i or AAV Luci were analyzed by echocardiography prior to (day 1) and post (day 8) induction of hypertrophy by isoprenaline treatment. Cardiac morphology and systolic function were investigated in B-mode and M-mode in the PLAX of the heart. Image in M-mode corresponds to the movement of the line displayed in B-mode over time. The corresponding ECG (green) and the respiration rate (yellow) is displayed below the M-mode images. The left ventricular internal diameter (LVID) and left ventricular posterior wall thickness (LVPW) in diastole and systole were measured in M-mode.

In addition, following treatment with isoprenaline left ventricular posterior wall thickness in systole was increased in AAV Luci as well as AAV β1i-injected β1i-deficient mice (Figure 16B). Similarly, the elevation of left ventricular posterior wall thickness in systole was higher in AAV Luci-treated control mice as compared to AAV β1i-injected β1i-deficient animals (Figure 16B). The analysis of left ventricular internal diameter in diastole upon exposure to isoprenaline revealed an increase in AAV Luci-injected control mice as well as in β1i-deficient mice into which β1i had been reintroduced (Figure 16C). In addition, following 7 days of isoprenaline treatment left ventricular internal diameter in systole was increased in AAV Luci and AAV β1i-injected β1i-deficient mice (Figure 16D). Notably, this increase was higher in the former (Figure 16D).

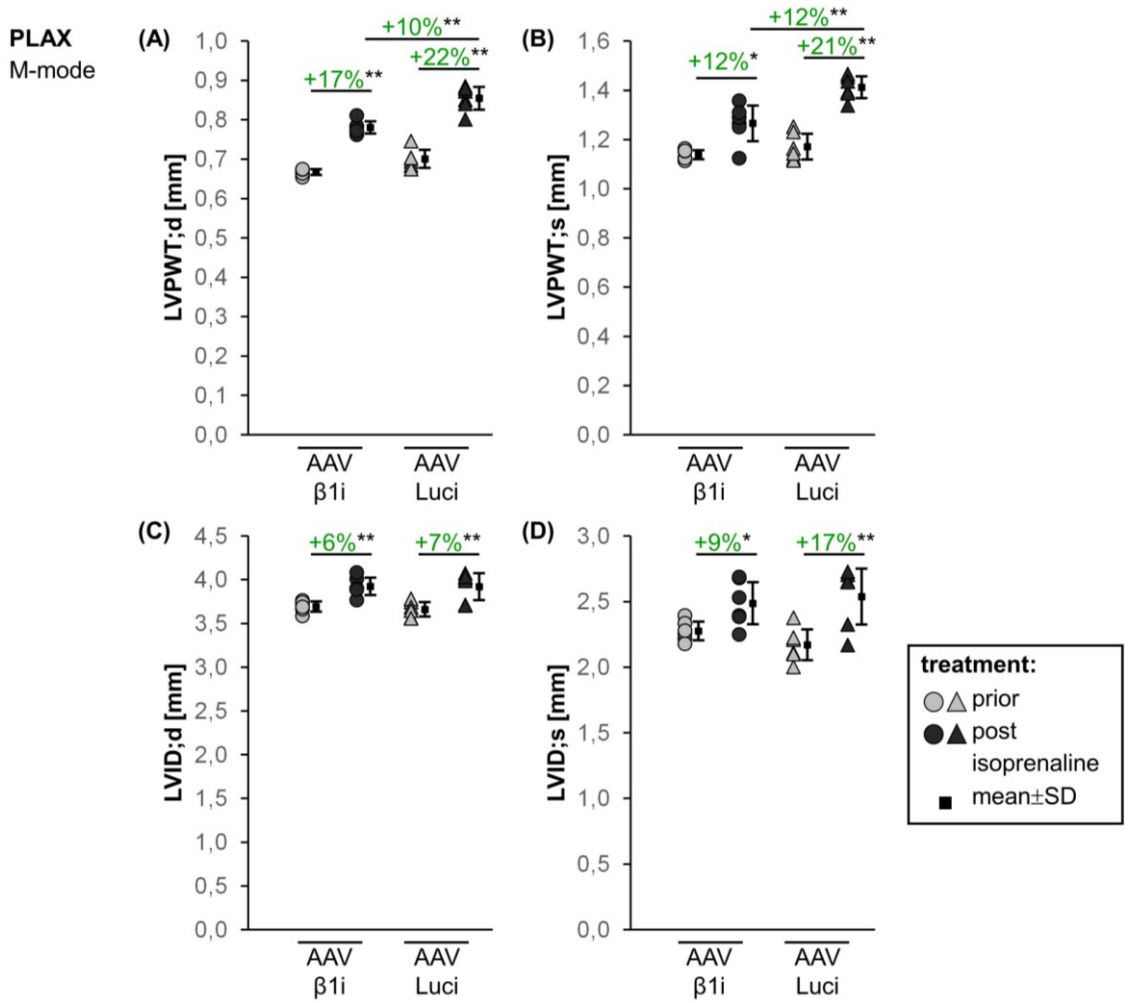

Figure 16. AAV9-based reintroduction of β1i in β1i-deficient mice attenuated the increase in left ventricular posterior wall thickness (LVPWT;d) following induction of hypertrophy.
Cardiac morphology (left ventricular posterior wall thickness (LVPWT) in diastole (LVPWT;d) **(A)** or systole (LVPWT;s) **(B)**, left ventricular internal diameter (LVID) in diastole (LVID;d) **(C)** or systole (LVID;s) **(D)**) was analyzed in parasternal long axis (PLAX) view in M-mode in AAV Luci or AAV β1i-injected β1i knockout mice prior to and post exposure to isoprenaline. * p<0.05, ** p<0.01. n=6.

The systolic function of the heart was analyzed in the parasternal long axis view in M-mode (Figure 17; Table 1). In accordance with the cardiac morphology, systolic function of AAV β1i and AAV Luci-injected β1i knockout mice was comparable prior to the initiation of isoprenaline treatment (Figure 17).

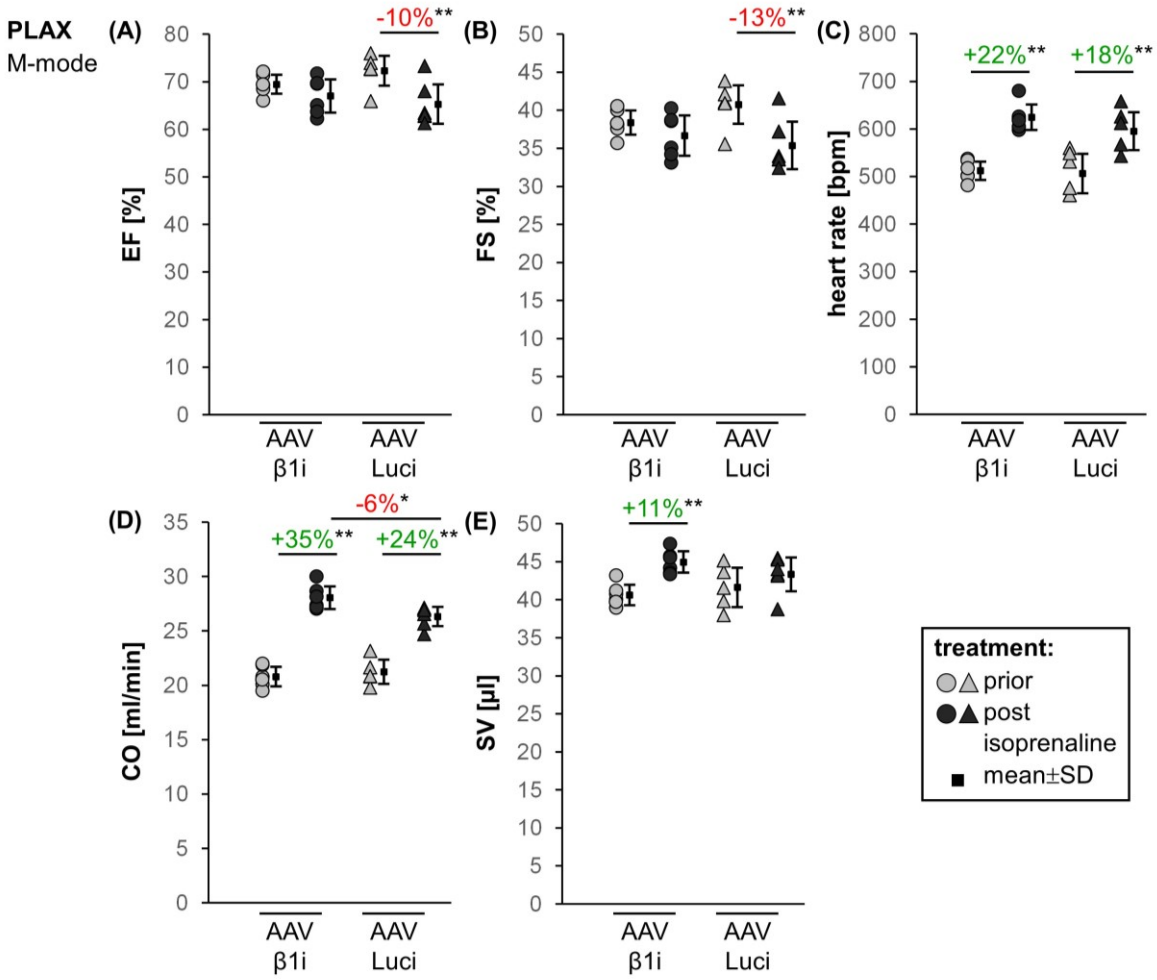

Figure 17. Systolic dysfunction was prevented by β1i reintroduction via AAV9 CMV/MLC0.26 β1i in β1i-deficient mice upon induction of hypertrophy.

Systolic function of the heart (ejection fraction (EF) **(A)**, fractional shortening (FS) **(B)**), cardiac output (CO) **(D)**, stroke volume (SV) **(E)**) was analyzed in parasternal long axis (PLAX) view in M-mode. In addition, the heart rate of AAV β1i or AAV Luci-injected β1i-deficient mice prior to and post isoprenaline treatment is indicated in **(C)**. * p<0.05, ** p<0.01. n=6.

Following isoprenaline treatment the analysis of the systolic function revealed a decrease of ejection fraction (Figure 17A) and fractional shortening (Figure 17B) in AAV Luci-injected mice indicating systolic dysfunction. On the contrary, systolic function upon exposure to isoprenaline was not altered after the reintroduction of β1i in β1i-deficient mice (Figure 17A, B). Due to the isoprenaline-dependent elevation of heart rate in AAV Luci as well as AAV β1i-treated mice

(Figure 17C), the ejected blood volume per minute (cardiac output) was increased in both groups albeit less in AAV Luci-treated mice (Figure 17D). The ejected blood volume during systole (stroke volume) was unchanged in AAV Luci-injected mice upon experimental hypertrophy (Figure 17E). In contrast, the stroke volume was increased following isoprenaline treatment in β1i-deficient mice into which β1i had been reintroduced (Figure 17E).

Furthermore, diastolic function was analyzed in the apical four chamber view using color and pulse wave Doppler mode (Figure 18, 19; Table 1).

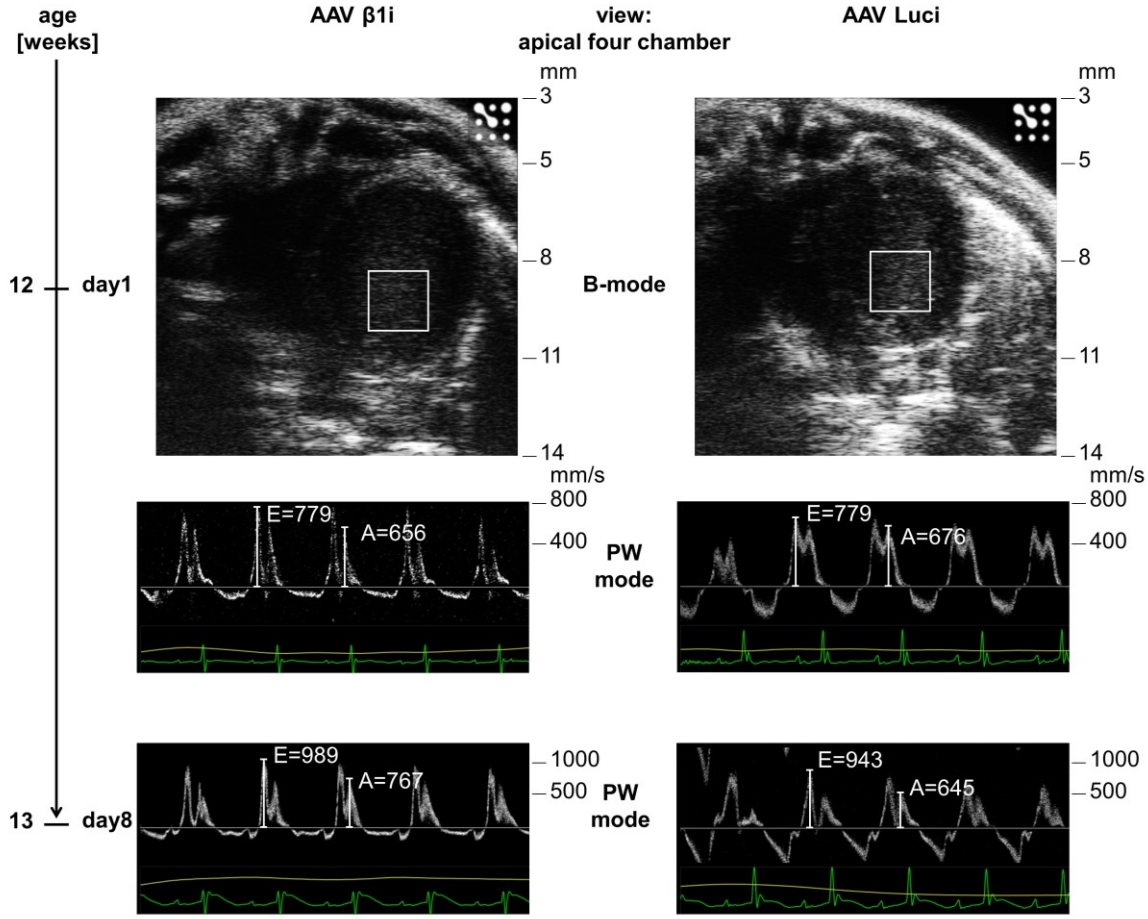

Figure 18. Representative echocardiographic images of the apical four chamber view.
Echocardiographic analysis of AAV β1i as well as AAV Luci-injected β1i-deficient mice was performed prior to (day 1) and post (day 8) exposure to isoprenaline. Diastolic function (E and A value) was analyzed using pulse wave (PW) Doppler mode in the apical four chamber view of the heart. For this purpose, the sample volume (square) was placed above the mitral valves. The corresponding ECG (green) and the respiration rate (yellow) is displayed in the M-mode images below.

Analysis of diastolic function indicated no significant differences between AAV β1i and AAV Luci-injected β1i-deficient mice prior to exposure to isoprenaline (Figure 18, 19).

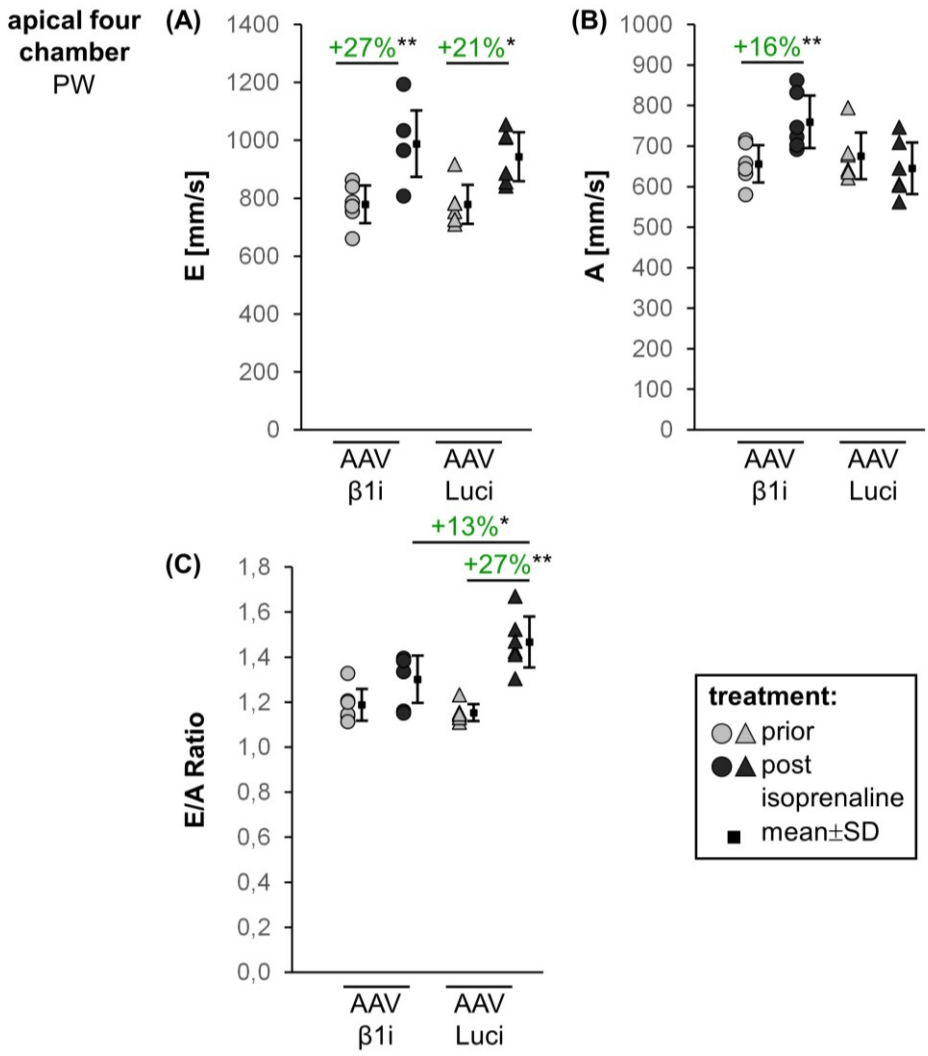

Figure 19. AAV9 based reintroduction of β1i in β1i knockout mice attenuated changes in the E/A ratio following exposure to a pro-hypertrophic stimulus.

Diastolic function (E value **(A)**, A value **(B)**, E/A ratio **(C)**) was analyzed in the apical four chamber view using pulse wave (PW) and color Doppler mode in AAV β1i or AAV Luci-injected β1i-deficient mice prior to and post exposure to isoprenaline. * $p<0.05$, ** $p<0.01$. n=6.

After induction of hypertrophy, the passive filling (E value) of the left ventricle was increased in both groups (Figure 19A). In contrast, upon isoprenaline treatment the active filling of the left ventricle during atrial systole (A value) was elevated in β1i-deficient mice into which β1i had been reintroduced, whereas this parameter was unchanged in AAV Luci-injected β1i knockout animals (Figure 19B). In consequence, the E/A ratio, commonly used as an indicator of diastolic function of the heart, was increased upon exposure to isoprenaline in AAV Luci-treated control mice (Figure 19C). In contrast, following induction of hypertrophy the E/A ratio remained at a level comparable to pretreatment values in β1i-deficient mice into which

β1i had been reintroduced (Figure 19C). Thus, after 7 days exposure to isoprenaline the increase in the E/A ratio was higher in AAV Luci-injected as compared to AAV β1i-treated β1i knockout mice (Figure 19C).

Table 1. Cardiac remodeling and function was improved by β1i reintroduction in β1i-deficient mice upon isoprenaline treatment.

	view	parameter	AAV β1i prior vs. post	AAV Luci prior vs. post
cardiac morphology	**PLAX** M-mode	LVPWT;d [mm]	↑	↑↑
		LVPWT;s [mm]	↑	↑↑
		LVID;d [mm]	↑	↑
		LVID;s [mm]	↑	↑
systolic function	**PLAX** M-mode	EF [%]	↔	↓
		FS [%]	↔	↓
		heart rate [bpm]	↑	↑
		CO [ml/min]	↑↑	↑
		SV [µl]	↑	↔
diastolic function	**apical four chamber** pulse wave	E [mm/s]	↑	↑
		A [mm/s]	↑	↔
		E/A ratio	↔	↑

Cardiac morphology and function of AAV β1i or AAV Luci-injected β1i knockout mice was analyzed prior to and post isoprenaline treatment. In the parasternal long axis (PLAX) view in M-mode, the cardiac morphology (left ventricular posterior wall thickness in diastole (LVPWT;d) or systole (LVPWT;s), left ventricular internal diameter (LVID) in diastole (LVID;d) or systole (LVID;s)) as well as the systolic function (ejection fraction (EF), fractional shortening (FS), cardiac output (CO), stroke volume (SV)) was analyzed. Moreover, the diastolic function (E value, A value, E/A ratio) was analyzed in the apical four chamber view using pulse wave and color Doppler mode.

4.5 Increased HW/BW ratio and cardiomyocyte cross-sectional area after isoprenaline treatment

The increase in left ventricular posterior wall thickness in diastole upon isoprenaline treatment was determined by echocardiographic analysis. Thus, the heart weight to body weight ratio (HW/BW ratio), an indicator of cardiac hypertrophy, was analyzed in AAV β1i or AAV Luci-injected and isoprenaline-treated β1i knockout mice. In addition, the cross-sectional area of cardiomyocytes was quantified in heart cryosections to determine cardiomyocyte size in these mice.

Notably, the HW/BW ratio was increased following 7 days of isoprenaline treatment in AAV Luci-injected mice as compared to AAV β1i-treated β1i-deficient animals (Figure 20).

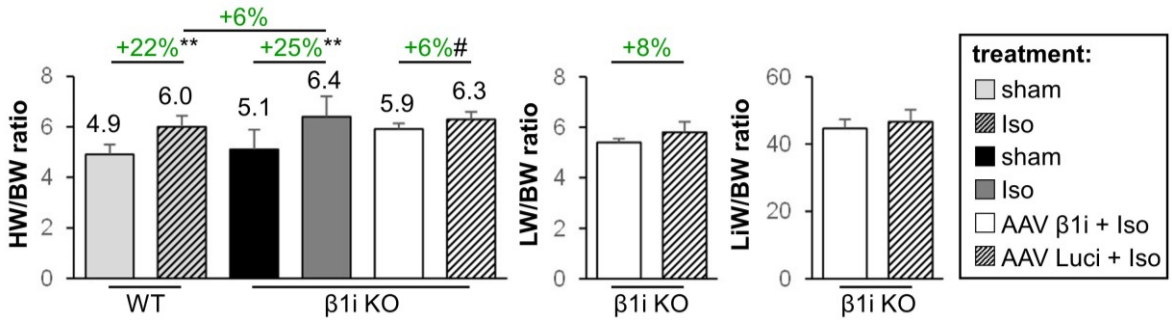

Figure 20. Attenuated isoprenaline-induced increase of the HW/BW ratio after β1i reintroduction.

The heart weight to body weight ratio (HW/BW ratio), lung weight to body weight ratio (LW/BW ratio) and liver weight to body weight ratio (LiW/BW ratio) was analyzed in AAV β1i or AAV Luci-injected β1i-deficient mice 7 days after starting the isoprenaline treatment. In addition, HW/BW ratios of the present study were compared to those in wild type (WT) and β1i knockout mice (β1i KO) performed by Lidia Gaal and Felix Trogisch, respectively. In these studies, the HW/BW ratio was analyzed following exposure to isoprenaline for 7 days or sham treatment in WT or β1i-deficient mice. Mean±SD. # $p=0.05$, ** $p<0.01$. n=6.

In order to evaluate the difference in the HW/BW ratio observed in the present study, present results were compared to those of parallel studies by our group performed by Lidia Gaal and Felix Trogisch. Following induction of hypertrophy by exposure to isoprenaline for 7 days the HW/BW ratio was increased in wild type mice as well as β1i knockout mice as compared to sham treated control animals (Figure 20). Moreover, the increase in HW/BW ratio was higher in β1i-deficient as compared to wild type mice following exposure to a pro-hypertrophic stimulus (Figure 20). Thus, the increase in the HW/BW ratio due to the reintroduction of β1i in β1i-deficient mice in the present study was comparable with the difference of the HW/BW ratio between wild type and β1i-deficient mice in parallel studies (Figure 20).

Moreover, the lung weight to body weight ratio (LW/BW ratio) and the liver weight to body weight ratio (LiW/BW ratio) was analyzed in the present study. The LW/BW ratio was greater after 7 days of isoprenaline treatment in AAV Luci as compared to AAV β1i-injected β1i knockout mice (Figure 20). In contrast, the LiW/BW ratio was not changed following induction of hypertrophy after the reintroduction of β1i in β1i-deficient mice as compared to AAV Luci-treated control mice (Figure 20).

The level of increase in HW/BW ratio matched those of the left ventricular posterior wall thickness in diastole in AAV Luci as well as AAV β1i-injected β1i-deficient mice (Figure 21).

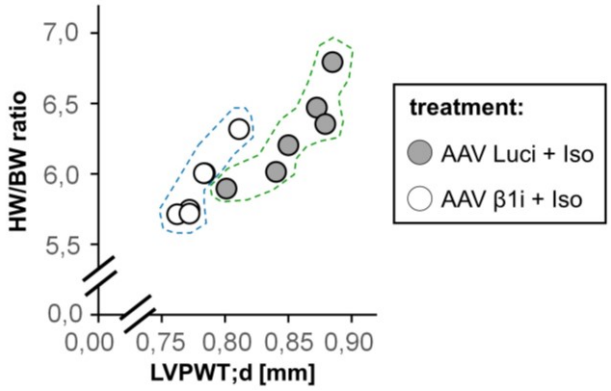

Figure 21. Association between heart weight to body weight ratio (HW/BW ratio) and left ventricular posterior wall thickness in diastole (LVPWT;d) after 7 days of isoprenaline treatment in AAV Luci-injected control mice as well as β1i-deficient animals into which β1i had been reintroduced.

The cross-sectional area of cardiomyocytes was quantified in hematoxylin and eosin (HE) stained heart cryosections.

According to analyses of a limited number of samples (n=1-2), the AAV9-based reintroduction of β1i into β1i knockout mice had no effect on cardiomyocyte size as compared to untreated β1i-deficient mice (Figure 22). On the contrary, cross-sectional area seemed to be increased after 7 days exposure to isoprenaline in AAV β1i-injected β1i knockout mice (Figure 22). Similarly, analysis of the cross-sectional area seemed to reveal an increase upon induction of hypertrophy in AAV Luci-injected β1i-deficient mice (Figure 22).

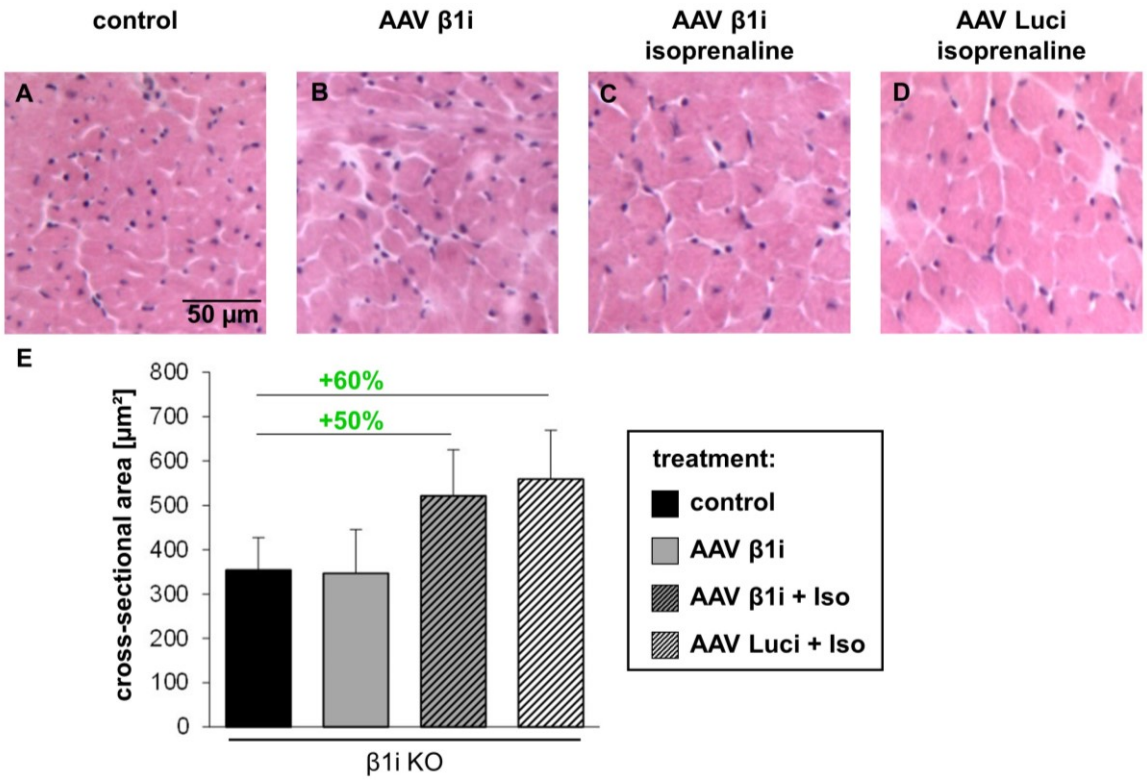

Figure 22. Isoprenaline treatment potentially induced an increase in the cardiomyocyte size in AAV β1i and AAV Luci-injected β1i knockout (β1i KO) mice.

Heart cryosections (base of the heart) of untreated β1i knockout mice (**A**, n=1), AAV β1i-injected β1i-deficient mice (**B**, n=2) as well as AAV β1i (**C**, n=2) or AAV Luci-injected (**D**, n=1) and isoprenaline-treated (7 days) β1i knockout mice were hematoxylin and eosin (HE) stained. The cross-sectional area was measured using ImageJ software in 15 areas of 3 cryosections per heart **(E)**. Statistical analysis was not performed due to limited number of samples. Mean±SD.

4.6 Areas with an increased myocardial collagen content were not observed after β1i reintroduction prior to hypertrophy induction in β1i knockout mice

Heart cryosections were stained with Masson's trichrome to analyze the myocardial collagen content after AAV injection and induction of hypertrophy in β1i knockout mice.

According to analyses of a limited number of samples (n=1-2), areas with an increased myocardial collagen content were neither observed in hearts of untreated or AAV β1i-injected β1i-deficient mice (Figure 23E, F) nor identified in hearts of β1i-deficient mice into which β1i had been reintroduced following exposure to isoprenaline (Figure 23G). In contrast, approximately one quarter of the tissue showed intrafibrillar blue staining indicating collagen following exposure to a pro-hypertrophic stimulus in AAV Luci-injected control mice (Figure 23H).

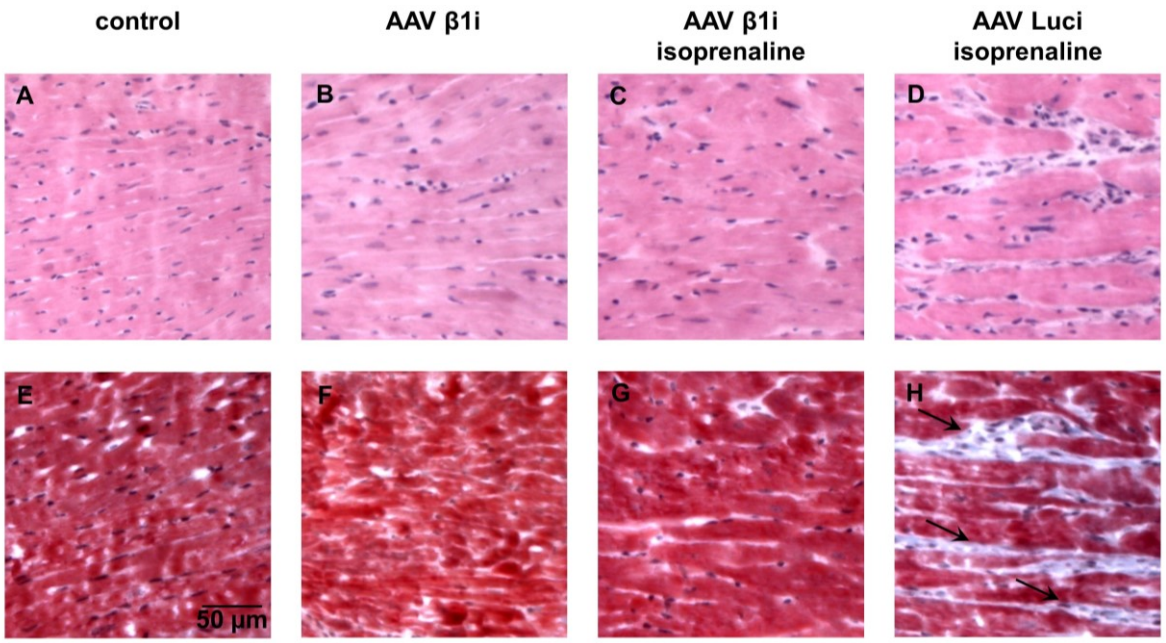

Figure 23. Reintroduction of β1i in β1i-deficient mice potentially prevents the formation of areas with an increased myocardial collagen content upon induction of hypertrophy

Hematoxylin and eosin (HE) stained heart cryosections (base of the heart) of untreated β1i-deficient mice (**A**, n=1), AAV β1i injected β1i knockout mice (**B**, n=2) as well as AAV β1i (**C**, n=2) or AAV Luci-injected (**D**, n=1) and 7 days to isoprenaline exposed β1i-deficient mice. Sections of the same samples were stained with Masson's Trichrome (**E-H**). Collagen is stained in blue. Areas with an increased myocardial collagen content are indicated by arrows (approximately 25% in **H**).

4.7 Beta1i or *Renilla* luciferase was expressed in the hearts after AAV injection

Cardiac function and left ventricular posterior wall thickness was modified after 7 days of isoprenaline treatment by reintroduction of β1i into β1i-deficient mice as compared to AAV Luci-injected control mice. In a subsequent step, potential regulation on the proteasomal level was investigated in this context. Initially, successful cardiac gene delivery via serotype 9 of adeno-associated viruses was analyzed on the protein level by Western blot analysis.

Renilla luciferase was not detected in untreated wild type or AAV β1i-injected and isoprenaline-treated β1i knockout mice (Figure 24A). In contrast, *Renilla* luciferase abundance was demonstrated after injection of AAV Luci in hypertrophic hearts of β1i-deficient mice (Figure 24A).

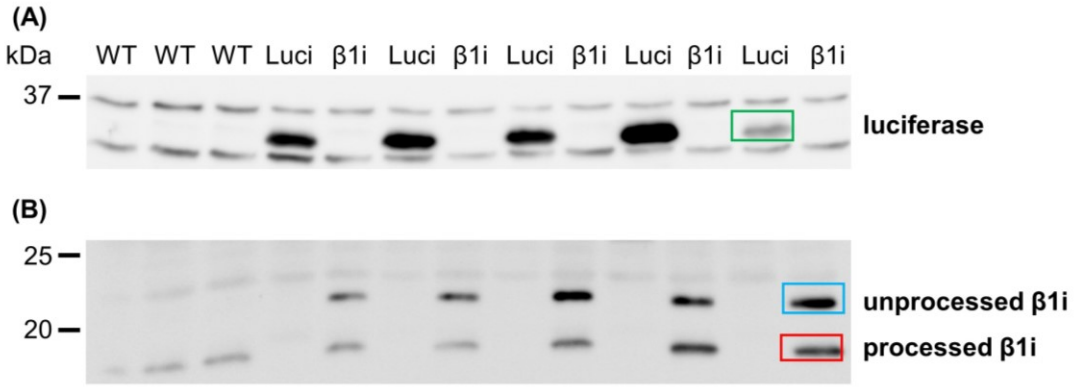

Figure 24. Beta1i and *Renilla* luciferase was detected after AAV β1i and AAV Luci injection, respectively, in hypertrophic hearts of β1i-deficient mice.

Heart homogenates (soluble fraction) of untreated wild type mice (WT) as well as AAV β1i (β1i) or AAV Luci-injected (Luci) and isoprenaline-treated (7 days) β1i knockout mice were analyzed for the abundance of *Renilla* luciferase (highlighted in green) **(A)** or β1i (highlighted in blue, red) **(B).**

In addition, β1i was detected in untreated wild type mice. In contrast, detection of β1i in AAV Luci and isoprenaline-treated β1i knockout mice was negative (Figure 24B). In accordance with previous results (Figure 14), β1i abundance was demonstrated in hypertrophic hearts of β1i-deficient mice upon AAV9-based reintroduction of β1i (Figure 24B). Moreover, two bands corresponding to β1i were detected in AAV β1i-injected β1i-deficient mice following 7 days of isoprenaline treatment while one band was observed in untreated wild type mice (Figure 24B). Notably, Western blot analysis indicated an inhomogeneous abundance of *Renilla* luciferase and β1i in hypertrophic hearts of AAV Luci and AAV β1i- injected β1i-deficient mice, respectively (Figure 24A, B).

In addition to the analysis of protein abundance, luciferase activity was analyzed using a *Renilla* luciferase activity assay to demonstrate the correct formation of the three dimensional structure of the protein.

Renilla luciferase activity was detected in all hypertrophic hearts of AAV Luci-injected β1i-deficient mice (Figure 25). Thus, the three dimensional structure of the protein was correctly formed. Notably, *Renilla* luciferase activity was inhomogeneous among the different samples of AAV Luci and isoprenaline-treated β1i knockout mice (Figure 25).

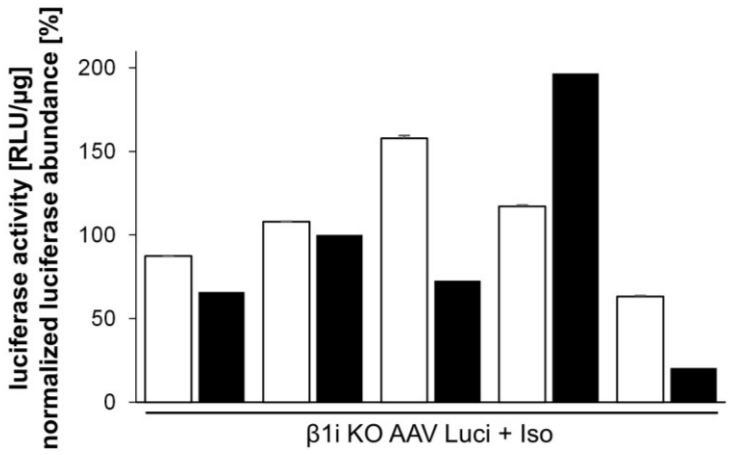

Figure 25. Detected *Renilla* luciferase activity revealed the expression of a correctly folded protein upon AAV9-based introduction of *Renilla* luciferase in β1i-deficient mice.
Following continuous exposure to isoprenaline (7 days) *Renilla* luciferase activity (indicated in white) in heart crude extracts of AAV Luci-injected β1i knockout mice was measured in triplicates. Mean±SD. The *Renilla* luciferase abundance (indicated in black) in heart homogenates (soluble fraction) of the same samples analyzed by Western blot analysis was normalized to Ponceau staining.

4.8 Neither 26S nor 20S proteasome activities were significantly changed by β1i reintroduction into β1i-deficient mice prior to induction of hypertrophy

The abundance of β1i in hypertrophic hearts was verified in AAV β1i-injected β1i knockout mice by Western blot analysis. In a subsequent step, the incorporation of the reintroduced β1i into active proteasome complexes was investigated using the activity based probe MVB003. Moreover, the effect of β1i incorporation into active proteasome complexes on proteasomal activity was analyzed using proteasome activity assays.

Active site labeling of heart homogenates using MVB003 revealed the incorporation of constitutive (β1, β2, β5) as well as inducible (β2i, β5i) proteolytic β subunits in proteasome complexes of hypertrophic hearts (Figure 26A). Moreover, an additional band presumably corresponding to β1i was detected in AAV β1i-injected as compared to AAV Luci-treated β1i-deficient mice following 7 days of isoprenaline treatment (Figure 26A).

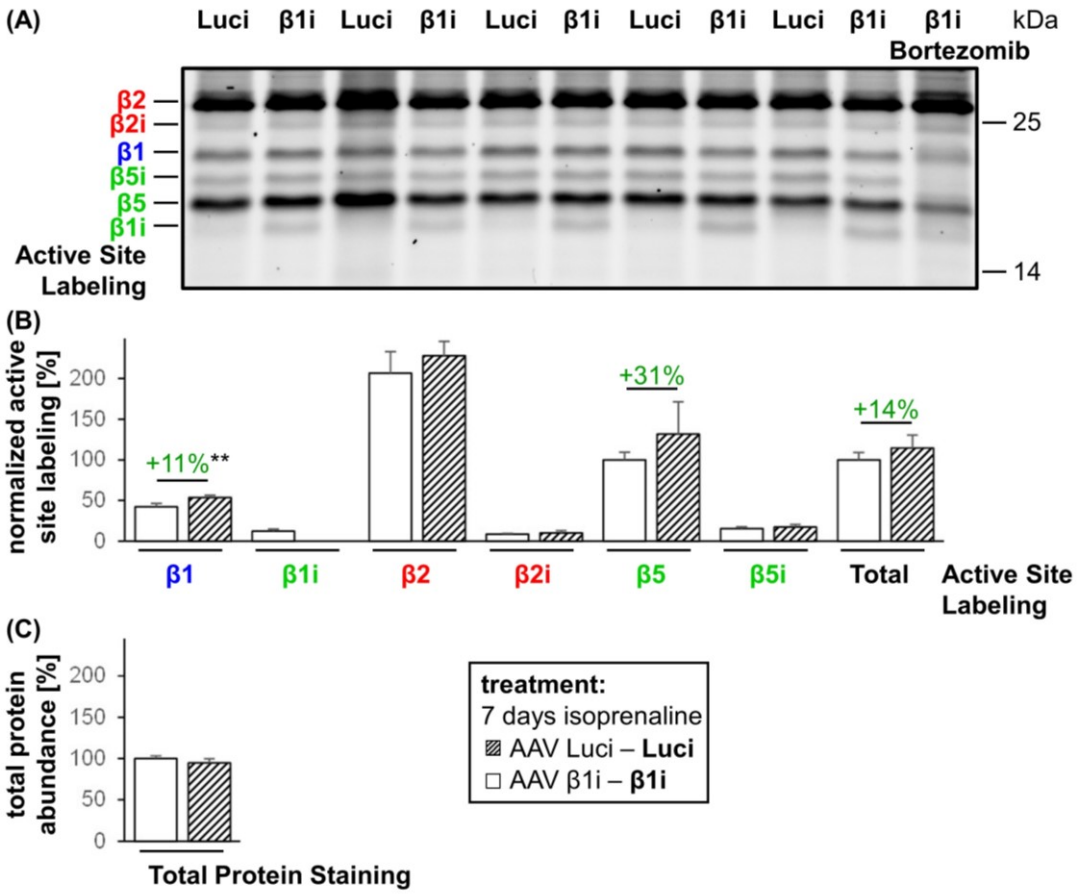

Figure 26. Beta1i was incorporated into active proteasome complexes.

(A) Proteasome active sites were labeled by MVB003 in heart homogenates of AAV β1i or AAV Luci-injected and isoprenaline-treated (7 days) β1i-deficient mice. The proteasome was inhibited using bortezomib prior to active site labeling in one of the samples to identify proteolytic β-subunits via a competitive assay. Proteasome subunits were designated according to previous publication (Florea et al. 2010). **(B)** The active site labeling was quantified and normalized by total protein staining using ruthenium **(C)**. Mean±SD. ** $p<0.01$. n=5.

In addition, the active site labeling was quantified and normalized by total protein staining using ruthenium (Figure 26B, C). The analysis indicated an increase in the incorporation of β1 subunits into proteasome complexes in AAV Luci as compared to AAV β1i-injected β1i-deficient mice upon exposure to isoprenaline (Figure 26B). Moreover, the incorporation of β5 subunits into proteasome complexes seemed elevated in AAV Luci as compared to AAV β1i-injected β1i knockout mice (Figure 26B). Notably, this elevation as well as the increase in the total incorporation of proteolytic subunits into proteasome complexes was not significant in AAV Luci as compared to AAV β1i-injected β1i-deficient mice following exposure to a pro-hypertrophic stimulus (Figure 26B).

In a subsequent step, the effect of β1i incorporation into proteasome complexes on proteasomal activity of hypertrophic hearts was analyzed by proteasome activity assays using heart homogenates.

None of the 26S or 20S proteasome activities were significantly changed in AAV β1i as compared to AAV Luci-injected β1i knockout mice following continuous exposure to isoprenaline (7 days) (Figure 27). Still, the 26S caspase-like activity and the 20S caspase-like activity seemed increased in AAV Luci-injected control mice as compared to β1i-deficient mice into which β1i had been reintroduced upon treatment with isoprenaline (Figure 27).

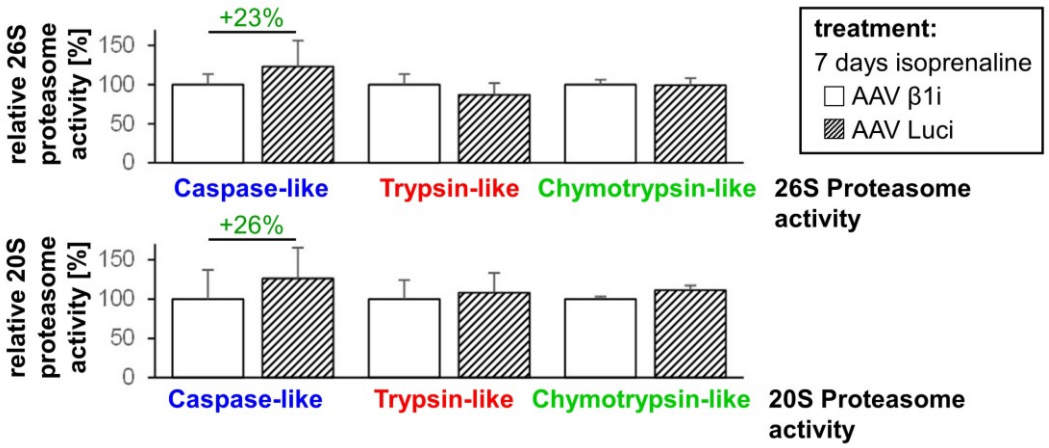

Figure 27. Beta1i reintroduction did not significantly change 26S and 20S proteasome activities in hypertrophic hearts of β1i-deficient mice.

Following exposure to isoprenaline for 7 days the proteasome activities were analyzed in heart homogenates of AAV β1i or AAV Luci-injected β1i knockout mice. Non-proteasomal activities, measured in the presence of specific proteasome inhibitors, were excluded from the figure. Mean±SD. n=5.

4.9 The abundance of other proteasome subunits than β1i was not significantly changed by reintroduction of β1i into hearts of β1i-deficient mice prior to induction of hypertrophy

The abundance of proteasome subunits was analyzed in heart homogenates of AAV β1i or AAV Luci-injected and isoprenaline-treated (7 days) β1i knockout mice to investigate the potential influence of reintroduction of β1i on the abundance of other proteolytic and structural proteasome subunits.

The abundance of structural subunits α7 and Rpt4 was not changed in hypertrophic hearts upon reintroduction of β1i in β1i-deficient mice as compared to AAV Luci-injected control animals (Figure 28). In contrast, the abundance of proteolytic subunits β1, β2, β5 and β5i

seemed higher in AAV Luci as compared to AAV β1i-injected β1i-deficient mice upon exposure to isoprenaline (Figure 28). This increase was not significant given the large SD (Figure 28).

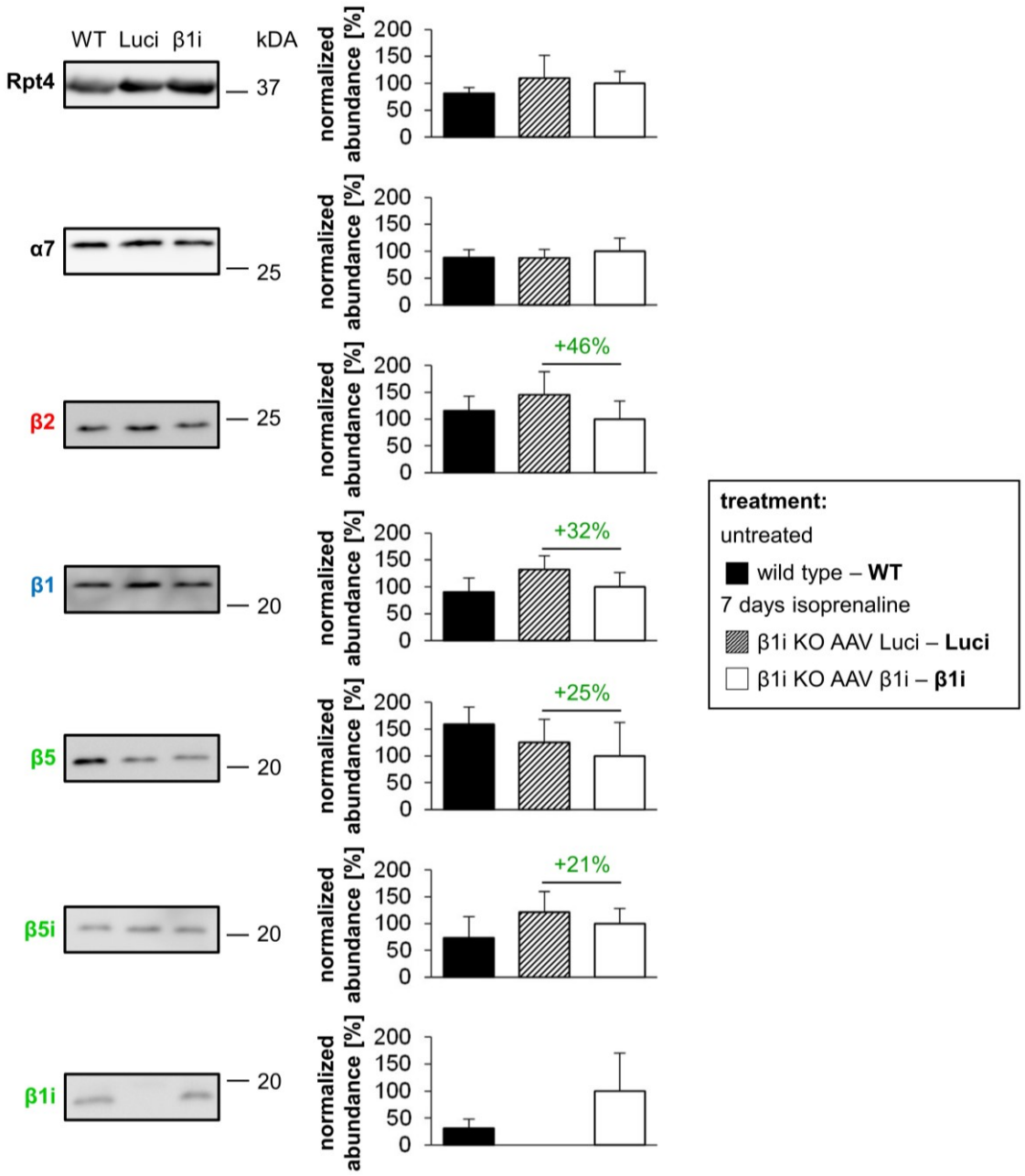

Figure 28. The abundance of other proteolytic and structural proteasome subunits than β1i was not significantly altered in hypertrophic hearts of β1i-deficient mice with prior reintroduction of β1i as compared to AAV Luci-injected control mice.

The abundance of structural subunits (α7, Rpt4) as well as proteolytic β-subunits (β1, β1i, β2, β5, β5i) normalized to Ponceau S staining was analyzed in heart homogenates by Western blot analysis in AAV β1i or AAV Luci-injected and isoprenaline-treated (7 days) β1i-deficient mice (n=5) and untreated wild type mice (n=3). Mean±SD.

The abundance of *Renilla* luciferase in AAV Luci-injected and isoprenaline-treated β1i knockout mice seemed not to be associated with the abundance of proteolytic (β1, β2, β5, β5i) or structural (Rpt4) proteasome subunits. In contrast, the abundance of α7 seemed to be increasing with increasing abundance of *Renilla* luciferase in AAV Luci-treated control mice following exposure to isoprenaline. In addition, the abundance of reintroduced β1i in AAV β1i-injected β1i knockout mice seemed to be associated with the abundance of β1 and β2. Following induction of hypertrophy, β1 and β2 abundance was lowest when abundance of β1i was highest in AAV β1i-injected β1i-deficient mice.

In addition, the abundance of proteasome subunits in hypertrophic hearts of AAV β1i or AAV Luci-injected β1i knockout mice was compared to untreated hearts of wild type mice to initially evaluate the potential effects of AAV β1i or AAV Luci injection and exposure to isoprenaline on proteasome subunit abundance.

The abundance of the structural subunit α7 was not changed in untreated wild type mice as compared to AAV-injected and isoprenaline-treated β1i knockout animals (Figure 28). Due to the large SD, the abundance of β1, β2, β5, β5i and Rpt4 was not significantly modified in hearts of untreated wild type mice as compared to hypertrophic hearts of AAV-injected β1i-deficient animals (Figure 28). The abundance of β1, β2, β5i and Rpt4 was higher while the abundance of β5 was lower in AAV Luci-injected and 7 days to isoprenaline exposed β1i knockout mice as compared to untreated wild type animals (Figure 28). Moreover, the abundance of β1, β5i and Rpt4 was elevated to a lower extent while the abundance of β2 and β5i was reduced to a higher extent in hypertrophic hearts of AAV β1i injected β1i-deficient mice as compared to hearts of untreated wild type mice (Figure 28).

4.10 The abundance of sarcomeric proteins was not significantly altered in hypertrophic hearts of β1i-defcient mice with prior β1i reintroduction

In a subsequent step, the influence of reintroduction of β1i on the abundance of sarcomeric proteins, which are reported targets of proteasomal degradation, was investigated. For this purpose, the abundance of sarcomeric proteins was analyzed in heart crude extracts or heart homogenates of AAV β1i or AAV Luci-injected and isoprenaline-treated β1i knockout mice.

The abundance of sarcomeric proteins actin, β-myosin heavy chain (β-MHC), ventricular myosin light chain 2 (MLC2v), α-tubulin, α-actinin and desmin were not altered in hypertrophic hearts of β1i-deficient mice into which β1i was reintroduced as compared to AAV Luci-injected β1i control animals (Figure 29). In contrast, the abundance of troponin I seemed lower in AAV Luci as compared to AAV β1i-injected β1i knockout mice following 7 days of isoprenaline treatment (Figure 29).

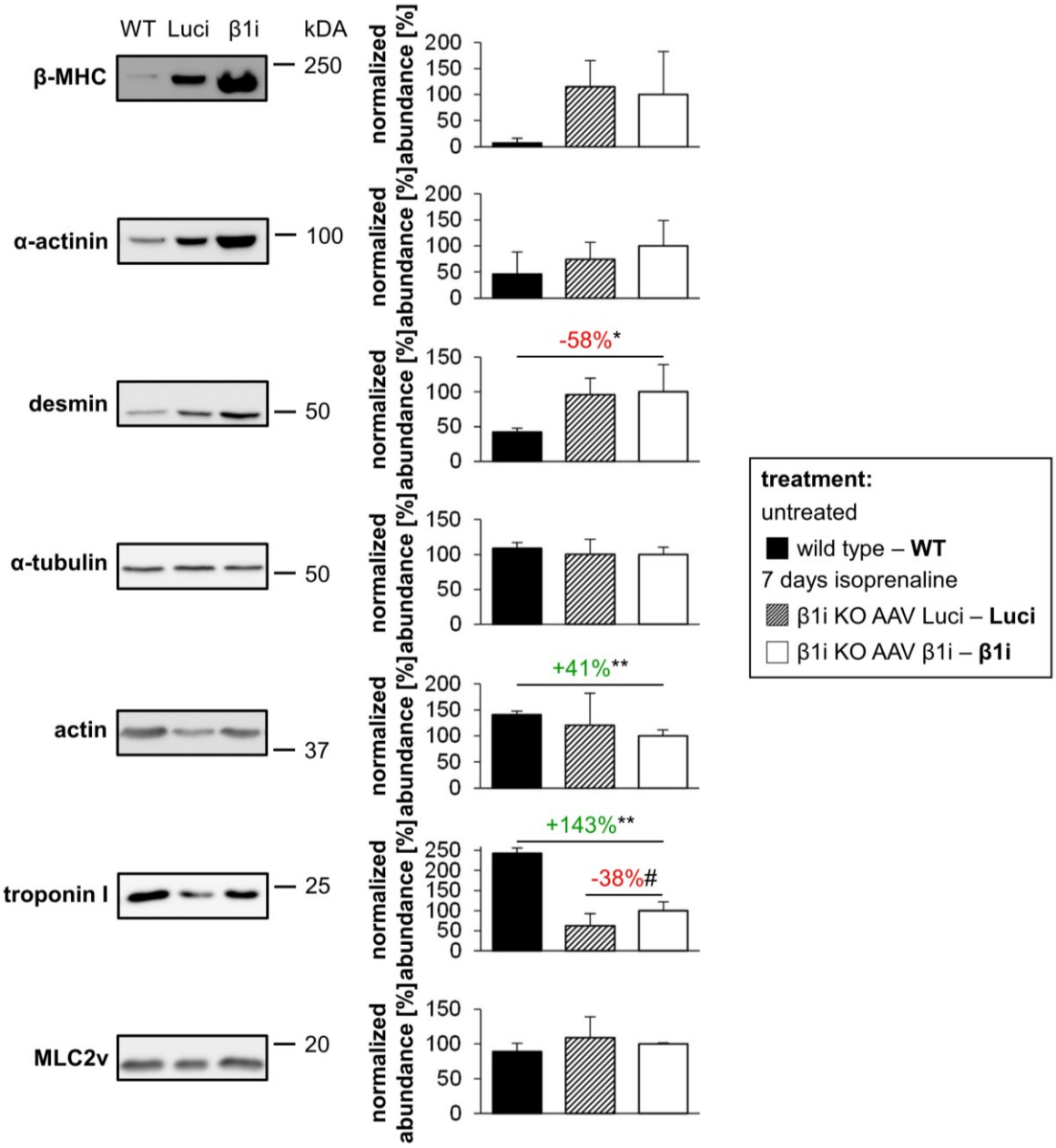

Figure 29. The abundance of sarcomeric proteins was not significantly altered in β1i knockout mice with β1i reintroduction prior to isoprenaline treatment.

The abundance of sarcomeric proteins β-myosin heavy chain (β-MHC) and α-actinin as well as desmin, α-tubulin, actin, troponin I and ventricular myosin light chain 2 (MLC2v=) normalized to Ponceau S staining was analyzed in AAV β1i or AAV Luci-injected and 7 days to isoprenaline exposed β1i-deficient mice (n=5) and in untreated wild type mice (n=3) by Western blot analysis. The former was investigated in heart crude extracts while the latter was analyzed in heart homogenates (soluble fraction). Mean±SD. # p=0.08, * p<0.05, ** p<0.01.

Moreover, the potential influence of isoprenaline treatment and AAV infection on the abundance of sarcomeric proteins was initially investigated by the analysis of these proteins in hypertrophic hearts of AAV-injected β1i-deficient mice as compared to untreated wild type mice.

The abundance of MLC2v and α-tubulin was not altered in untreated wild type mice as compared to AAV β1i or AAV Luci-injected and isoprenaline-treated β1i knockout mice (Figure 29). In contrast, the abundance of β-MHC, α-actinin and desmin was decreased in untreated wild type mice as compared to AAV β1i-injected β1i-deficient mice following exposure to isoprenaline (Figure 29). However, this decrease, with the exception of desmin, was not significant due to the large SD. Moreover, the analysis revealed an increase of the abundance of actin and troponin I in untreated wild type mice as compared to AAV β1i and isoprenaline-treated β1i knockout mice (Figure 29).

4.11 Desmin localization was not modified by induction of hypertrophy in hearts of β1i-deficient mice receiving gene transfer

Desmin was analyzed in heart cryosections of untreated, AAV β1i-treated as well as AAV β1i or AAV Luci-injected and 7 days to isoprenaline exposed β1i knockout mice by immunofluorescence staining to investigate whether the localization of desmin within cardiomyocytes was altered in a disease-dependent manner.

According to analyses of a limited number of samples (n=1-2), desmin seemed to be located in Z-disks and intercalated disks in hearts of untreated or AAV β1i-injected β1i knockout mice (Figure 30A, B). Moreover, the localization seemed not to be modified upon induction of hypertrophy in AAV β1i or AAV Luci-treated β1i-deficient mice (Figure 30C, D). However, the analysis suggested a higher increase of the desmin fluorescence intensity in AAV β1i versus AAV Luci-injected β1i knockout mice following 7 days of isoprenaline treatment as compared to untreated animals (Figure 30E).

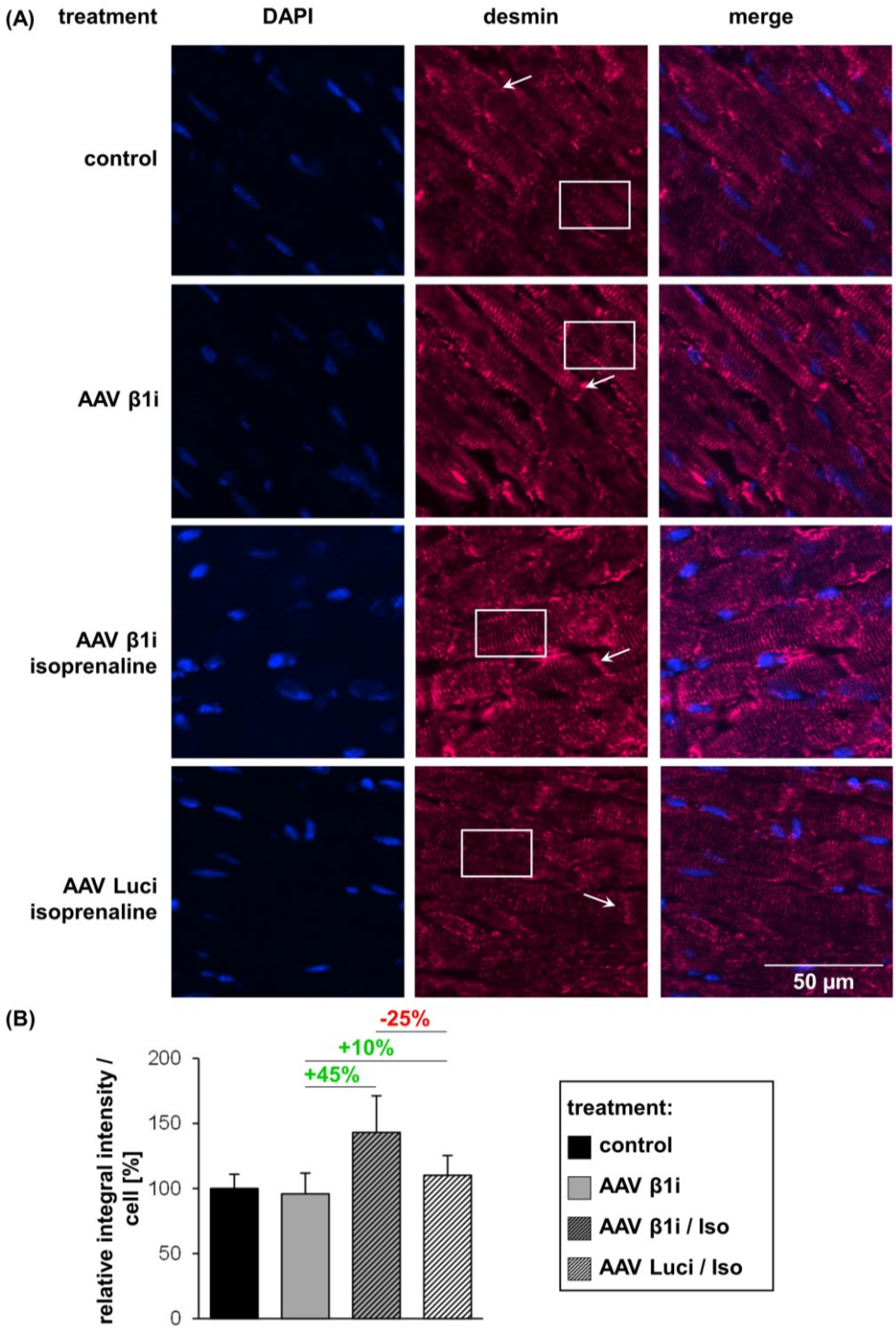

Figure 30. Desmin localization seemed to be unchanged by induction of hypertrophy in hearts of β1i knockout mice receiving gene transfer.

Heart cryosections (base of the heart) of untreated β1i knockout mice (**A**, n=1), AAV β1i-injected β1i-deficient mice (**B**, n=2) as well as AAV β1i (**C**, n=2) or AAV Luci-injected (**D**, n=1) and isoprenaline-treated (7 days) β1i knockout mice were analyzed for desmin abundance and localization by immunofluorescence analysis. Localization of desmin in Z-disks and intercalated disks is visualized by rectangles and arrows, respectively. The desmin fluorescence intensity per cell was analyzed in 15 areas of 3 cryosections per sample using Olympus Xcellence software **(E)**. Statistical analysis was not performed due to limited number of samples. Mean±SD.

4.12 Heart weight to body weight ratio was not significantly altered in aged as compared to young mice

In collaboration with Dr. Kleinbongard (Dept. of Pathophysiology, University Hospital Essen), age-related alterations of the cardiac proteome and proteasome system were analyzed in 4 versus 26 months old mice as well as in 3, 9 and 30 months old animals. Notably, the health status of the old (26 and 30 months old) mice was different (communicated by Dr. Kleinbongard, Dept. of Pathophysiology, University Hospital Essen). The 26 months old mice were sacrificed due to visible signs of distress, suggesting a poor health condition. In contrast, the 30 month group showed no visible signs of distress. Furthermore, cardiac function of the 3, 9 and 30 months old mice was analyzed by echocardiography through our collaborators (data not shown). Accordingly to this data, hearts of the 30 months old animals did not show pathological abnormalities.

Initially, the heart weight (HW) and the heart weight to body weight ratio (HW/BW ratio) of differentially aged mice were analyzed by our collaborators.

The HW and HW/BW ratio were not significantly altered in old (26 and 30 months old) mice as compared to young (4 and 3 months old) animals (Figure 31A, B).

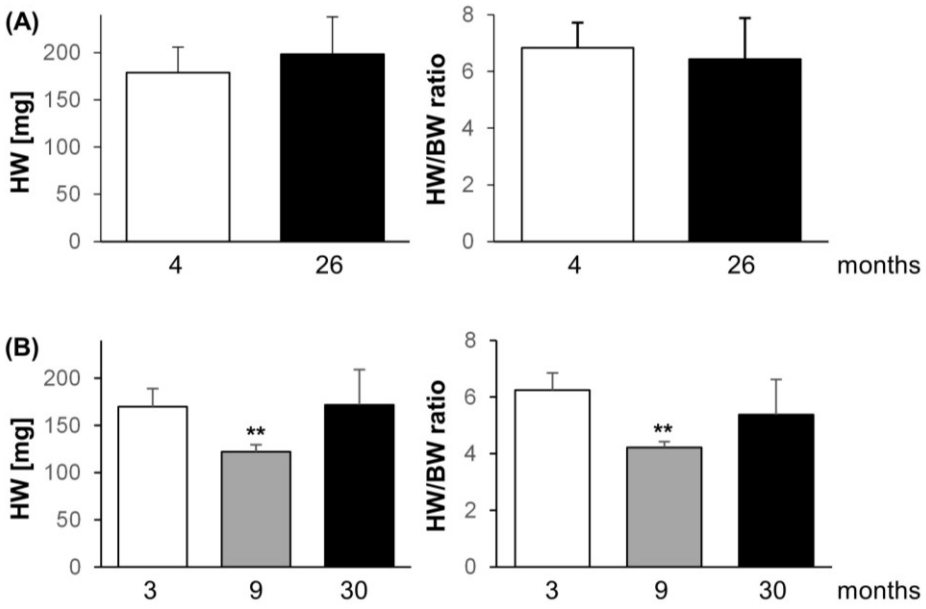

Figure 31. The heart weight (HW) and heart weight to body weight ratio (HW/BW ratio) were not different in aged as compared to young wild type mice.

The HW and HW/BW ratio was analyzed in 4 and 26 months old mice (n=5) **(A)** as well as in 3, 9 and 30 months old animals (n=5-6) **(B)**. Mean±SD. ** $p<0.01$ versus 3 months old animals.

In contrast, the HW and HW/BW ratio were decreased in 9 versus 3 months old mice (Figure 31B). The HW as well as BW data were kindly provided by our collaborators (Dr. Kleinbongard, Dept. of Pathophysiology, University Hospital Essen).

4.13 Increased 26S proteasome activities in aged hearts

Cardiac 20S and 26S proteasome activities were analyzed in heart homogenates from 4 versus 26 months old mice and 3, 9 and 30 months old animals.

Cardiac 20S proteasome activities were not significantly increased in 4 as compared to 26 months old mice (Figure 32). Comparing the heart homogenates from 3, 9 and 30 months old mice, the caspase-, trypsin- and chymotrypsin-like 20S proteasome activities were likewise unaltered (Figure 33).

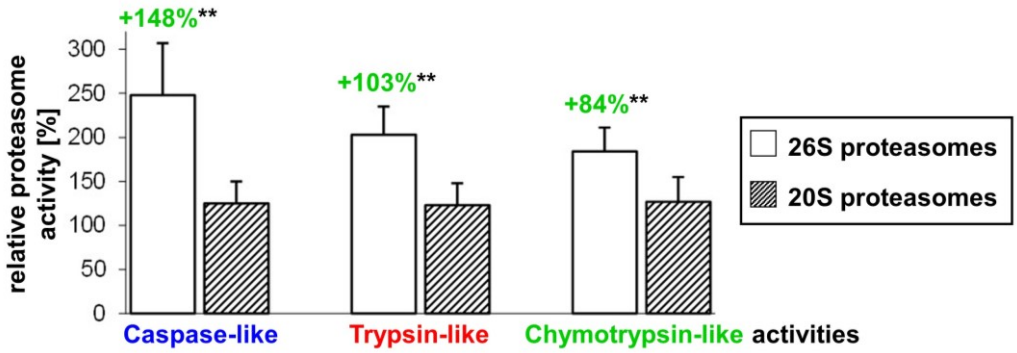

Figure 32. The 26S proteasome activities were increased in hearts of aged mice.
Proteasome activities were analyzed in heart homogenates from 4 and 26 months old mice. Non-proteasomal activities measured in the presence of a specific proteasome inhibitor have been subtracted from the values shown. Activities in 26 months old mice are indicated as percentage of those in 4 months old animals. Mean±SD. ** $p<0.01$ versus 4 months old animals. n=5.

In contrast, the caspase-, trypsin- and chymotrypsin-like 26S proteasome activities were increased in hearts from 26 as compared to 4 months old mice. (Figure 32). These activities were elevated to a lesser extend in 30 months old as compared to the 3 months old mice (Figure 33). Moreover, the 26S proteasome activities seemed to increase successively with age in the latter study (Figure 33).

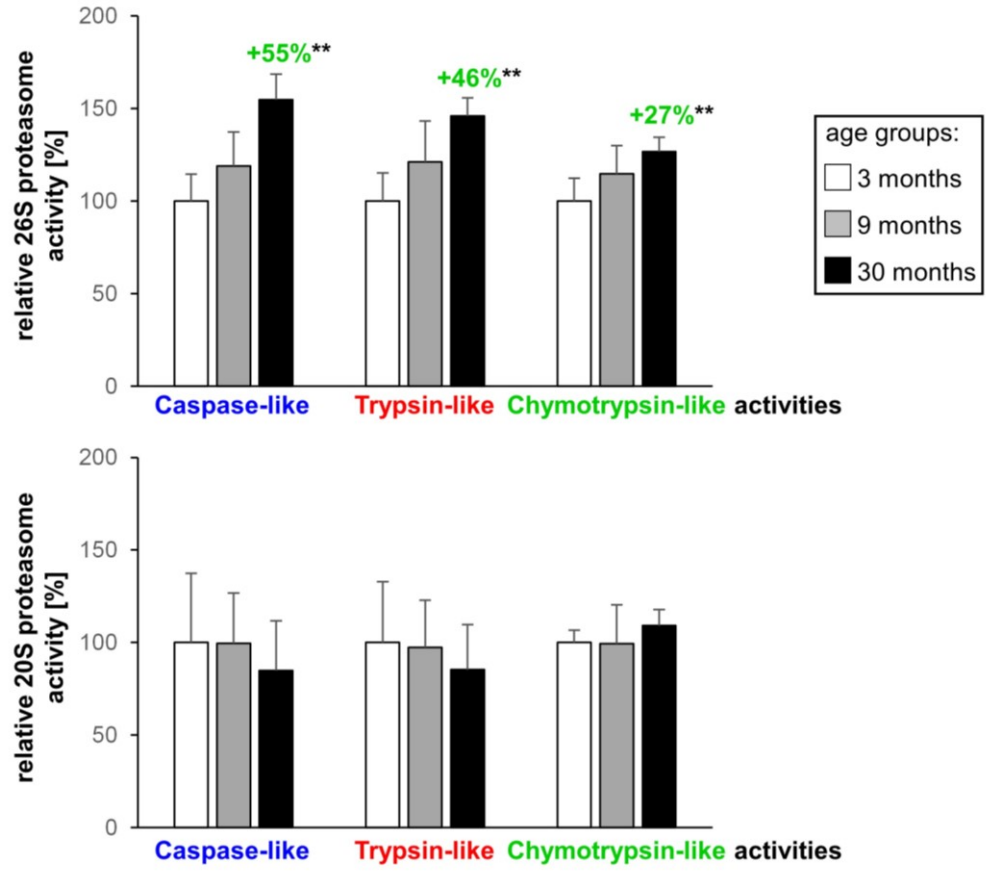

Figure 33. The 26S proteasome activities were elevated with age.

26S and 20S proteasome activities were analyzed in heart homogenates from 3, 9 and 30 months old wild type mice. Non-proteasomal activities have been subtracted from the values shown (see figure 32). Mean±SD. ** $p<0.01$ versus 3 months old animals. n=5-6.

4.14 Differential alteration of the proteasome assembly in aged mice

Proteasome assembly in differentially aged wild type mice was investigated in heart homogenates by active site labeling using the activity based probe MV151 given that 26S proteasome activities were significantly increased in aged as compared to young hearts.

The active site labeling of heart homogenates revealed the incorporation of constitutive proteolytic subunits β1, β2 and β5 into proteasome complexes of differentially aged mice (Figure 34A; 35A). In addition, the active site labeling was quantified and normalized to total protein staining using ruthenium (Figure 34B, C; 35B, C). Comparing 4 versus 26 months or 3 versus 9 or 30 months old mice with regard to total protein abundance showed no differences with statistical significance (Figure 34B; 35B). Still, incorporation of β1, β2 and β5 into proteasome complexes seemed to be increased in 26 months old as compared to 4 months old mice (Figure 34C). This increase was not significant due to the large SD. Incorporation of constitutive proteolytic subunits into proteasome complexes was unchanged in 30 as compared to 3 or 9 months old mice (Figure 35C).

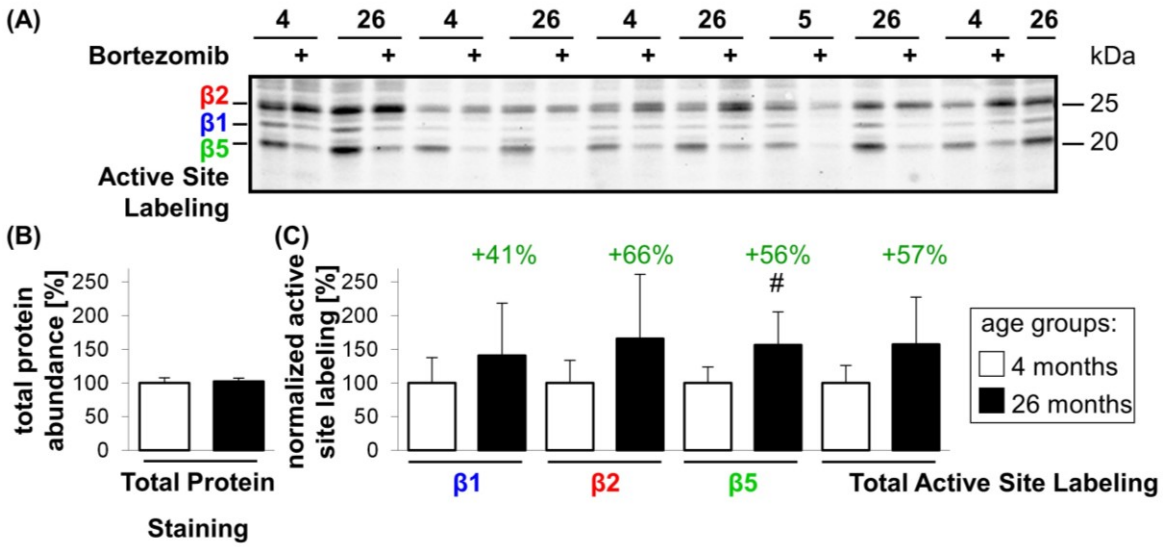

Figure 34. The incorporation of proteolytic β-subunits in proteasome complexes was not significantly increased in 26 as compared to 4 months old mice.

(A) Proteasome active sites were labeled by MV151 in heart homogenates from 4 versus 26 months old mice. In addition, proteasome active site labeling (in particular β1 and β5) was inhibited by using bortezomib prior to labeling to identify proteolytic β-subunits through a competitive assay. Designation of proteasome subunits was performed according to previous publication (Verdoes et al. 2010). **(C)** The active site labeling was quantified and normalized to total protein staining using ruthenium **(B)**. Mean±SD. # p=0.06. n=5.

Accordingly, total incorporation of proteolytic subunits into proteasome complexes seemed elevated in 26 versus 4 months old mice (Figure 34C) while this was not altered in 30 versus 3 or 9 months old animals (Figure 35C).

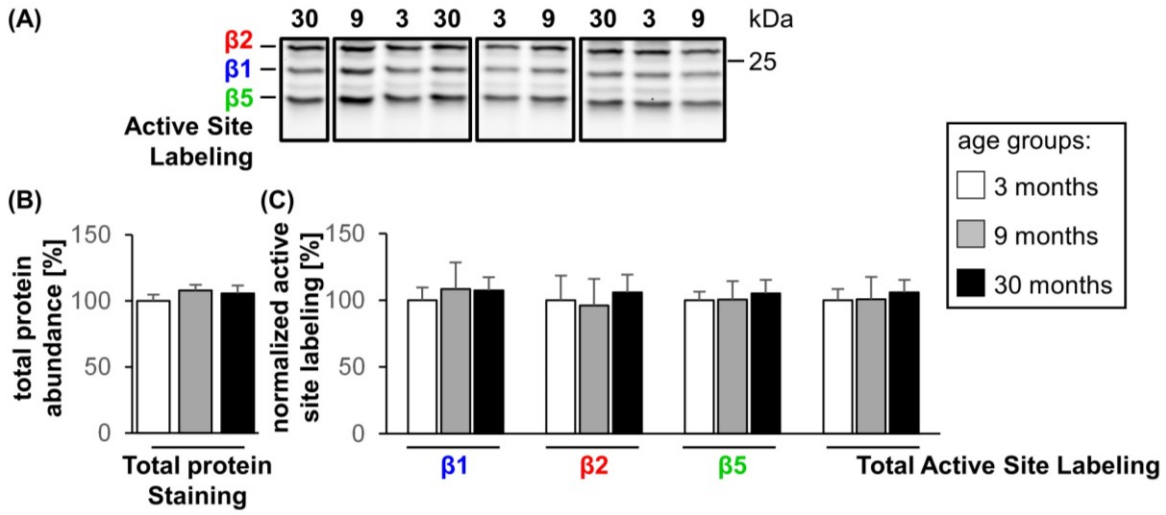

Figure 35. The incorporation of proteolytic β-subunits into cardiac proteasome complexes was unchanged in the context of aging.

(A) Active sites of proteasome complexes were labeled by MV151 in heart homogenates from 3, 9 and 30 months old mice. Proteasome subunits were designated according to previous publication (Verdoes et al. 2010). **(C)** The active site labeling was quantified and normalized to total protein staining using ruthenium **(B)**. Mean±SD. n=5-6.

In addition, the abundance of proteasomal subunits was analyzed in heart homogenates from 3, 9 as well as 30 months old mice by Western blot analysis.

Comparing 9 versus 3 months old mice, the abundance of the structural subunits Rpt4 and α7 as well as the proteolytic subunits β1, β2, β5, β5i and β1i was not altered with statistical significance (Figure 36). The abundance of all analyzed structural and proteolytic proteasome subunits seemed elevated in the hearts of 30 months old mice as compared to 3 months old animals (Figure 36). This increase was statistically significant for the abundance of β5 and β5i (Figure 36).

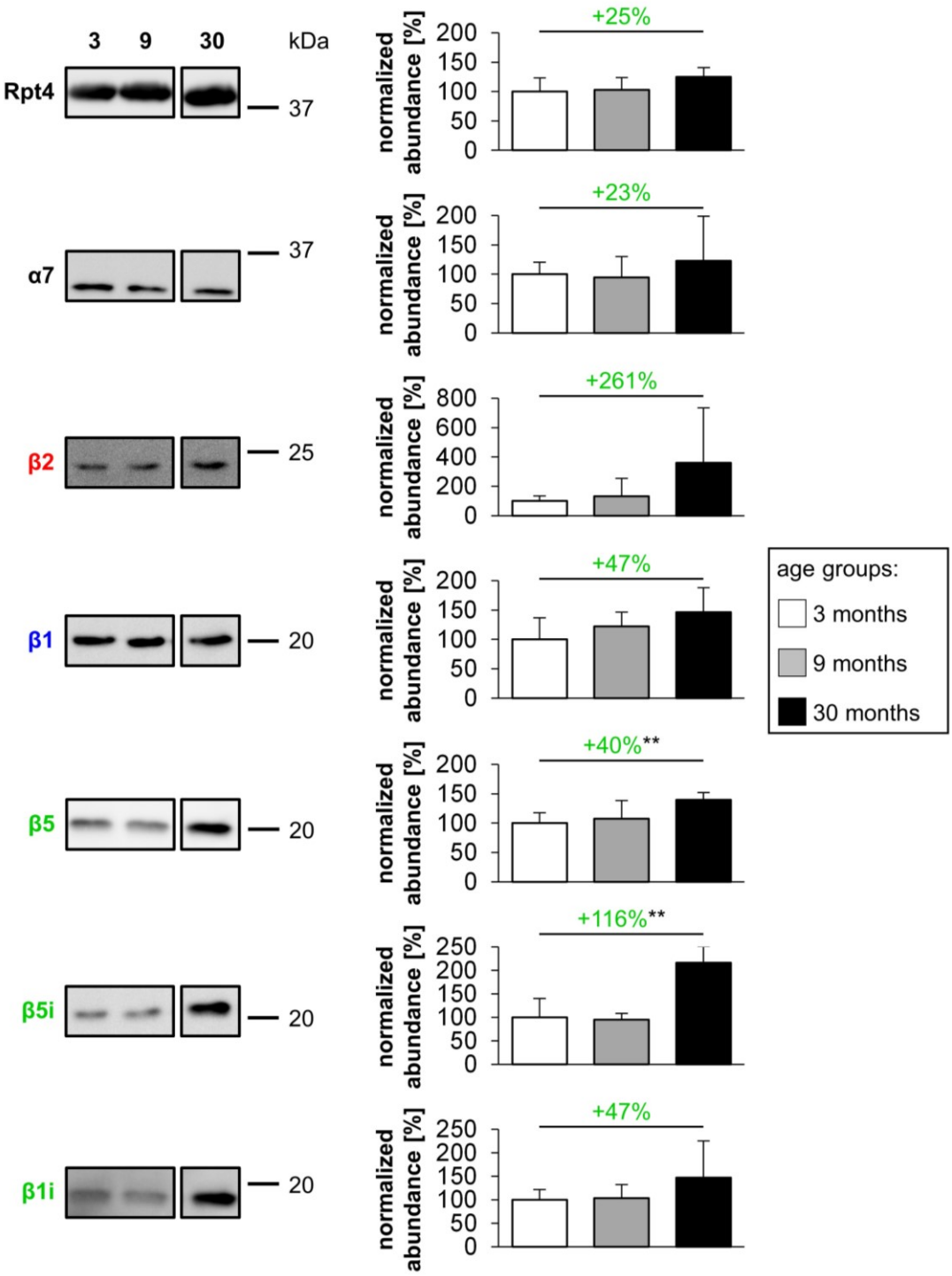

Figure 36. Proteasome subunits with altered abundance in cardiac aging.

The abundance of proteolytic β-subunits as well as structural subunits (α7, Rpt4) normalized to Ponceau S staining was investigated in heart homogenates from 3, 9 as well as 30 months old mice by Western blot analysis. Mean±SD. ** $p<0.01$. n=5-6.

4.15 Differentially altered cardiac proteome in aged as compared to young mice

In addition to the alteration of cardiac proteasome complexes in the context of aging, age-related alteration of cardiac proteomes was analyzed by total protein staining after 1D and 2D gel electrophoresis using heart homogenates from differentially aged wild type mice.

Using 1D gel electrophoresis, 30 bands were quantified in 4 versus 26 months old mice of which 15 bands were unchanged (Figure 37). When comparing 3, 9 and 30 months old animals, a total of 26 bands was quantified of which 17 remained unaltered (Figure 38).

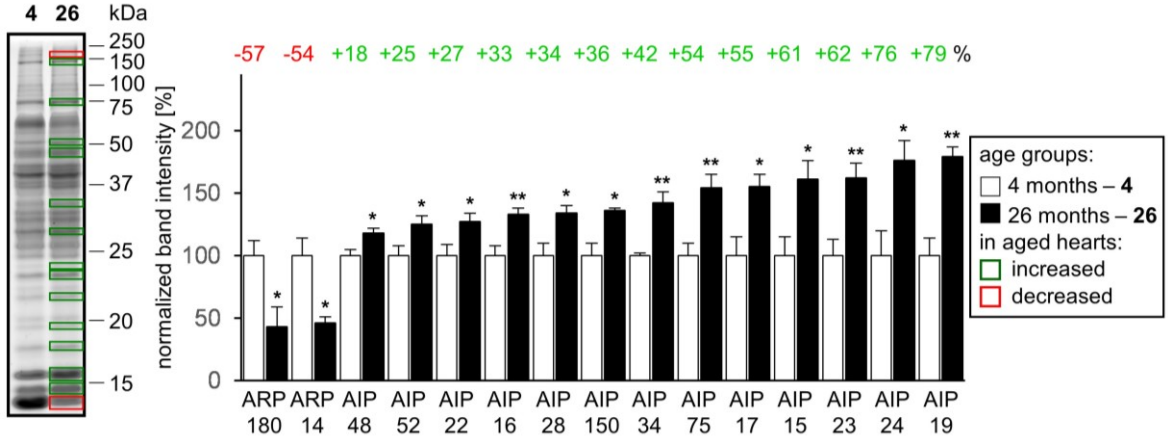

Figure 37. More than 10 abundant protein bands were increased in aged hearts of wild type mice.

Total protein staining using ruthenium of heart homogenates from 4 and 26 months old mice was analyzed after 1D gel electrophoresis. Significantly elevated age induced protein bands (AIP) (green) or decreased age reduced protein bands (ARP) (red) were highlighted. Protein bands were named according to their molecular weight (kDa). Mean±SD. * $p<0.05$, ** $p<0.01$. n=5.

Quantified protein bands were named according to their molecular weight (kDa) and indicated as age reduced proteins (ARP) or age induced proteins (AIP) depending on whether their abundance in old animals was significantly decreased or increased as compared to young mice. Comparing 26 versus 4 months old mice, 2 protein bands were decreased and 13 protein bands increased (Figure 37). On the contrary, when comparing the 3, 9 and 30 months old animals by 1D gel electrophoresis only 3 protein bands were significantly affected (Figure 38). The intensity of protein band ARP 64 was decreased in 9 versus 3 months old mice while that of protein band ARP 18 was decreased in 30 as compared to 3 months old animals. Moreover, the intensity of protein band AIP 25 was increased in 9 and 30 months old mice as compared to 3 months old animals (Figure 38).

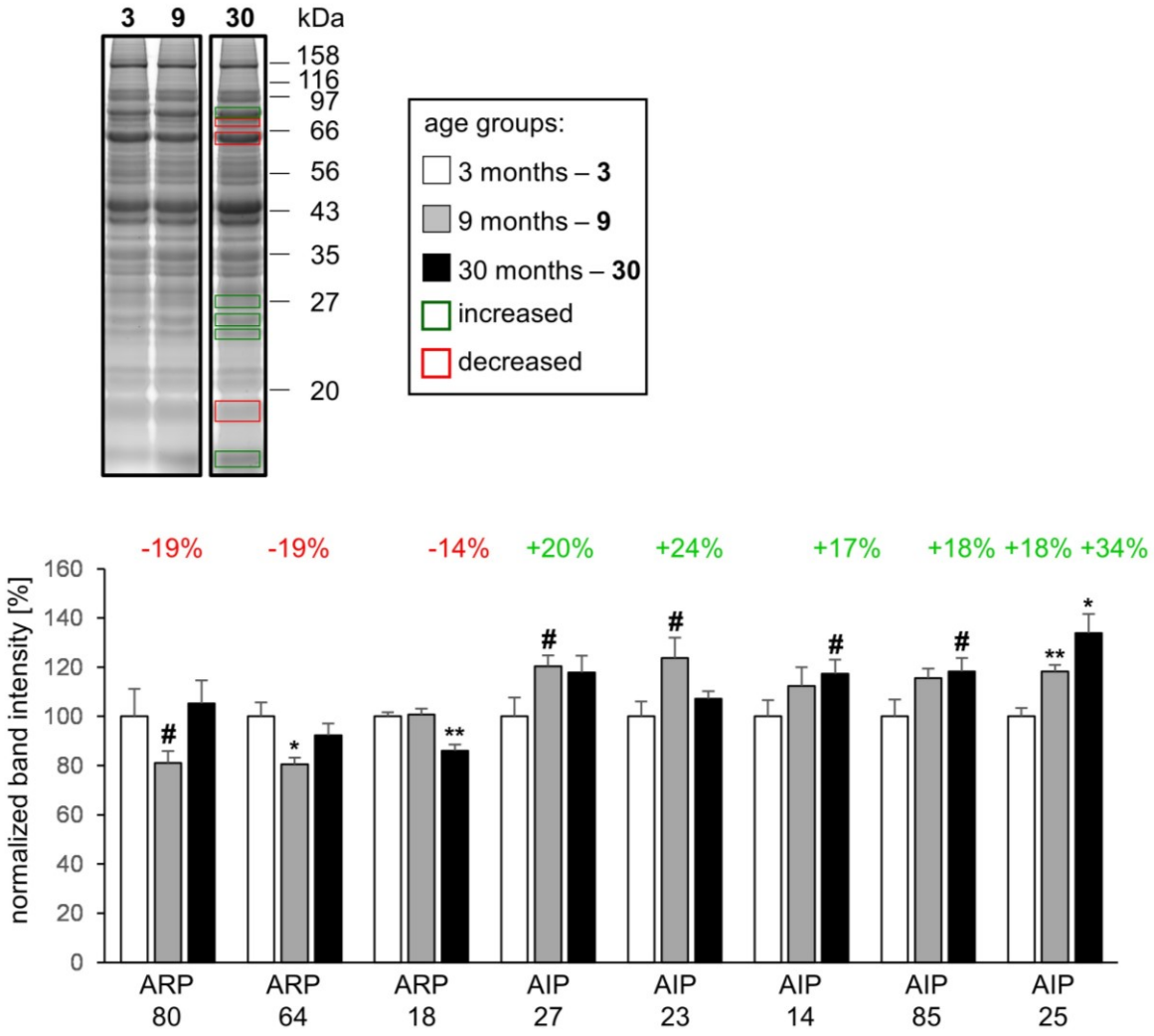

Figure 38. The abundance of eight protein bands was changed in cardiac aging.

Total protein of heart homogenates from 3, 9 as well as 30 months old mice was stained after 1D gel electrophoresis using ruthenium. Increased age induced protein bands (AIP) (green) or decreased age reduced protein bands (ARP) (red) were highlighted and named according to their molecular weight (kDa). Mean±SD. # $p \leq 0.1$, * $p < 0.05$, ** $p < 0.01$. n=5-6.

The comparison of the total protein staining after 1D gel electrophoresis of heart homogenates revealed a similar band pattern in 4 or 26 months old mice as compared to 3, 9 or 30 months old animals (Figure 39). However, bands altered with statistical significance were quite different between the two studies (Figure 39).

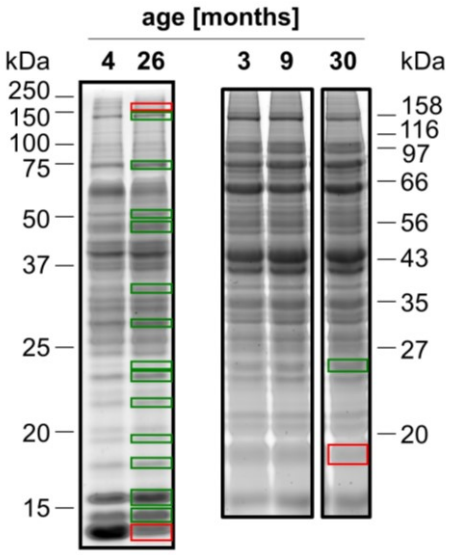

Figure 39. Marked difference in significantly altered protein bands in 26 as compared to 30 months old mice.
After 1D gel electrophoresis total protein staining using ruthenium of heart homogenates from 4 and 26 months old mice was compared to this of 3, 9 and 30 months old animals. Increased age induced protein bands (AIP) were highlighted in green and decreased age reduced protein bands (ARP) were highlighted in red.

The heart homogenates from 4 and 26 months old mice were further analyzed by 2D gel electrophoresis to separate bands into individual proteins and facilitate protein identification.

Spots, which potentially corresponded to the ARPs or AIPs identified via 1D gel electrophoresis, were compared to 2D gels of published reference gels of a cardiac proteome database (HP-2DPAGE: http://web.mpiib-berlin.mpg.de/hp-2dpage/heart1.html). According to this, four of these spots seemed to correspond to essential structural (myosin light chain 3, ventricular myosin light chain 2) and functional proteins (transferrin, myoglobin) (Figure 40). AIP 75 potentially corresponds to transferrin, AIP 24 to myosin light chain 3 (MLC3), AIP 19 to ventricular myosin light chain 2 (MLC2v) and AIP 16 to myoglobin. Quantification of the spots on representative 2D gel electrophoresis gels supports the notion that MLC3 and myoglobin were increased in 26 months old mice as compared to 4 months old animals (Figure 40).

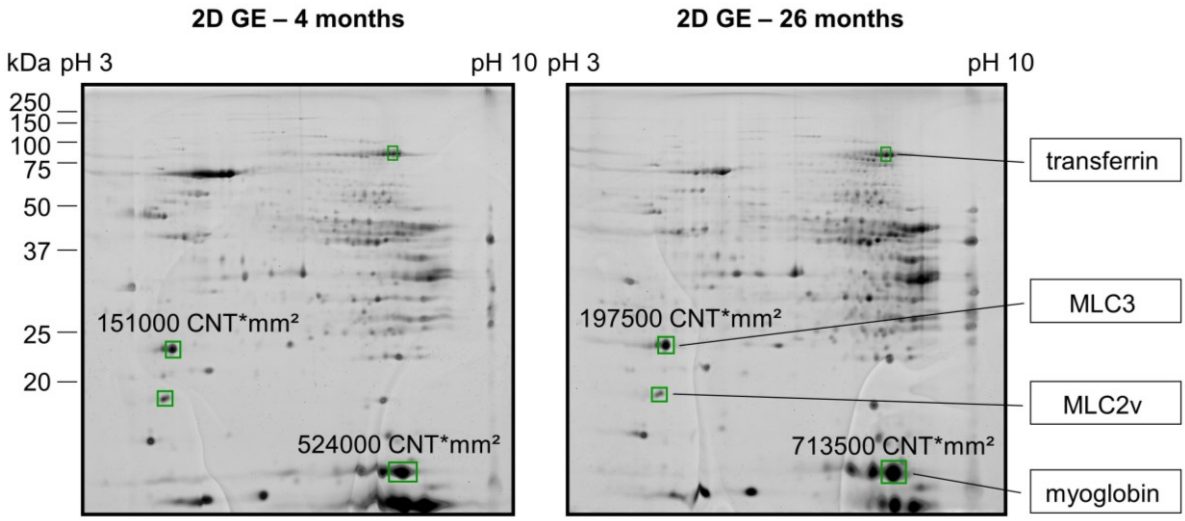

Figure 40. Proteins with putative changes in cardiac aging.

2D gel electrophoresis of heart homogenates from 4 as well as 26 months old mice and proteins were stained using ruthenium complex (performed by M. Lorenz and Dr. O. Drews). Spot volume (CNT*mm² = counts*mm²) was analyzed using Quantity One software. Marked proteins correspond to the following proteins of published reference gels from a cardiac proteome database (HP-2DPAGE: http://web.mpiib-berlin.mpg.de/hp-2dpage/heart1.html): transferrin, myosin light chain 3 (MLC3), ventricular myosin light chain 2 (MLC2v) and myoglobin.

4.16 Altered abundance of sarcomeric proteins in context of aging

The abundance of sarcomeric proteins, which are reported targets of proteasomal degradation, were analyzed in heart homogenates of 3, 9 and 30 months old wild type mice by Western blot analysis due to the published alteration of the contractility in aged hearts.

Comparing 9 versus 3 months old mice, the abundance of ventricular myosin light chain 2 (MLC2v), β-myosin heavy chain (β-MHC), α-tubulin, actin and troponin I was not altered. Moreover, an increase in α-actinin and desmin abundance in 9 as compared to 3 months old mice was not statistically significant (Figure 41). The abundance of α-tubulin and MLC2v was unchanged while the abundance of β-MHC, actin, α-actinin and desmin was increased in 30 months old mice as compared to 3 month old animals (Figure 41). However, this increase was not statistically significant. The abundance of troponin I was decreased in 30 months old mice (Figure 41).

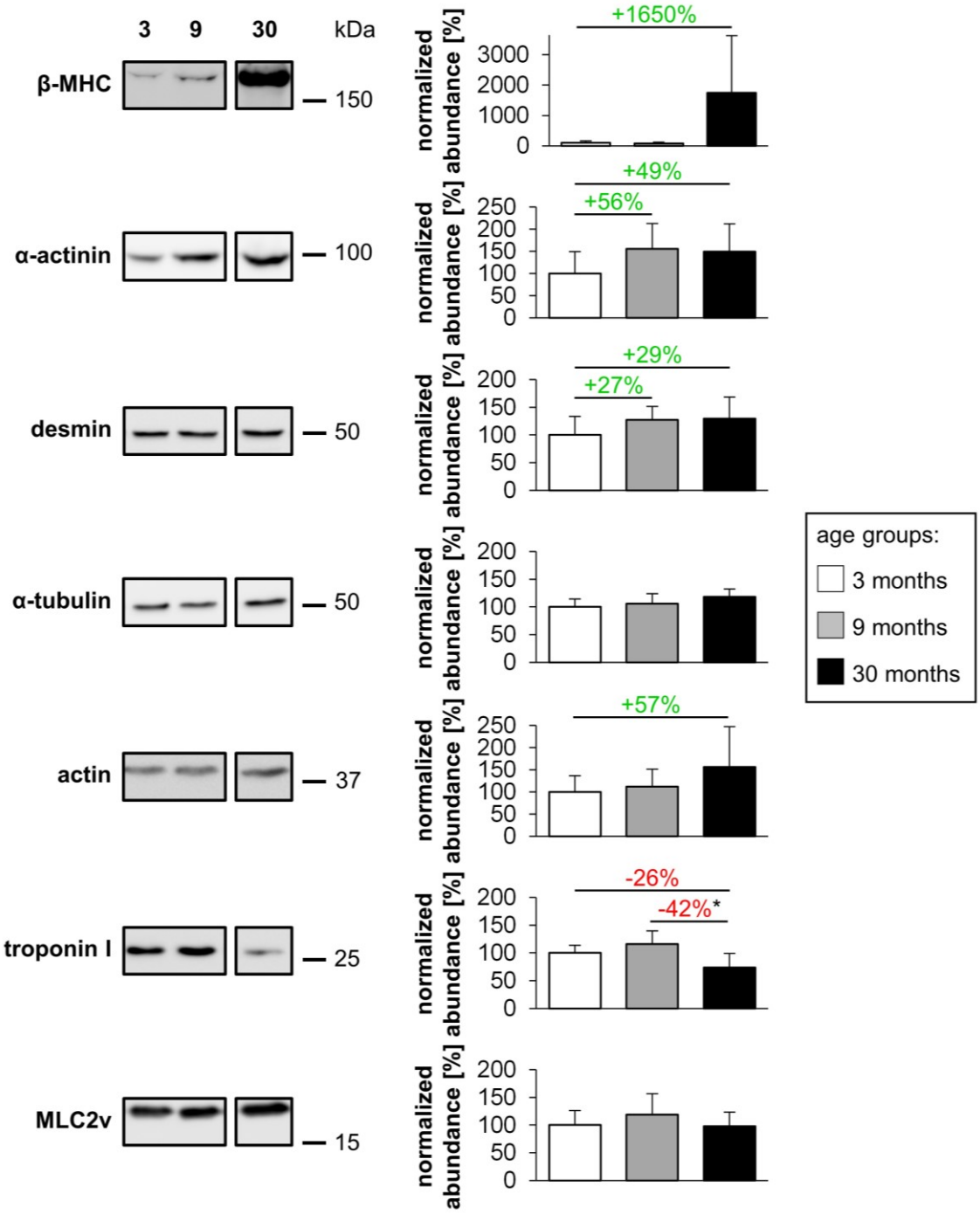

Figure 41. Abundance of sarcomeric proteins in the context of aging.

The abundance of the sarcomeric proteins β-myosin heavy chain (β-MHC), α-actinin, desmin, α-tubulin, actin, troponin I and ventricular myosin light chain 2 (MLC2v) normalized to Ponceau S staining was analyzed in heart homogenates from 3, 9 and 30 months old mice by Western blot analysis. Mean±SD. * $p<0.05$. n=5-6.

5 Discussion

Cardiovascular diseases result in the highest mortality worldwide. Moreover, the prevalence of cardiac hypertrophy and heart failure dramatically increases with age (Lakatta et al. 2003). Proteasomal degradation accounts for the regulation of multiple pathways involved in heart disease (Willis et al. 2010). However, systematic studies regarding the mechanisms of proteasomal regulation and their role in the pathogenesis of heart disease are currently limited. The present study demonstrated for the first time that following induction of hypertrophy the heart-specific incorporation of β1i into proteasome complexes of β1i-deficient mice attenuates hypertrophy development and prevents manifestation of systolic and diastolic dysfunction. Thus, the previously reported increase in the incorporation of inducible β-subunits into cardiac proteasomes complexes in wild type mice following isoprenaline exposure (Drews et al. 2010) seems to be an important protective mechanism in cardiac remodeling. A first analysis of the sarcomer structure in the cardiomyocytes following continuous β-adrenergic stimulation indicated that the observed phenotype of the β1i-deficient animals is not related to a disturbance of this structure or a deregulated degradation of contractile proteins. However, increased levels of troponin I upon treatment with isoprenaline and reintroduction of β1i in β1i-deficient mice potentially contributed to the maintenance of cardiac function in these animals. In the context of aging, marked alterations of the cardiac proteome were associated with significantly increased 26S proteasome activities. Moreover, this increase seemed to be adaptive with respect to the extent of the alterations in the cardiac proteome, and may be generally associated with a poor health status and serve to maintain protein homeostasis and cardiac function in the aging animal.

5.1 NRCMs – the preferable *in vitro* system to verify correct transgene expression using AAV CMV/MLC0.26 vectors

A standard cloning approach is the direct cloning of PCR products into target vectors (Scharf et al. 1986). For this purpose, two different restriction sites at the 5’ and 3’ end of the gene of interest are inserted via PCR using overhang primers. Subsequently, the gene of interest is inserted into the target vector via cohesive-end ligation after restriction digestion of the PCR product and the vector (Kaufman et al. 1990). A drawback of this approach is that it is not possible to figure out, which (intermediate) step fails in a failing cloning procedure. Alternatively, the PCR product containing the restriction sites is inserted into a standard vector via blunt-end ligation (Innis et al. 2012). This procedure has the advantage to verify the inserted sequence before its insertion into the target vector and to restart the cloning procedure at a higher level if the cohesive-end ligation into the target has failed.

Using the AAV CMV/MLC0.26 target vector, it is particularly recommended to use this intermediate step due to low transformation efficiency, which was also observed in the present study. Moreover, an additional intermediate step was necessary due to the small yield by PCR using reverse transcribed cDNA from the liver of C57BL/6J wild type mice as a template and 'β1i overhang primers' in this study. Thus, the β1i gene was initially amplified from reverse transcribed cDNA using 'β1i direct primers' and inserted via blunt-end ligation into a standard cloning vector. This standard vector containing β1i was subsequently used as a template for PCR using 'β1i overhang primers'.

HEK-293 cells are commonly used to verify the correct expression of a transgene encoded by adeno-associated viral vectors containing a CMV promoter and packaged into AAV2 particles (Hagstrom et al. 2000, Kaspar et al. 2002, Shimpo et al. 2002). In previous studies using AAV vectors containing a transgene under the control of a combined CMV/MLC promoter, NRCMs were used to analyze correct expression of the transgene following infection by AAV6 particles (Geisler et al. 2011, Friedrich et al. 2014, Weber et al. 2014). In the present study, correct expression of β1i was verified in HEK-293 cells and NRCMs using the AAV CMV/MLC0.26 β1i vector packaged into appropriate AAV particles. Thus, both approaches are applicable for verifying functionality of the adeno-associated viral vector system used. However, rodent cardiac cells (NRCMs) seem preferable due to the higher degree of similarity to the *in vivo* conditions (rodent hypertrophy model).

5.2 Effective reintroduction of β1i in hearts of β1i knockout mice via AAV9 CMV/MLC0.26 β1i

To my knowledge, the proteasome subunit β1i has not been reintroduced into a β1i-deficient model organism, e.g. by way of viral gene transfer, so far. Using AAV9 harboring expression constructs under the control of a CMV-enhanced myosin light chain promoter, transgene expression in the heart was demonstrated in different disease models (Kaya et al. 2011, Pleger et al. 2011, Schinkel et al. 2012). In a porcine model of myocardial infarction, myocardial expression of S100A1, a positive regulator of myocardial contractility, was moderately increased through AAV9 CMV/MLC0.26 S100A1 gene transfer using 1.5×10^{13} vector genomes per animal (Pleger et al. 2011). Serum levels of interleukin-10 (IL-10), a potent anti-inflammatory cytokine, were markedly elevated by AAV9 CMV/MLC0.26 IL-10 gene transfer using 10^{12} vector genomes per animal in a mouse model of autoimmune myocarditis (Kaya et al. 2011). In the present study, the expression of β1i in β1i-deficient mice was similar to that of wild type animals after AAV9 CMV/MLC0.26 β1i gene transfer using 10^{11} vector genomes, demonstrating sufficient transgene expression using an even lower number of vector genomes per animal.

The proteasome subunit β1i is synthesized in a precursor form consisting of a N-terminal propeptide (18 AA) and a C-terminal tail (201 AA), and lacks proteolytic activity (Murata et al. 2009). The N-terminal propeptide is cleaved off during the dimerization of the two half-proteasomes to the 20S core complex via autolysis to expose the catalytic threonine residue of the C-terminal tail hence enabling proteolytic activity (Murata et al. 2009). Thus, the observed two β1i bands likely correspond to the β1i precursor form (23.4 kDa) and the processed form of β1i (21.3 kDa) (Figure 14, 24). Detection of the processed form of β1i can be interpreted as an indication for incorporation of the reintroduced β1i into proteasome complexes in AAV β1i-injected β1i-deficient mice.

The incorporation of all constitutive and inducible proteasome subunits in proteasome complexes has previously been reported for thymus homogenates of wild type mice by active site labeling using the activity based probe MVB003 (BODIPY-epoxomicin) (Florea et al. 2010). The labeling pattern of the proteasome subunits, observed in the present study, was slightly modified as compared to the aforementioned labeling pattern (Florea et al. 2010). Thus, distinct β5 and β5i bands were observed in the mouse heart but only one band corresponded to the β5 and β5i subunit in the labeling pattern from the mouse thymus (Florea et al. 2010). The presence of distinct β5 and β5i bands in the present study might be due to differential posttranslational modifications of these β-subunits in the mouse thymus and the mouse heart, respectively, namely in view of the reported cardiac-specific phosphorylation sites of the β5 subunit (Cui et al. 2014). The lowest band, observed in the MVB003 labeling pattern in heart homogenates of AAV β1i-injected β1i knockout mice, most likely corresponds to β1i when considering that the processed form of β1i is the smallest proteasome subunit. Accordingly, the lowest band of the active site labeling in the mouse thymus has been designated β1i, too (Florea et al. 2010). This β1i-like band was detected in AAV β1i-injected but not AAV Luci-injected β1i knockout mice. This may point to the incorporation of β1i in proteolytically active proteasome complexes in AAV β1i-injected β1i knockout mice following isoprenaline treatment.

5.3 Beta1i reintroduction in β1i knockout mice attenuates cardiac hypertrophy development upon isoprenaline exposure

Continuous stimulation of the β-adrenergic pathway through isoprenaline infusion is a well-established model of cardiac hypertrophy in various model organisms (reviewed in (Osadchii 2007)). In previous studies, 7-day treatment using an infusion rate of 30 mg * kg^{-1} * d^{-1} of isoprenaline has been commonly used to induce cardiac hypertrophy in mice (Saadane et al. 1999, Drews et al. 2010, Lukowski et al. 2010). In these studies, the heart weight to body weight ratio (HW/BW ratio) was used as a marker for cardiac hypertrophy. In C57BL/6J wild type mice and β1i knockout mice, the HW/BW ratio was strongly increased

following isoprenaline exposure pointing to the development of cardiac hypertrophy (ongoing studies) (Liem D 2012). In this context, the HW/BW ratio of AAV Luci-injected β1i-deficient mice was similar to that of untreated β1i knockout mice while the HW/BW ratio of AAV β1i-treated β1i-deficient mice was equivalent when compared to wild type animals. Moreover, the HW/BW ratio was markedly increased after isoprenaline treatment in AAV Luci-injected control mice as compared to AAV β1i-treated β1i knockout mice. Thus, the reintroduction of β1i reduced the development of cardiac hypertrophy in the β1i-deficient mice to the level of the isoprenaline-treated wild type mice.

Echocardiography is a well-established non-invasive method to analyze cardiovascular structure and function in mice (Rottman et al. 2007, Stypmann 2007, Scherrer-Crosbie et al. 2008). In addition to the HW/BW ratio, the left ventricular posterior wall thickness in diastole (LVPWT;d) is an established hypertrophy indicator (Freund et al. 2005, Galindo et al. 2009, Li et al. 2013). One advantage of the non-invasive monitioring of this parameter is its determination prior to and post induction of cardiac hypertrophy. In the present study, changes in LVPWT;d in the different experimental groups mirrored those of the HW/BW ratio, again suggesting that the AAV9-based reintroduction of β1i into β1i-deficient mice normalized the hypertrophy-associated increase in wall thickness to the level of wild type mice that had been exposed to isoprenaline for 7 days.

Cardiac hypertrophy is commonly classified to be concentric (symmetrical) or eccentric (asymmetrical) based on an alteration of the distribution of the muscle mass resulting in a modification of the heart's shape and ventricular volume (reviewed in (Heineke et al. 2006, Maillet et al. 2013)). Besides remodeling of the extracellular matrix and coordinated angiogenesis, an increase in cardiomyocyte size due to the addition of sarcomeres in parallel or in series is the pivotal element of hypertrophic growth of the heart. In concentric hypertrophy, the thickness of the ventricular wall and septum is irregularly increased in proportion to the ventricular volume, which is maintained or even reduced, due to the predominant addition of sarcomeres in parallel. In the isoprenaline hypertrophy model, a concentric hypertrophy ensues evidenced by the fact that the cross-sectional area of the cardiomyocytes is significantly increased (Galindo et al. 2009, Lukowski et al. 2010). Accordingly, the cardiomyocyte cell width to cell length ratio, represented by the cross-sectional area, was strongly increased following isoprenaline treatment both in AAV Luci and AAV β1i-injected β1i-deficient mice, suggesting that the missing incorporation of β1i into cardiac proteasome complexes does not have a major effect on the structural changes in the heart following exposure to a pro-hypertrophic stimulus. Nonetheless, concentric hypertrophy seemed to be more pronounced in AAV Luci as compared to AAV β1i-injected β1i-deficient animals (preliminary results). Thus, the less severe cardiac hypertrophy upon reintroduction of β1i in β1i-deficient mice, as indicated by the HW/BW ratio and the left ventricular posterior wall

thickness in diastole, might be due to a somewhat different remodeling process that requires further investigation.

After 7 days of isoprenaline treatment, the systolic function of the heart is increased in wild type mice (Drews et al. 2010, Lukowski et al. 2010, Shan et al. 2010). In contrast, ejection fraction (EF) and fractional shortening (FS) – two parameters indicative of systolic function – are reduced upon isoprenaline treatment in β1i knockout mice (ongoing studies) (Liem D 2012). Herein, the same was true for the isoprenaline-treated AAV Luci-injected β1i-deficient animals. Thus, the presumed loss of β1i incorporation into cardiac proteasome complexes resulted in an accelerated systolic dysfunction following continuous exposure to isoprenaline. EF and FS were not altered in isoprenaline-treated AAV β1i-injected β1i-deficient mice pointing to an effective prevention of systolic dysfunction. There was, however, no increase in systolic function in these animals as it normally occurs in wild type mice (Drews et al. 2010, Lukowski et al. 2010, Shan et al. 2010). This lack of an increased systolic function following 7 days of isoprenaline treatment might be a different adaptive response of the heart to β-adrenergic overstimulation in the absence of β1i or a negative effect of the systemic loss of β1i that was not recovered by the heart-specific reintroduction of β1i.

Assessment of left ventricular diastolic function by echocardiography is a part of the standard procedure for the diagnosis of heart diseases in humans (reviewed in (Nagueh et al. 2009)). In this context, the transmitral filling patterns, and in particular the so-called E/A ratio, are used as parameters indicative of diastolic dysfunction (Nagueh et al. 2009). Currently, the number of studies using echocardiography in mice is limited, due to the lack of appropriate echocardiography instruments for small laboratory animals such as mice with adequate spatial and temporal resolution. With the introduction of high-resolution digital ultrasound imaging this situation has recently been significantly improved, especially for the analysis of small rodents such as mice. In previous studies, diastolic dysfunction characterized by a significant alteration of the E/A ratio, has been reported for the transverse aortic constriction (TAC) model of pressure overload-induced concentric hypertrophy and heart failure in mice (Dirkx et al. 2013, Wang et al. 2014, Carley et al. 2015). In the present study, diastolic function of the heart was altered due to the lusitropic effect of isoprenaline. Thus, the accelerated relaxation in diastole results in an increased passive filling of the ventricle (E value). Similarly, its positive ionotropic effect results in an increased active filling of the ventricle (A value) due to the enhanced contractility. Thus, the E/A ratio was not changed in response to isoprenaline in wild type mice in previous studies from our laboratory (ongoing studies) (Drews et al. 2010).

In the present study, diastolic function deteriorated (increased E/A ratio) in the presence of isoprenaline in AAV Luci but not AAV β1i-injected β1i-deficient mice, suggesting that the reintroduction of β1i prevents the development of diastolic dysfunction. The E value increased

following treatment with isoprenaline both in AAV Luci and AAV β1i-injected β1i-deficient animals but this effect was more pronounced in the reconstituted β1i knockout mice. Upon isoprenaline treatment, the A value was increased in the AAV β1i-injected but not in the AAV Luci-treated β1i-deficient mice indicating that diastolic dysfunction in these animals is caused by a decreased contractility of the atria. In addition, the present study confirmed the applicability of the E/A ratio as an indicator of diastolic dysfunction in the isoprenaline model of cardiac hypertrophy in mice.

The progression of normal diastolic function towards severe dysfunction is represented by four different transmitral inflow patterns in humans (Nagueh et al. 2009) and in mice (Du et al. 2008). These patterns include normal filling (E>A), impaired left ventricular relaxation (E<A), pseudonormal filling (E>A) and restrictive filling (E>>A) (Du et al. 2008, Nagueh et al. 2009). Analysis of cardiac function at an intermediate step might enable a better judgement of the rapid progression of diastolic dysfunction (Gao et al. 2011). Thus, cardiac function should be investigated after 3 or 4 days of isoprenaline exposure (Saadane et al. 1999) when the E value is likely to be elevated already. This seems less clear for the A value, reflecting the contractility of the atria, which may in fact be increased earlier and more transiently in AAV Luci-injected β1i knockout mice. Along these lines it would also be interesting to analyze whether systolic function in these animals is increased at such an earlier time point. In summary, investigating the aforementioned parameters after 3-4 days isoprenaline exposure may provide a better insight into the mechanisms underlying the deteriorating cardiac function associated with the loss of β1i in these animals, which could be restored by the AAV9-based reintroduction of β1i into (the active proteasomes of) the heart.

Myocardial fibrosis is closely associated with cardiac remodeling in various cardiovascular diseases (Lorell et al. 2000, Kitamura et al. 2001, Moreo et al. 2009). In previous studies using the isoprenaline hypertrophy model, myocardial collagen content was analyzed by Masson's trichrome staining (Saadane et al. 1999, Matkovich et al. 2006, Galindo et al. 2009). In C57BL/6 wild type mice no sign of fibrosis (Saadane et al. 1999) or marginal fibrosis (Matkovich et al. 2006) was reported after a 14-day isoprenaline treatment. In the present study, preliminary results suggest that there is essentially no myocardial fibrosis in AAV β1i-injected β1i knockout mice after 7 days exposure to isoprenaline while this was present in an AAV Luci-injected control animal. Clearly, the validity of this finding must be corroborated in further studies. However, myocardial fibrosis potentially contributed to the observed diastolic dysfunction in the AAV Luci-injected β1i knockout mice, given the association of myocardial fibrosis with increased myocardial stiffness and hence impaired diastolic relaxation, as previously reported for this experimental hypertrophy model (reviewed in (Osadchii 2007)).

The development of myocardial fibrosis is either due to the remodeling of the extracellular matrix (reactive fibrosis) or the replacement of lost cardiomyocytes (replacement fibrosis) (reviewed in (Krenning et al. 2010)). Reactive fibrosis is predominantly observed in pressure overload-induced cardiac hypertrophy due to enhanced biomechanical stress resulting in the remodeling of the extracellular matrix (reviewed in (Fan et al. 2012)). On the contrary, replacement fibrosis compensates for lost cardiomyocytes due to apoptosis or necrosis for example after myocardial infarction or in the terminal stages of heart failure (reviewed in (Fan et al. 2012)). One characteristic feature of replacement fibrosis due to cardiomyocyte necrosis is the recruitment of inflammatory cells (Fan et al. 2012). Cardiac fibroblast proliferation as well as recruitment and differentiation of circulating bone-marrow-derived cells to cardiac fibroblast in replacement fibrosis results in the formation of fibrotic scar tissue (Fan et al. 2012).

In the isoprenaline hypertrophy model, replacement fibrosis due to cardiomyocyte necrosis has been reported after acute treatment using high doses of isoprenaline (5 days, 100 mg * kg^{-1} * d^{-1}) in Swiss-Webster mice (Brooks et al. 2009) and A/J mice (Faulx et al. 2005). Notably, the resulting fibrosis is strain-dependent, thus the extent of fibrosis in C57BL/6 mice is much lower than that in A/J mice (Faulx et al. 2005). Replacement fibrosis has been further shown in C57BL/6 mice after chronic stimulation with a moderate dose of isoprenaline (10 days, 40 mg * kg^{-1} * d^{-1}) (Galindo et al. 2009). The fibrosis observed upon isoprenaline treatment of AAV Luci-injected β1i-deficient mice (preliminary results) may represent the replacement fibrosis type, given the absence of cell debris or immune cells in the fibrotic tissue. Further analyses of preceding cardiomyocyte necrosis or apoptosis may elucidate the exact type of cardiac fibrosis in these animals. Considering the presence of marginal fibrosis in C57BL/6 mice after 14 days isoprenaline treatment at a dose of 30 mg * kg^{-1} * d^{-1} (Matkovich et al. 2006), the development of fibrosis in these animals may potentially be accelerated depending on the dose of and duration of treatment with isoprenaline.

5.4 Sarcomeric proteins – targets of β1i-specific degradation upon isoprenaline treatment?

In a previous study from our laboratory, an increased expression and incorporation of inducible proteasome subunits into proteasome complexes, enhanced assembly of 26S proteasomes resulting in the increase of all three 26S proteasome activities as well as an increased sensitivity of the 20S proteasome to activation via cAMP-dependent PKA has been reported for a 7-day treatment protocol with isoprenaline (30 mg * kg^{-1} * d^{-1}) in mice (Drews et al. 2010). In the TAC model, an increase of the 26S chymotrypsin-like activity has previously been shown in mice 5 days to 3 weeks following the aortic constriction (Depre et al. 2006, Hedhli et al. 2008). In another study using TAC in mice, the 26S proteasome activities were reduced for 2

to 4 weeks after the TAC procedure (Tsukamoto et al. 2006). Thus, regulation of the activity of the proteasome may depend on the level of aortic constriction resulting in a differing development of hypertrophy or transition towards heart failure, given that a decreased activity of the 26S proteasome is associated with heart failure in humans (reviewed in (Drews et al. 2014)). Therefore, proteasome function and activity seems to be markedly altered in cardiac hypertrophy and heart failure. In the present study, proteasome subunit expression, assembly as well as activity were not significantly altered upon treatment with isoprenaline of β1i-deficient mice in which this subunit had been reintroduced by cardiac-specific gene transfer.

Previously, increased expression of inducible proteolytic subunits was associated with enhanced incorporation of these subunits into (active) proteasome complexes upon exposure to isoprenaline in wild type mice (Drews et al. 2010). Thus, the uniform albeit insignificant elevation of the expression of the proteolytic subunits β1, β2, β5 and β5i in AAV Luci-injected β1i knockout mice may potentially be associated with an increased incorporation of these subunits into proteasome complexes, as shown by active site labeling. Moreover, this may be associated with the more pronounced pro-hypertrophic response to isoprenaline of these mice.

Reintroduction of β1i influences the activity of the proteasome, given that the constitutive counterpart β1 accounts for the caspase-like activity, whereas the inducible subunit β1i contributes to the chymotrypsin-like activity of the proteasome. However, considering the preference of the activity-based probe MVB003 for proteasome subunits with chymotrypsin-like or trypsin-like activity, the proteasome subunit β1i was incorporated into proteasome complexes only to a small extent in relation to its constitutive counterpart β1 in AAV β1i-injected β1i knockout mouse hearts following β-adrenergic overstimulation. Contrariwise, the 26S and 20S caspase-like activities were both moderately albeit insignificantly reduced in these hearts, so that the level of incorporation of β1i into cardiac proteasome complexes did not correspond to the alterations in proteolytic activity. Thus, there must be additional mechanisms regulating proteasomal function. Considering the involvement of PKA in controlling proteasomal activity in this hypertrophy model (Drews et al. 2010), this might be regulated via phosphorylation, given that several phosphorylation sites exist both in the β1 and β1i subunit (reviewed in (Cui et al. 2014)). Alternatively, the slight difference in proteasomal function upon treatment with isoprenaline of AAV β1i as compared to AAV Luci-injected β1i-deficient mice might be associated with the differential regulation of several non-proteasomal proteins, resulting in the reduced development of hypertrophy and prevention of cardiac dysfunction.

Chronic β-adrenergic stimulation by isoprenaline induces a (pathological) concentric cardiac hypertrophy. One characteristic of hypertrophic growth is the remodeling of cardiomyocytes

through the addition of sarcomeres. Consequently, the turnover of sarcomeric proteins is increased. The UPS likely accounts for the maintenance of cardiomyocyte function by the targeted degradation of structural, functional and signaling proteins (Drews et al. 2014). Thus, differences in the expression of sarcomeric proteins, which are targets of the UPS, potentially contribute to the observed systolic and diastolic dysfunction upon treatment with isoprenaline in AAV Luci-injected β1i-deficient mice. Sarcomeric contractile proteins that are targeted by the UPS comprise, e.g. actin (Solomon et al. 1996), β-myosin heavy chain (β-MHC) (Fielitz et al. 2007) and ventricular myosin light chain 2 (MLC2v) (Witt et al. 2005) as well as cardiac troponin I (Kedar et al. 2004). Moreover, sarcomeric structural proteins such as α-tubulin (Poruchynsky et al. 2008), desmin (Ye et al. 2014) or α-actinin (Spaich et al. 2012) can also be degraded via the UPS. Neither the abundance of actin, β-MHC or MLC2v nor that of α-tubulin were altered upon treatment with isoprenaline in AAV Luci as compared to AAV β1i-injected β1i-deficient mice. Thus, neither the myofilaments, which are part of the force-generating machinery, nor the microtubules, which alter cardiomyocyte contraction capacity due to modifying flexibility of the cytoskeleton, seem to be subjected to differential proteasomal degradation upon reintroduction of β1i, and therefore may not be related to the observed beneficial effects on cardiac function in these animals.

In contrast, the level of cardiac troponin I seemed to be moderately decreased in AAV Luci as compared to AAV β1i-injected β1i-deficient mouse hearts. Troponin I is a key regulator of striated muscle contraction and relaxation due to its control of the actin-myosin cross bridge cycle. Previously, phosphorylation of cardiac troponin I via PKA upon β-adrenergic stimulation, resulting in accelerated relaxation (lusitropic effect), has been demonstrated (Zhang et al. 1995). In addition to diastolic function, systolic function may also be improved through phosphorylation of cardiac troponin I via β-adrenergic stimulation (Takimoto et al. 2004). Moreover, deprivation of cardiac troponin I has been associated with diastolic dysfunction due to impaired cardiomyocyte relaxation (Fentzke et al. 1999). Thus, the moderately decreased level of cardiac troponin I in AAV Luci as compared to AAV β1i-injected β1i-deficient mouse hearts may have contributed to the observed systolic and diastolic dysfunction in these animals. Consequently, reincorporation of β1i into (active) proteasome complexes potentially reduces degradation of cardiac troponin I by the proteasome. This interesting hypothesis warrants further investigation.

The overall abundance of α-actinin, which links adjacent sarcomeres at the Z-discs, and desmin, which aligns myofibrils to three dimensional networks at the Z-discs and intercalated disks, was not significantly altered in AAV Luci as compared to AAV β1i-injected β1i-deficient mouse hearts. However, the ordered localization of α-actinin and desmin is of particular interest, given that disorganization of desmin (Heling et al. 2000) and α-actinin (Hein et al. 2009) has previously been shown in patients with heart failure. This was not altered following

isoprenaline exposure in the AAV Luci as compared to AAV β1i-injected β1i-deficient mouse hearts (α-actinin – data not shown). Moreover, atypical α-actinin clusters (Heling et al. 2000) or a disturbed cross-striation pattern of desmin (Hein et al. 2009), which have been shown in human failing hearts, were not observed following isoprenaline treatment in AAV Luci as compared to AAV β1i-injected β1i-deficient mouse hearts (α-actinin – data not shown). Thus, the observed systolic and diastolic dysfunction in AAV Luci-injected β1i knockout seems to be unrelated to a disorganization of the sarcomeres, given that sarcomere integrity was not disturbed.

5.5 Increased 26S proteasome activities in the context of aging: effort to maintain protein homeostasis?

Considering the regulation of proteasome function in cardiac hypertrophy and heart failure, the potential regulation of proteasome function in the context of aging is intriguing, given the increased prevalence of cardiac hypertrophy and heart failure in the elderly. While the E/A ratio (diastolic function) is decreased, ejection fraction (systolic function) is preserved in healthy humans (Lakatta et al. 2003). Similar alterations in cardiac function can be observed in aging mice (Dai et al. 2009). Moreover, a reduced regenerative capacity of the aged heart has been reported for both men (Bergmann et al. 2009) and mice (Senyo et al. 2013). Thus, cardiac aging in mice seems to recapitulate the alterations in the human heart with increasing age. Consequently, mice seem to be a suitable model for the analysis of cardiac aging.

Previous studies reported an increase (Palpant et al. 2008, Hua et al. 2015) as well as no change (Li et al. 2007, Wu et al. 2007, Kiper et al. 2013) of the heart weight to body weight ratio (HW/BW ratio) in young versus old wild type mice. In the present study, the HW/BW ratio was not significantly altered in old as compared to young mice but in middle-aged mice this was significantly reduced (Kiper et al. 2013). Thus, cardiac aging may be not associated with marked alterations of cardiac morphology, such as cardiac hypertrophy, in general. Notably, systolic dysfunction was detected in 24 versus 2 months old mice despite no change in the HW/BW ratio (Kiper et al. 2013). In the present study, the 26 months old mice most likely had a rather poor general health status since they had to be sacrificed because of this. Contrariwise, no pathologic abnormalities were observed in 30 versus 3 months old mice by echocardiography analysis. Considering the similar alteration of the HW/BW ratio in the 26 and 30 months old mice as compared to their young (4 or 3 months old) counterparts this parameter may not be suitable as a reliable indicator of normal cardiac function.

Aging is associated with the accumulation and aggregation of damaged proteins, which can be cytotoxic, resulting in the reinforcement of the aging process. It is commonly hypothesized that proteasome function is impaired in the context of aging due to the key role of the UPS in

maintaining protein homeostasis (reviewed in (Kevei et al. 2014)). Moreover, the UPS accounts for the regulation of key regulator pathways of aging (reviewed in (Kenyon 2010)), such as the insulin or the insulin-like growth factor 1 (IGF-1) signaling pathway. For this purpose, the UPS regulates the stability of multiple components of the IGF-1 signaling pathway (Han et al. 2012). Thus, an impaired regulation of these regulatory pathways with aging potentially results in the reinforcement of the aging process due to a decline of the function of the UPS. However, the number of studies regarding this topic are rather limited. Regulation of the 20S proteasomal activities in the heart has been investigated in the context of aging in only one study (Bulteau et al. 2002) which revealed that the caspase-, trypsin- and chymotrypsin-like activities of the 20S proteasome were significantly reduced in the hearts of 26 as compared to 8 months old rats. In the present study, the 20S proteasome activities were altered neither in hearts of 26 versus 4 months old mice nor in those of 30 versus 3 months old animals. These differing results may be explained by using different reference groups and a different general health status and/or cardiac performance and, most importantly, different species with a different normal life span.

In contrast to the cardiac 20S proteasome, the caspase-, trypsin- and chymotrypsin-like activities of the 26S proteasome were strongly increased in old as compared to young mice. Interestingly, this difference was accentuated in the 26 versus 4 months old mice as compared to the 30 versus 3 months old animals, potentially related to the poorer general health status of the 26 months old mice. Previously, the decline of proteasome activity with age has been linked to the formation of protein aggregates, which interfere with the activity of the proteasome, e.g. in yeast (Andersson et al. 2013). Thus, impaired proteasome activity and protein aggregate formation are potentially induced if the degradation capacity of the proteasome is exceeded. Apparently, this threshold has not been reached in the old mice in the present study, given that the 26S proteasome activities were significantly higher than in young mice, and even higher when their general health status was quite poor.

Proteasome activity is regulated by multiple mechanisms, such as the increased assembly of proteasome complexes, the association of regulatory particles or post-translational modifications (Jung et al. 2009). In the present study, the incorporation of proteolytic β-subunits, analyzed via active site labeling, was not altered, whereas the abundance of all proteolytic subunits, analyzed by Western blot, was uniformly elevated in 30 versus 3 months old mice. Thus, the age-related increase of proteasome activities in these animals seems to be regulated via alternative mechanisms, such as the association with regulatory particles or post-translational modifications. In addition, such a disparity between abundance and incorporation of proteasome subunits has previously been reported in the context of cardiac hypertrophy (Drews et al. 2010). In contrast, incorporation of proteolytic β-subunits was uniformly increased in 26 versus 4 months old mice in the present study. Thus, the markedly

higher increase of the 26S proteasome activities in the 26 months old as compared to the 30 months old mouse hearts is potentially due to an increased assembly of proteasome complexes that may be associated with the comparatively poor general health status of these mice. Consequently, 26S proteasome activities are potentially increased through the association with regulatory particles or post-translational modifications with age in healthy mice, whereas the assembly of proteasome complexes may be linked to the manifestation of a poor general health status.

Association of the 11S regulatory particle is potentially involved in the increase of the 26S proteasome activities, given that the 11S acts as an activator (Dubiel et al. 1992). Moreover, hybrid proteasomes consisting of a 20S core particles, capped by one 19S and one 11S regulatory particle, have been reported previously (Tanahashi et al. 2000). Post-translational modifications are a key regulatory mechanism of proteasome structure and function, such as proteolytic activity and interaction with associating partner proteins (reviewed in (Scruggs et al. 2012, Cui et al. 2014)). In this context, phosphorylation is one of the most frequent post-translational modifications in the proteasome (Cui et al. 2014). Moreover, several cardiac-specific phosphorylation sites have been reported (Cui et al. 2014) that are partially targeted by PKA and when phosphorylated cause an increase in proteasomal activity (Lu et al. 2008). Thus, the activity of the proteasome may be affected by changes in β-adrenergic signaling in the context of aging.

Cardiac aging is associated with structural and functional changes of cardiomyocytes (reviewed in (Lakatta 2003)), resulting in alterations of cardiac function such as a decline in diastolic function. In the context of aging, the number of cardiomyocytes may be reduced due to necrosis or apoptosis resulting in the enlargement of the remaining cardiomyoyctes and myocardial fibrosis (reviewed in (Strait et al. 2012)). Moreover, cardiomyocyte contraction is modified with increasing age due to changes in the ion channel and intracellular Ca^{2+}-handling properties of these cells (reviewed in (Feridooni et al. 2014)). Modifications of contractile proteins, such as a decreased phosphorylation of troponin I (Campbell et al. 2013) or a switch from the fast α-MHC to the slower β-MHC isoform (Wahr et al. 2000) contribute to alterations in contractility with increasing age. These extensive structural and functional changes also imply alterations of the cardiac proteome in the context of aging. In the present study, proteome analysis via total protein staining after 1D-gel electrophoresis revealed significant alterations in the proteome of aged hearts as compared to young hearts. Again, these alterations were more pronounced in the 26 months old mice as compared to the 30 months old animals, presumably due to their different general health status and the aforementioned differences in the 26S proteasome activities.

Previously, alterations of the cardiac proteome with increasing age have been investigated in rats and mice by way of 2D-gel electrophoresis and tandem mass spectrometry analyses (Dai et al. 2008, Richardson et al. 2008, Grant et al. 2009). In the present study, proteins were identified by comparison of their position (spot) on a 2D-gel with that in a published reference gel representing a cardiac proteome database (HP-2DPAGE: http://web.mpiib-berlin.mpg.de/hp-2dpage/heart1.html). Notably, alterations in the cardiac proteome were quantified in 2D-gels of samples from young and aged hearts. The analysis revealed an increased abundance of myosin light chain 3 (MLC3) but not ventricular myosin light chain 2 (MLC2v) and myoglobin in 26 versus 4 months mouse hearts. An increased abundance of the essential isoform MLC1/3 and of the regulatory isoform MLC2v as well as an enhanced expression of MHCs has previously been shown in the hearts of 34 versus 4 months old rats (Richardson et al. 2008).

Considering the structure of the myosin complex, which is a hexamer consisting of two MHCs, two essential MLCs and two regulatory MLCs, cardiac expression of all components of this myosin complex was increased in the aged rats (Richardson et al. 2008). Contrariwise, abundance of the essential MLC, but not of the regulatory MLC2v, was higher in the hearts from the 26 months old mice in the present study. Thus, formation of the myosin complex may be impaired in these animals due to the limited abundance of the regulatory MLC2v or an alternative regulatory MLC isoform, which has not been identified or quantified, is incorporated into the myosin complex. It may be therefore that MLC isoforms are potentially switched with increasing age in mice as previously shown for MHC isoforms (Wahr et al. 2000). In the context of aging, cardiac contraction seems to be decelerated due to a switch from the α-MHC isoform to the slower β-MHC isoform (Wahr et al. 2000). Similarly, the ventricular MLC2 (MLC2v) isoform may be replaced by the atrial MLC2 (MLC2a) isoform, also resulting in an altered contractility (Pawloski-Dahm et al. 1998).

A decreased abundance of myoglobin has previously been shown in 23 versus 3 months old mice (Dai et al. 2008). In contrast, myoglobin levels were increased in 26 versus 4 months old mice in the present study. Considering the role of myoglobin in the antioxidant defence of the heart (Flogel et al. 2004), the increased abundance of myoglobin in the heart of the 26 months old mice in the present study might be linked to the poor general health status of these animals

The abundance of MLC2v in the 30 months old mouse hearts as compared to the 3 or 9 months old animals was not altered like in the 26 months old animals, arguing against an influence of the general health status. In contrast, abundance of the slow β-MHC was also markedly increased in 30 versus 3 months old mouse hearts, suggesting that this is the predominant MHC isoform in the heart of old mice (Wahr et al. 2000). Moreover, troponin I levels were moderately decreased in 30 versus 9 months old mouse hearts, implying that this is potentially

linked to the decline of diastolic function (Fentzke et al. 1999) in aged mice. Notably, the ubiquitin ligase muscle RING finger 1 (MuRF1) accounts for the targeted degradation of the slow β-MHC isoform (Fielitz et al. 2007) and of troponin I (Kedar et al. 2004). Consequently, targeted degradation of proteins via the UPS seems to be differentially regulated via additional regulatory mechanisms, given that β-MHC seems to be less avidly degraded, whereas degradation of troponin I appears to be upregulated in aged hearts.

Deubiquitinating enzymes (DUBs) preserve ubiquitin-tagged proteins from proteasomal degradation via the removal of ubiquitin (reviewed in (Komander et al. 2009)). Thus, β-MHC might be shielded from proteasomal degradation by DUBs, whereas troponin I is directly degraded via the proteasome. In addition, protein synthesis of β-MHC and troponin I might be differentially regulated in the context of aging. Furthermore, the significantly increased 26S proteasome activities might be associated with the differential regulation of proteins other than sarcomeric proteins due to the limited alteration of sarcomeric proteins with increasing age. Previously, an altered expression of multiple signaling, metabolic and antioxidant proteins, as well as proteins involved in the energy and fatty acid metabolism in the context of aging has been reported (Dai et al. 2008, Richardson et al. 2008, Grant et al. 2009). Thus, the observed increased 26S proteasome activities might be associated with the regulation of these proteins. This hypothesis warrants further investigation.

5.6 Proposed model of proteasome function during the development of cardiac hypertrophy and aging

In β1i knockout mice exposed to isoprenaline incorporation of the subunit β1i into cardiac proteasome complexes prevented the development of an exacerbated hypertrophy. Thus, the lack of β1i incorporation into cardiac proteasome complexes rather than systemic β1i deficiency most likely has resulted in the observed phenotype of the β1i-deficient mice when exposed to β-adrenergic overstimulation. In fact, increased incorporation of inducible subunits into cardiac proteasome complexes following hypertrophy induction, previously reported for wild type mice (Drews et al. 2010), seems to be an important mechanism in cardiac remodeling (Figure 42).

The observed phenotype in the isoprenaline-treated β1i-deficient mice does not seem to be related to a disturbance of the sarcomeric structure while incorporation of β1i instead of β1 into the cardiac proteasome complexes seems to be associated with increased levels of troponin I compared to the control group, potentially contributing to maintenance of cardiac function. Alternatively, the observed phenotype may also be linked to a potential downregulation or desensitization of β-adrenergic receptors, as previously reported in patients with heart failure (reviewed in (Hamdani et al. 2012)).

Cardiac aging is associated with significant alterations within the cardiac proteome that may be exacerbated in the context of a poor general health status. Moreover, the extent of these alterations seems to be associated with an adaptive increase of the 26S proteasome activities, which may maintain protein homeostasis and cardiac function in the context of aging (Figure 42). Considering previous reports on a decline of proteasome activity with increasing age that is accompanied or caused by an enhanced formation of protein aggregates (Andersson et al. 2013), aggregate formation may occur if the capacity of the UPS is reached resulting in the impairment of proteasome function (reviewed in (Vernace et al. 2007)).

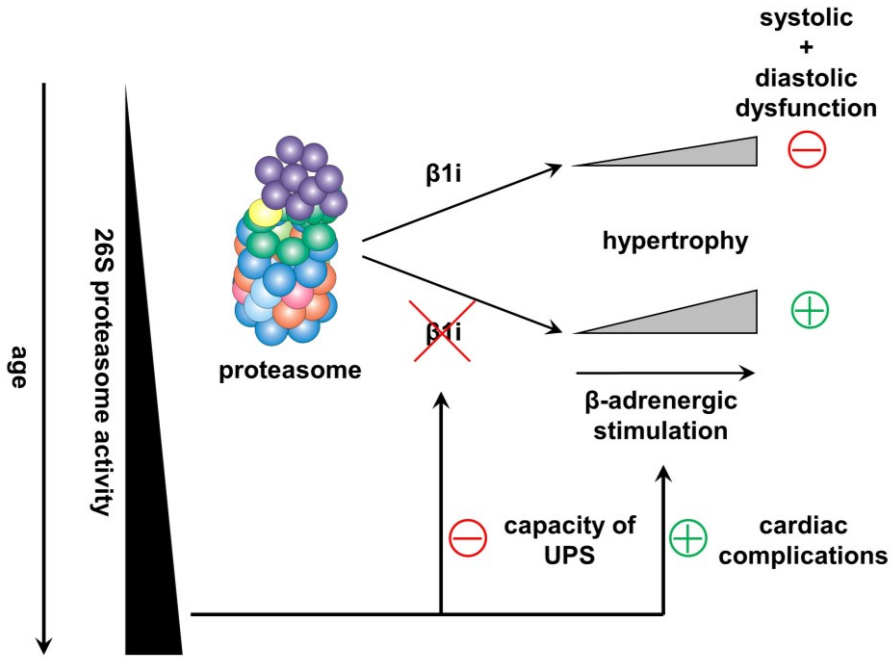

Figure 42. Proposed model of proteasome function during aging and the development of cardiac hypertrophy.

Incorporation of β1i into cardiac proteasome complexes prevents the development of an exacerbated hypertrophy and premature occurrence of systolic and diastolic dysfunction following continuous β-adrenergic stimulation. The 26S proteasome activity seems to rise with increasing age. This increase potentially limits the capacity of the UPS to counteract pro-hypertrophic stimuli in aged organisms potentially resulting in cardiac complications, e.g. pathological hypertrophy.

In patients older than 60 years, cardiotoxicity of the proteasome inhibitor bortezomib, used in tumor therapy, has been reported (Enrico et al. 2007). Further case reports associate the pathogenesis of cardiac disorders with the utilization of proteasome inhibitors targeting all proteasome complexes in tumor therapy (reviewed in (Drews et al. 2014)). Contrariwise, maladaptive cardiac remodeling has been reported to be prevented and cardiac function preserved by proteasome inhibition in models of pathological hypertrophy (Depre et al. 2006, Hedhli et al. 2008, Stansfield et al. 2008). Notably, submaximal inhibition of proteasomal

activity in association with its duration seem to be critical for the beneficial effects of proteasome inhibition in the context of maladaptive cardiac hypertrophy. Considering the treatment regimen typically used for tumor therapy, cardiac proteasome inhibition is presumably more pronounced in tumor patients than in cardiac hypertrophy.

Moreover, the difference in age also seems to be a critical factor. Considering the augmented 26S proteasome activities with increasing age to maintain protein homeostasis and cardiomyocyte function, the more aggressive proteasome inhibition in tumor patients may limit the degradation capacity of the UPS, resulting in the formation of protein aggregates, which in turn exacerbate its impairment. About 50% of tumor patients with cardiac complications treated with proteasome inhibitors develop heart failure (Enrico et al. 2007). Thus, the increased prevalence of pathological cardiac hypertrophy in the elderly might be due to the limited capacity of the UPS to maintain protein homeostasis and thus cardiomyocyte function (Figure 42). Further studies on the beneficial or detrimental effects of proteasome inhibition on cardiac function are needed to minimize adverse effects of proteasome inhibitors used in tumor therapy or against other diseases.

5.7 Perspectives

Considering the aforementioned proposed model of proteasome function during the development of cardiac hypertrophy and aging, the following interesting questions arise which need to be answered by further investigations.

a) What is the underlying mechanism responsible for the augmented cardiac hypertrophy and dysfunction in β1i-deficient mice following induction of hypertrophy? Further experiments have to be done to compare the changes, e.g. in heart weight, between the isoprenaline treated groups with sham treated mice. In addition, detected differences in troponin I levels between hearts of isoprenaline administered AAV β1i and AAV Luci-treated β1i knockout mice require statistical validation. Again, comparison with matching sham treated animals will indicate whether intracellular troponin I levels are comparable with those in wild type hearts and indeed decreased in cardiac hypertrophy. Other observations, such as the onset of fibrosis require validation as well.

b) Can cardiac β1i overexpression in wild type mice (gain of function) decrease or even prevent the development of pathological hypertrophy following isoprenaline exposure? Cardiac function and morphology as well as proteasome regulation have to be analyzed. Verification that increased β1i incorporation into cardiac proteasome complexes is beneficial would reinforce interest in the underlying mechanism.

c) Is the increase of 26S proteasome activities with increasing age related to the deteriorating general health status? In order to confirm this hypothesis the abundance of proteins indicating increased cellular stress could be analyzed. Investigation of the pool of ubiquitinated and oxidized proteins might elucidate whether proteasome activity is increased in response to a higher demand in their turnover. In turn, this may be associated with increased levels of proteins participating in antioxidant defence or protein folding.

d) Is AAV9-based gene transfer, e.g. of β1i, a realistic therapeutic option to maintain proteasome function and activity and hence protein homeostasis in the aging heart to prevent cardiac hypertrophy and/or its transition to heart failure? This is a particularly interesting question that requires the setting up of a cardiac hypertrophy model in aging mice with the potential of a transition to heart failure that are treated with the adeno-associated viral vector-based CMV/MLC0.26-driven β1i expression construct established herein. Mechanistically, this approach might also reveal whether there really is a link between the hypertrophy and age-related deterioration of cardiac function with regard to changes in the function and/or activity of the 26S proteasome that could only be marked off in the present study.

References

Adams, G. M., B. Crotchett, C. A. Slaughter, G. N. DeMartino and E. P. Gogol (1998). "Formation of proteasome-PA700 complexes directly correlates with activation of peptidase activity." Biochemistry **37**(37): 12927-12932.

Agha, S. A., A. P. Kalogeropoulos, J. Shih, V. V. Georgiopoulou, G. Giamouzis, P. Anarado, D. Mangalat, I. Hussain, W. Book, S. Laskar, A. L. Smith, R. Martin and J. Butler (2009). "Echocardiography and risk prediction in advanced heart failure: incremental value over clinical markers." J Card Fail **15**(7): 586-592.

Andersson, V., S. Hanzen, B. Liu, M. Molin and T. Nystrom (2013). "Enhancing protein disaggregation restores proteasome activity in aged cells." Aging (Albany NY) **5**(11): 802-812.

Angeles, A., G. Fung and H. Luo (2012). "Immune and non-immune functions of the immunoproteasome." Front Biosci (Landmark Ed) **17**: 1904-1916.

Bancroft, J. D. and M. Gamble (2008a). Theory and Practice of Histological Techniques. The Hematoxylins and Eosin, Churchill Livingstone. **Volume 6:** pp. 121-134.

Bancroft, J. D. and M. Gamble (2008b). Theory and Practice of Histological Techniques. Connective Tissues and Stains, Churchill Livingstone. **Volume 6**.

Bancroft, J. D. and M. Gamble (2008c). Theory and Practice of Histological Techniques. Laser Microdissection, Churchill Livingstone. **Volume 6:** pp. 575-584.

Bar-Nun, S. and M. H. Glickman (2012). "Proteasomal AAA-ATPases: structure and function." Biochim Biophys Acta **1823**(1): 67-82.

Barki-Harrington, L., C. Perrino and H. A. Rockman (2004). "Network integration of the adrenergic system in cardiac hypertrophy." Cardiovasc Res **63**(3): 391-402.

Berenji, K., M. H. Drazner, B. A. Rothermel and J. A. Hill (2005). "Does load-induced ventricular hypertrophy progress to systolic heart failure?" Am J Physiol Heart Circ Physiol **289**(1): H8-H16.

Bergmann, O., R. D. Bhardwaj, S. Bernard, S. Zdunek, F. Barnabe-Heider, S. Walsh, J. Zupicich, K. Alkass, B. A. Buchholz, H. Druid, S. Jovinge and J. Frisen (2009). "Evidence for cardiomyocyte renewal in humans." Science **324**(5923): 98-102.

Bernardo, B. C., K. L. Weeks, L. Pretorius and J. R. McMullen (2010). "Molecular distinction between physiological and pathological cardiac hypertrophy: Experimental findings and therapeutic strategies." Pharmacology & Therapeutics **128**(1): 191-227.

Birnboim, H. C. and J. Doly (1979). "A rapid alkaline extraction procedure for screening recombinant plasmid DNA." Nucleic Acids Res **7**(6): 1513-1523.

Bisping, E., P. Wakula, M. Poteser and F. R. Heinzel (2014). "Targeting cardiac hypertrophy: toward a causal heart failure therapy." J Cardiovasc Pharmacol **64**(4): 293-305.

Bochtler, M., L. Ditzel, M. Groll, C. Hartmann and R. Huber (1999). "The proteasome." Annu Rev Biophys Biomol Struct **28**: 295-317.

Bonner, P. L. R. and A. J. Hargreaves (2011). Basic Bioscience Laboratory Techniques: A Pocket Guide, Wiley.

Brooks, W. W. and C. H. Conrad (2009). "Isoproterenol-induced myocardial injury and diastolic dysfunction in mice: structural and functional correlates." Comp Med **59**(4): 339-343.

Buckingham, L. (2011). Molecular Diagnostics: Fundamentals, Methods and Clinical Applications. Nucleic Acid Extraction Methods, F.A. Davis Company**:** pp. 69-86.

Bulteau, A. L., L. I. Szweda and B. Friguet (2002). "Age-dependent declines in proteasome activity in the heart." Arch Biochem Biophys **397**(2): 298-304.

Burgess, M. L., J. Buggy, R. L. Price, F. L. Abel, L. Terracio, A. M. Samarel and T. K. Borg (1996). "Exercise- and hypertension-induced collagen changes are related to left ventricular function in rat hearts." Am J Physiol **270**(1 Pt 2): H151-159.

Campbell, S. G., P. Haynes, W. Kelsey Snapp, K. E. Nava and K. S. Campbell (2013). "Altered ventricular torsion and transmural patterns of myocyte relaxation precede heart failure in aging F344 rats." Am J Physiol Heart Circ Physiol **305**(5): H676-686.

Carley, A. N., D. M. Taglieri, J. Bi, R. J. Solaro and E. D. Lewandowski (2015). "Metabolic efficiency promotes protection from pressure overload in hearts expressing slow skeletal troponin I." Circ Heart Fail **8**(1): 119-127.

Chen, P. and M. Hochstrasser (1996). "Autocatalytic subunit processing couples active site formation in the 20S proteasome to completion of assembly." Cell **86**(6): 961-972.

Ciechanover, A. and A. L. Schwartz (1989). "How are substrates recognized by the ubiquitin-mediated proteolytic system?" Trends Biochem Sci **14**(12): 483-488.

Cui, Z., S. B. Scruggs, J. E. Gilda, P. Ping and A. V. Gomes (2014). "Regulation of cardiac proteasomes by ubiquitination, SUMOylation, and beyond." J Mol Cell Cardiol **71**: 32-42.

Dai, D. F., L. F. Santana, M. Vermulst, D. M. Tomazela, M. J. Emond, M. J. MacCoss, K. Gollahon, G. M. Martin, L. A. Loeb, W. C. Ladiges and P. S. Rabinovitch (2009). "Overexpression of catalase targeted to mitochondria attenuates murine cardiac aging." Circulation **119**(21): 2789-2797.

Dai, Q., G. P. Escobar, K. W. Hakala, J. M. Lambert, S. T. Weintraub and M. L. Lindsey (2008). "The left ventricle proteome differentiates middle-aged and old left ventricles in mice." J Proteome Res **7**(2): 756-765.

Depre, C., Q. Wang, L. Yan, N. Hedhli, P. Peter, L. Chen, C. Hong, L. Hittinger, B. Ghaleh, J. Sadoshima, D. E. Vatner, S. F. Vatner and K. Madura (2006). "Activation of the cardiac proteasome during pressure overload promotes ventricular hypertrophy." Circulation **114**(17): 1821-1828.

Deveraux, Q., V. Ustrell, C. Pickart and M. Rechsteiner (1994). "A 26 S protease subunit that binds ubiquitin conjugates." J Biol Chem **269**(10): 7059-7061.

Dirkx, E., M. M. Gladka, L. E. Philippen, A. S. Armand, V. Kinet, S. Leptidis, H. El Azzouzi, K. Salic, M. Bourajjaj, G. J. da Silva, S. Olieslagers, R. van der Nagel, R. de Weger, N. Bitsch, N. Kisters, S. Seyen, Y. Morikawa, C. Chanoine, S. Heymans, P. G. Volders, T. Thum, S. Dimmeler, P. Cserjesi, T. Eschenhagen, P. A. da Costa Martins and L. J. De Windt (2013). "Nfat and miR-25 cooperate to reactivate the transcription factor Hand2 in heart failure." Nat Cell Biol **15**(11): 1282-1293.

Drews, O. and H. Taegtmeyer (2014). "Targeting the ubiquitin-proteasome system in heart disease: the basis for new therapeutic strategies." Antioxid Redox Signal **21**(17): 2322-2343.

Drews, O., O. Tsukamoto, D. Liem, J. Streicher, Y. Wang and P. Ping (2010). "Differential regulation of proteasome function in isoproterenol-induced cardiac hypertrophy." Circ Res **107**(9): 1094-1101.

Drews, O., R. Wildgruber, C. Zong, U. Sukop, M. Nissum, G. Weber, A. V. Gomes and P. Ping (2007). "Mammalian proteasome subpopulations with distinct molecular compositions and proteolytic activities." Mol Cell Proteomics **6**(11): 2021-2031.

Du, J., J. Liu, H. Z. Feng, M. M. Hossain, N. Gobara, C. Zhang, Y. Li, P. Y. Jean-Charles, J. P. Jin and X. P. Huang (2008). "Impaired relaxation is the main manifestation in transgenic mice expressing a restrictive cardiomyopathy mutation, R193H, in cardiac TnI." Am J Physiol Heart Circ Physiol **294**(6): H2604-2613.

Dubiel, W., G. Pratt, K. Ferrell and M. Rechsteiner (1992). "Purification of an 11 S regulator of the multicatalytic protease." J Biol Chem **267**(31): 22369-22377.

Ehsani, A. A., J. M. Hagberg and R. C. Hickson (1978). "Rapid changes in left ventricular dimensions and mass in response to physical conditioning and deconditioning." Am J Cardiol **42**(1): 52-56.

Enrico, O., B. Gabriele, C. Nadia, G. Sara, V. Daniele, C. Giulia, S. Antonio and P. Mario (2007). "Unexpected cardiotoxicity in haematological bortezomib treated patients." Br J Haematol **138**(3): 396-397.

Fan, D., A. Takawale, J. Lee and Z. Kassiri (2012). "Cardiac fibroblasts, fibrosis and extracellular matrix remodeling in heart disease." Fibrogenesis Tissue Repair **5**(1): 15.

Faulx, M. D., P. Ernsberger, D. Vatner, R. D. Hoffman, W. Lewis, R. Strachan and B. D. Hoit (2005). "Strain-dependent beta-adrenergic receptor function influences myocardial responses to isoproterenol stimulation in mice." Am J Physiol Heart Circ Physiol **289**(1): H30-36.

Feldman, D. S., C. A. Carnes, W. T. Abraham and M. R. Bristow (2005). "Mechanisms of disease: beta-adrenergic receptors--alterations in signal transduction and pharmacogenomics in heart failure." Nat Clin Pract Cardiovasc Med **2**(9): 475-483.

Fentzke, R. C., S. H. Buck, J. R. Patel, H. Lin, B. M. Wolska, M. O. Stojanovic, A. F. Martin, R. J. Solaro, R. L. Moss and J. M. Leiden (1999). "Impaired cardiomyocyte relaxation and diastolic function in transgenic mice expressing slow skeletal troponin I in the heart." J Physiol **517 (Pt 1)**: 143-157.

Ferguson, S. S. (2001). "Evolving concepts in G protein-coupled receptor endocytosis: the role in receptor desensitization and signaling." Pharmacol Rev **53**(1): 1-24.

Feridooni, H. A., K. M. Dibb and S. E. Howlett (2014). "How cardiomyocyte excitation, calcium release and contraction become altered with age." J Mol Cell Cardiol.

Fernandis, A. Z., R. P. Cherla, R. D. Chernock and R. K. Ganju (2002). "CXCR4/CCR5 down-modulation and chemotaxis are regulated by the proteasome pathway." J Biol Chem **277**(20): 18111-18117.

Fielitz, J., M. S. Kim, J. M. Shelton, S. Latif, J. A. Spencer, D. J. Glass, J. A. Richardson, R. Bassel-Duby and E. N. Olson (2007). "Myosin accumulation and striated muscle myopathy result from the loss of muscle RING finger 1 and 3." J Clin Invest **117**(9): 2486-2495.

Flogel, U., A. Godecke, L. O. Klotz and J. Schrader (2004). "Role of myoglobin in the antioxidant defense of the heart." FASEB J **18**(10): 1156-1158.

Florea, B. I., M. Verdoes, N. Li, W. A. van der Linden, P. P. Geurink, H. van den Elst, T. Hofmann, A. de Ru, P. A. van Veelen, K. Tanaka, K. Sasaki, S. Murata, H. den Dulk, J. Brouwer, F. A. Ossendorp, A. F. Kisselev and H. S. Overkleeft (2010). "Activity-based profiling reveals reactivity of the murine thymoproteasome-specific subunit beta5t." Chem Biol **17**(8): 795-801.

Frank, D., C. Kuhn, B. Brors, C. Hanselmann, M. Ludde, H. A. Katus and N. Frey (2008). "Gene expression pattern in biomechanically stretched cardiomyocytes: evidence for a stretch-specific gene program." Hypertension **51**(2): 309-318.

Freund, C., R. Schmidt-Ullrich, A. Baurand, S. Dunger, W. Schneider, P. Loser, A. El-Jamali, R. Dietz, C. Scheidereit and M. W. Bergmann (2005). "Requirement of nuclear factor-kappaB in angiotensin II- and isoproterenol-induced cardiac hypertrophy in vivo." Circulation **111**(18): 2319-2325.

Friedrich, F. W., S. Reischmann, A. Schwalm, A. Unger, D. Ramanujam, J. Munch, O. J. Muller, C. Hengstenberg, E. Galve, P. Charron, W. A. Linke, S. Engelhardt, M. Patten, P. Richard, J. van der Velden, T. Eschenhagen, R. Isnard and L. Carrier (2014). "FHL2 expression and variants in hypertrophic cardiomyopathy." Basic Res Cardiol **109**(6): 451.

Gaczynska, M., P. A. Osmulski, Y. Gao, M. J. Post and M. Simons (2003). "Proline- and arginine-rich peptides constitute a novel class of allosteric inhibitors of proteasome activity." Biochemistry **42**(29): 8663-8670.

Galderisi, M. (2005). "Diastolic dysfunction and diastolic heart failure: diagnostic, prognostic and therapeutic aspects." Cardiovasc Ultrasound **3**: 9.

Galindo, C. L., M. A. Skinner, M. Errami, L. D. Olson, D. A. Watson, J. Li, J. F. McCormick, L. J. McIver, N. M. Kumar, T. Q. Pham and H. R. Garner (2009). "Transcriptional profile of isoproterenol-induced cardiomyopathy and comparison to exercise-induced cardiac hypertrophy and human cardiac failure." BMC Physiol **9**: 23.

Gao, S., D. Ho, D. E. Vatner and S. F. Vatner (2011). "Echocardiography in Mice." Curr Protoc Mouse Biol **1**: 71-83.

Gauthier, C., V. Leblais, L. Kobzik, J. N. Trochu, N. Khandoudi, A. Bril, J. L. Balligand and H. Le Marec (1998). "The negative inotropic effect of beta3-adrenoceptor stimulation is mediated by activation of a nitric oxide synthase pathway in human ventricle." J Clin Invest **102**(7): 1377-1384.

Geisler, A., A. Jungmann, J. Kurreck, W. Poller, H. A. Katus, R. Vetter, H. Fechner and O. J. Muller (2011). "microRNA122-regulated transgene expression increases specificity of cardiac gene transfer upon intravenous delivery of AAV9 vectors." Gene Ther **18**(2): 199-209.

Ghali, J. K., Y. Liao, B. Simmons, A. Castaner, G. Cao and R. S. Cooper (1992). "The prognostic role of left ventricular hypertrophy in patients with or without coronary artery disease." Ann Intern Med **117**(10): 831-836.

Gomes, A. C., I. Falcao-Pires, A. L. Pires, C. Bras-Silva and A. F. Leite-Moreira (2013). "Rodent models of heart failure: an updated review." Heart Fail Rev **18**(2): 219-249.

Gomes, A. V., G. W. Young, Y. Wang, C. Zong, M. Eghbali, O. Drews, H. Lu, E. Stefani and P. Ping (2009). "Contrasting proteome biology and functional heterogeneity of the 20 S proteasome complexes in mammalian tissues." Mol Cell Proteomics **8**(2): 302-315.

Gomes, A. V., C. Zong, R. D. Edmondson, X. Li, E. Stefani, J. Zhang, R. C. Jones, S. Thyparambil, G. W. Wang, X. Qiao, F. Bardag-Gorce and P. Ping (2006). "Mapping the murine cardiac 26S proteasome complexes." Circ Res **99**(4): 362-371.

Gorg, A., Drews, O., and Weiss, W. (2004). "Separation of proteins using two-dimensional gel electrophoresis." Purifying Proteins for Proteomics: a Laboratory Manual (Si mpson, R. J., ed), Cold Spring Harbor Laboratory Press, Cold Spring Harbor, NY 391– 430.

Gorg, A., W. Postel and S. Gunther (1988). "The current state of two-dimensional electrophoresis with immobilized pH gradients." Electrophoresis **9**(9): 531-546.

Grant, J. E., A. D. Bradshaw, J. H. Schwacke, C. F. Baicu, M. R. Zile and K. L. Schey (2009). "Quantification of protein expression changes in the aging left ventricle of Rattus norvegicus." J Proteome Res **8**(9): 4252-4263.

Grayburn, P. A., C. P. Appleton, A. N. DeMaria, B. Greenberg, B. Lowes, J. Oh, J. F. Plehn, P. Rahko, M. St John Sutton, E. J. Eichhorn and B. T. E. S. Investigators (2005). "Echocardiographic predictors of morbidity and mortality in patients with advanced heart failure: the Beta-blocker Evaluation of Survival Trial (BEST)." J Am Coll Cardiol **45**(7): 1064-1071.

Groettrup, M., S. Khan, K. Schwarz and G. Schmidtke (2001). "Interferon-gamma inducible exchanges of 20S proteasome active site subunits: why?" Biochimie **83**(3-4): 367-372.

Groll, M., M. Bajorek, A. Kohler, L. Moroder, D. M. Rubin, R. Huber, M. H. Glickman and D. Finley (2000). "A gated channel into the proteasome core particle." Nat Struct Biol **7**(11): 1062-1067.

Grune, T., K. Merker, G. Sandig and K. J. Davies (2003). "Selective degradation of oxidatively modified protein substrates by the proteasome." Biochem Biophys Res Commun **305**(3): 709-718.

Haas, A. L. and I. A. Rose (1982). "The mechanism of ubiquitin activating enzyme. A kinetic and equilibrium analysis." J Biol Chem **257**(17): 10329-10337.

Hagstrom, J. N., L. B. Couto, C. Scallan, M. Burton, M. L. McCleland, P. A. Fields, V. R. Arruda, R. W. Herzog and K. A. High (2000). "Improved muscle-derived expression of human coagulation factor IX from a skeletal actin/CMV hybrid enhancer/promoter." Blood **95**(8): 2536-2542.

Haider, A. W., M. G. Larson, E. J. Benjamin and D. Levy (1998). "Increased left ventricular mass and hypertrophy are associated with increased risk for sudden death." J Am Coll Cardiol **32**(5): 1454-1459.

Hamdani, N. and W. A. Linke (2012). "Alteration of the beta-adrenergic signaling pathway in human heart failure." Curr Pharm Biotechnol **13**(13): 2522-2531.

Hames, B. D. (1998). Gel Electrophoresis of Proteins : A Practical Approach: A Practical Approach, OUP Oxford.

Han, Y., H. Lee, J. C. Park and G. S. Yi (2012). "E3Net: a system for exploring E3-mediated regulatory networks of cellular functions." Mol Cell Proteomics **11**(4): O111 014076.

Harrison, M. A. and I. F. Rae (1997). General Techniques of Cell Culture. Cell Culture, Cambridge University Press. **Volume 1:** pp. 69-88.

Hasenfuss, G. (1998). "Animal models of human cardiovascular disease, heart failure and hypertrophy." Cardiovasc Res **39**(1): 60-76.

Hedhli, N., P. Lizano, C. Hong, L. F. Fritzky, S. K. Dhar, H. Liu, Y. Tian, S. Gao, K. Madura, S. F. Vatner and C. Depre (2008). "Proteasome inhibition decreases cardiac remodeling after initiation of pressure overload." Am J Physiol Heart Circ Physiol **295**(4): H1385-1393.

Hein, S., T. Block, R. Zimmermann, S. Kostin, T. Scheffold, T. Kubin, W. P. Klovekorn and J. Schaper (2009). "Deposition of nonsarcomeric alpha-actinin in cardiomyocytes from patients with dilated cardiomyopathy or chronic pressure overload." Exp Clin Cardiol **14**(3): e68-75.

Heineke, J. and J. D. Molkentin (2006). "Regulation of cardiac hypertrophy by intracellular signalling pathways." Nat Rev Mol Cell Biol **7**(8): 589-600.

Heling, A., R. Zimmermann, S. Kostin, Y. Maeno, S. Hein, B. Devaux, E. Bauer, W. P. Klovekorn, M. Schlepper, W. Schaper and J. Schaper (2000). "Increased expression of cytoskeletal, linkage, and extracellular proteins in failing human myocardium." Circ Res **86**(8): 846-853.

Hirano, Y., H. Hayashi, S. Iemura, K. B. Hendil, S. Niwa, T. Kishimoto, M. Kasahara, T. Natsume, K. Tanaka and S. Murata (2006). "Cooperation of multiple chaperones required for the assembly of mammalian 20S proteasomes." Mol Cell **24**(6): 977-984.

Hirano, Y., K. B. Hendil, H. Yashiroda, S. Iemura, R. Nagane, Y. Hioki, T. Natsume, K. Tanaka and S. Murata (2005). "A heterodimeric complex that promotes the assembly of mammalian 20S proteasomes." Nature **437**(7063): 1381-1385.

Hirano, Y., T. Kaneko, K. Okamoto, M. Bai, H. Yashiroda, K. Furuyama, K. Kato, K. Tanaka and S. Murata (2008). "Dissecting beta-ring assembly pathway of the mammalian 20S proteasome." EMBO J **27**(16): 2204-2213.

Hobbs, F. D., A. K. Roalfe, R. C. Davis, M. K. Davies, R. Hare and C. Midlands Research Practices (2007). "Prognosis of all-cause heart failure and borderline left ventricular systolic dysfunction: 5 year mortality follow-up of the Echocardiographic Heart of England Screening Study (ECHOES)." Eur Heart J **28**(9): 1128-1134.

Hogg, K., K. Swedberg and J. McMurray (2004). "Heart failure with preserved left ventricular systolic function; epidemiology, clinical characteristics, and prognosis." J Am Coll Cardiol **43**(3): 317-327.

Hua, Y., T. J. Robinson, Y. Cao, G. P. Shi, J. Ren and S. Nair (2015). "Cathepsin K knockout alleviates aging-induced cardiac dysfunction." Aging Cell.

Hunter, J. J. and K. R. Chien (1999). "Signaling pathways for cardiac hypertrophy and failure." N Engl J Med **341**(17): 1276-1283.

Husnjak, K., S. Elsasser, N. Zhang, X. Chen, L. Randles, Y. Shi, K. Hofmann, K. J. Walters, D. Finley and I. Dikic (2008). "Proteasome subunit Rpn13 is a novel ubiquitin receptor." Nature **453**(7194): 481-488.

Iaizzo, P. A. (2007). Handbook of Cardiac Anatomy, Physiology, and Devices. General Features of the Cardiovascular System. P. A. Iaizzo, Springer. **Volume 1:** pp. 3-11.

Innis, M. A., D. H. Gelfand, J. J. Sninsky and T. J. White (2012). PCR Protocols: A Guide to Methods and Applications, Elsevier Science.

Jin, H., R. Yang, W. Li, H. Lu, A. M. Ryan, A. K. Ogasawara, J. Van Peborgh and N. F. Paoni (2000). "Effects of exercise training on cardiac function, gene expression, and apoptosis in rats." Am J Physiol Heart Circ Physiol **279**(6): H2994-3002.

Jung, T., B. Catalgol and T. Grune (2009). "The proteasomal system." Mol Aspects Med **30**(4): 191-296.

Kaspar, B. K., B. Vissel, T. Bengoechea, S. Crone, L. Randolph-Moore, R. Muller, E. P. Brandon, D. Schaffer, I. M. Verma, K. F. Lee, S. F. Heinemann and F. H. Gage (2002). "Adeno-associated virus effectively mediates conditional gene modification in the brain." Proc Natl Acad Sci U S A **99**(4): 2320-2325.

Kaufman, D. L. and G. A. Evans (1990). "Restriction endonuclease cleavage at the termini of PCR products." Biotechniques **9**(3): 304, 306.

Kaya, Z., C. Leib, S. Werfel, S. Goser, R. Ottl, B. Leuchs, G. Pfitzer, H. A. Katus and O. J. Muller (2011). "Comparison of IL-10 and MCP-1-7ND gene transfer with AAV9 vectors for protection from murine autoimmune myocarditis." Cardiovasc Res **91**(1): 116-123.

Kedar, V., H. McDonough, R. Arya, H. H. Li, H. A. Rockman and C. Patterson (2004). "Muscle-specific RING finger 1 is a bona fide ubiquitin ligase that degrades cardiac troponin I." Proc Natl Acad Sci U S A **101**(52): 18135-18140.

Kenyon, C. J. (2010). "The genetics of ageing." Nature **464**(7288): 504-512.

Kevei, E. and T. Hoppe (2014). "Ubiquitin sets the timer: impacts on aging and longevity." Nat Struct Mol Biol **21**(4): 290-292.

Keyaerts, M., I. Remory, V. Caveliers, K. Breckpot, T. J. Bos, J. Poelaert, A. Bossuyt and T. Lahoutte (2012). "Inhibition of firefly luciferase by general anesthetics: effect on in vitro and in vivo bioluminescence imaging." PLoS One **7**(1): e30061.

Kiper, C., B. Grimes, G. Van Zant and J. Satin (2013). "Mouse strain determines cardiac growth potential." PLoS One **8**(8): e70512.

Kitamura, M., M. Shimizu, H. Ino, K. Okeie, M. Yamaguchi, N. Funjno, H. Mabuchi and I. Nakanishi (2001). "Collagen remodeling and cardiac dysfunction in patients with hypertrophic cardiomyopathy: the significance of type III and VI collagens." Clin Cardiol **24**(4): 325-329.

Klein, L., C. M. O'Connor, W. A. Gattis, M. Zampino, L. de Luca, A. Vitarelli, F. Fedele and M. Gheorghiade (2003). "Pharmacologic therapy for patients with chronic heart failure and reduced systolic function: review of trials and practical considerations." Am J Cardiol **91**(9A): 18F-40F.

Koegl, M., T. Hoppe, S. Schlenker, H. D. Ulrich, T. U. Mayer and S. Jentsch (1999). "A novel ubiquitination factor, E4, is involved in multiubiquitin chain assembly." Cell **96**(5): 635-644.

Komander, D., M. J. Clague and S. Urbe (2009). "Breaking the chains: structure and function of the deubiquitinases." Nat Rev Mol Cell Biol **10**(8): 550-563.

Krenning, G., E. M. Zeisberg and R. Kalluri (2010). "The origin of fibroblasts and mechanism of cardiac fibrosis." J Cell Physiol **225**(3): 631-637.

Kusmierczyk, A. R., M. J. Kunjappu, M. Funakoshi and M. Hochstrasser (2008). "A multimeric assembly factor controls the formation of alternative 20S proteasomes." Nat Struct Mol Biol **15**(3): 237-244.

Lakatta, E. G. (2003). "Arterial and cardiac aging: major shareholders in cardiovascular disease enterprises: Part III: cellular and molecular clues to heart and arterial aging." Circulation **107**(3): 490-497.

Lakatta, E. G. and D. Levy (2003). "Arterial and cardiac aging: major shareholders in cardiovascular disease enterprises: Part II: the aging heart in health: links to heart disease." Circulation **107**(2): 346-354.

Le Tallec, B., M. B. Barrault, R. Courbeyrette, R. Guerois, M. C. Marsolier-Kergoat and A. Peyroche (2007). "20S proteasome assembly is orchestrated by two distinct pairs of chaperones in yeast and in mammals." Mol Cell **27**(4): 660-674.

Lee, T. H., M. A. Hamilton, L. W. Stevenson, J. D. Moriguchi, G. C. Fonarow, J. S. Child, H. Laks and J. A. Walden (1993). "Impact of left ventricular cavity size on survival in advanced heart failure." Am J Cardiol **72**(9): 672-676.

Levy, D., R. J. Garrison, D. D. Savage, W. B. Kannel and W. P. Castelli (1990). "Prognostic implications of echocardiographically determined left ventricular mass in the Framingham Heart Study." N Engl J Med **322**(22): 1561-1566.

Levy, D., D. D. Savage, R. J. Garrison, K. M. Anderson, W. B. Kannel and W. P. Castelli (1987). "Echocardiographic criteria for left ventricular hypertrophy: the Framingham Heart Study." Am J Cardiol **59**(9): 956-960.

Li, Q. and J. Ren (2007). "Influence of cardiac-specific overexpression of insulin-like growth factor 1 on lifespan and aging-associated changes in cardiac intracellular Ca2+ homeostasis, protein damage and apoptotic protein expression." Aging Cell **6**(6): 799-806.

Li, Z., Y. Song, R. Xing, H. Yu, Y. Zhang, Z. Li and W. Gao (2013). "Heat shock protein 70 acts as a potential biomarker for early diagnosis of heart failure." PLoS One **8**(7): e67964.

Liem D, K. F., Tsukamoto O, Wang Y, Hecker M, Ping P, Drews O. (2012). Reduced proteasome heterogeneity augments cardiac remodeling. American Heart Association (AHA) 2012 Scientific Sessions. Los Angeles, USA.

Lips, D. J., L. J. deWindt, D. J. van Kraaij and P. A. Doevendans (2003). "Molecular determinants of myocardial hypertrophy and failure: alternative pathways for beneficial and maladaptive hypertrophy." Eur Heart J **24**(10): 883-896.

Liu, C. W., X. Li, D. Thompson, K. Wooding, T. L. Chang, Z. Tang, H. Yu, P. J. Thomas and G. N. DeMartino (2006). "ATP binding and ATP hydrolysis play distinct roles in the function of 26S proteasome." Mol Cell **24**(1): 39-50.

Lohse, M. J., S. Engelhardt and T. Eschenhagen (2003). "What is the role of beta-adrenergic signaling in heart failure?" Circ Res **93**(10): 896-906.

Lorell, B. H. and B. A. Carabello (2000). "Left ventricular hypertrophy: pathogenesis, detection, and prognosis." Circulation **102**(4): 470-479.

Lorenz, K., J. P. Schmitt, E. M. Schmitteckert and M. J. Lohse (2009a). "A new type of ERK1/2 autophosphorylation causes cardiac hypertrophy." Nat Med **15**(1): 75-83.

Lorenz, K., J. P. Schmitt, M. Vidal and M. J. Lohse (2009b). "Cardiac hypertrophy: targeting Raf/MEK/ERK1/2-signaling." Int J Biochem Cell Biol **41**(12): 2351-2355.

Lu, H., C. Zong, Y. Wang, G. W. Young, N. Deng, P. Souda, X. Li, J. Whitelegge, O. Drews, P. Y. Yang and P. Ping (2008). "Revealing the dynamics of the 20 S proteasome phosphoproteome: a combined CID and electron transfer dissociation approach." Mol Cell Proteomics **7**(11): 2073-2089.

Lukowski, R., S. D. Rybalkin, F. Loga, V. Leiss, J. A. Beavo and F. Hofmann (2010). "Cardiac hypertrophy is not amplified by deletion of cGMP-dependent protein kinase I in cardiomyocytes." Proc Natl Acad Sci U S A **107**(12): 5646-5651.

Lyon, A. R., M. Sato, R. J. Hajjar, R. J. Samulski and S. E. Harding (2008). "Gene therapy: targeting the myocardium." Heart **94**(1): 89-99.

Maillet, M., J. H. van Berlo and J. D. Molkentin (2013). "Molecular basis of physiological heart growth: fundamental concepts and new players." Nat Rev Mol Cell Biol **14**(1): 38-48.

Malumbres, M., R. Mangues, N. Ferrer, S. Lu and A. Pellicer (1997). "Isolation of high molecular weight DNA for reliable genotyping of transgenic mice." Biotechniques **22**(6): 1114-1119.

Maron, B. J., A. Pelliccia, A. Spataro and M. Granata (1993). "Reduction in left ventricular wall thickness after deconditioning in highly trained Olympic athletes." Br Heart J **69**(2): 125-128.

Matkovich, S. J., A. Diwan, J. L. Klanke, D. J. Hammer, Y. Marreez, A. M. Odley, E. W. Brunskill, W. J. Koch, R. J. Schwartz and G. W. Dorn, 2nd (2006). "Cardiac-specific ablation of G-protein receptor kinase 2 redefines its roles in heart development and beta-adrenergic signaling." Circ Res **99**(9): 996-1003.

Mollova, M., K. Bersell, S. Walsh, J. Savla, L. T. Das, S. Y. Park, L. E. Silberstein, C. G. Dos Remedios, D. Graham, S. Colan and B. Kuhn (2013). "Cardiomyocyte proliferation contributes to heart growth in young humans." Proc Natl Acad Sci U S A **110**(4): 1446-1451.

Moreo, A., G. Ambrosio, B. De Chiara, M. Pu, T. Tran, F. Mauri and S. V. Raman (2009). "Influence of myocardial fibrosis on left ventricular diastolic function: noninvasive assessment by cardiac magnetic resonance and echo." Circ Cardiovasc Imaging **2**(6): 437-443.

Müller, O. J., H. A. Katus and R. Bekeredjian (2007). "Targeting the heart with gene therapy-optimized gene delivery methods." Cardiovasc Res **73**(3): 453-462.

Murata, S., H. Yashiroda and K. Tanaka (2009). "Molecular mechanisms of proteasome assembly." Nat Rev Mol Cell Biol **10**(2): 104-115.

Nagueh, S. F., C. P. Appleton, T. C. Gillebert, P. N. Marino, J. K. Oh, O. A. Smiseth, A. D. Waggoner, F. A. Flachskampf, P. A. Pellikka and A. Evangelisa (2009). "Recommendations for the evaluation of left ventricular diastolic function by echocardiography." Eur J Echocardiogr **10**(2): 165-193.

Nandi, D., E. Woodward, D. B. Ginsburg and J. J. Monaco (1997). "Intermediates in the formation of mouse 20S proteasomes: implications for the assembly of precursor beta subunits." EMBO J **16**(17): 5363-5375.

Ortega, J., J. B. Heymann, A. V. Kajava, V. Ustrell, M. Rechsteiner and A. C. Steven (2005). "The axial channel of the 20S proteasome opens upon binding of the PA200 activator." J Mol Biol **346**(5): 1221-1227.

Osadchii, O. E. (2007). "Cardiac hypertrophy induced by sustained beta-adrenoreceptor activation: pathophysiological aspects." Heart Fail Rev **12**(1): 66-86.

Pagan, J., T. Seto, M. Pagano and A. Cittadini (2013). "Role of the ubiquitin proteasome system in the heart." Circ Res **112**(7): 1046-1058.

Palpant, N. J., S. M. Day, T. J. Herron, K. L. Converso and J. M. Metzger (2008). "Single histidine-substituted cardiac troponin I confers protection from age-related systolic and diastolic dysfunction." Cardiovasc Res **80**(2): 209-218.

Pawloski-Dahm, C. M., G. Song, D. L. Kirkpatrick, J. Palermo, J. Gulick, G. W. Dorn, 2nd, J. Robbins and R. A. Walsh (1998). "Effects of total replacement of atrial myosin light chain-2 with the ventricular isoform in atrial myocytes of transgenic mice." Circulation **97**(15): 1508-1513.

Pickart, C. M. and I. A. Rose (1985). "Functional heterogeneity of ubiquitin carrier proteins." J Biol Chem **260**(3): 1573-1581.

Pleger, S. T., C. Shan, J. Ksienzyk, R. Bekeredjian, P. Boekstegers, R. Hinkel, S. Schinkel, B. Leuchs, J. Ludwig, G. Qiu, C. Weber, P. Raake, W. J. Koch, H. A. Katus, O. J. Muller and P. Most (2011). "Cardiac AAV9-S100A1 gene therapy rescues post-ischemic heart failure in a preclinical large animal model." Sci Transl Med **3**(92): 92ra64.

Pluim, B. M., A. H. Zwinderman, A. van der Laarse and E. E. van der Wall (2000). "The athlete's heart. A meta-analysis of cardiac structure and function." Circulation **101**(3): 336-344.

Poruchynsky, M. S., D. L. Sackett, R. W. Robey, Y. Ward, C. Annunziata and T. Fojo (2008). "Proteasome inhibitors increase tubulin polymerization and stabilization in tissue culture cells: a possible mechanism contributing to peripheral neuropathy and cellular toxicity following proteasome inhibition." Cell Cycle **7**(7): 940-949.

Powell, S. R., J. Herrmann, A. Lerman, C. Patterson and X. Wang (2012). "The ubiquitin-proteasome system and cardiovascular disease." Prog Mol Biol Transl Sci **109**: 295-346.

Prasad, K. M., Y. Xu, Z. Yang, S. T. Acton and B. A. French (2011). "Robust cardiomyocyte-specific gene expression following systemic injection of AAV: in vivo gene delivery follows a Poisson distribution." Gene Ther **18**(1): 43-52.

Reiss, Y., H. Heller and A. Hershko (1989). "Binding sites of ubiquitin-protein ligase. Binding of ubiquitin-protein conjugates and of ubiquitin-carrier protein." J Biol Chem **264**(18): 10378-10383.

Richardson, M. R., X. Lai, S. B. Mason, S. J. Miller and F. A. Witzmann (2008). "Differential protein expression during aging in ventricular myocardium of Fischer 344 x Brown Norway hybrid rats." Exp Gerontol **43**(10): 909-918.

Ritter, O. and L. Neyses (2003). "The molecular basis of myocardial hypertrophy and heart failure." Trends Mol Med **9**(7): 313-321.

Rockman, H. A., W. J. Koch and R. J. Lefkowitz (2002). "Seven-transmembrane-spanning receptors and heart function." Nature **415**(6868): 206-212.

Rottman, J. N., G. Ni and M. Brown (2007). "Echocardiographic evaluation of ventricular function in mice." Echocardiography **24**(1): 83-89.

Rozec, B., M. Erfanian, K. Laurent, J. N. Trochu and C. Gauthier (2009). "Nebivolol, a vasodilating selective beta(1)-blocker, is a beta(3)-adrenoceptor agonist in the nonfailing transplanted human heart." J Am Coll Cardiol **53**(17): 1532-1538.

Saadane, N., L. Alpert and L. E. Chalifour (1999). "Expression of immediate early genes, GATA-4, and Nkx-2.5 in adrenergic-induced cardiac hypertrophy and during regression in adult mice." Br J Pharmacol **127**(5): 1165-1176.

Sambrook, J. and D. W. Russell (1989). Molecular Cloning: A Laboratory Manual, Cold Spring Harbor Laboratory Press.

Schannwell, C. M., T. Zimmermann, M. Schneppenheim, G. Plehn, R. Marx and B. E. Strauer (2002). "Left ventricular hypertrophy and diastolic dysfunction in healthy pregnant women." Cardiology **97**(2): 73-78.

Scharf, S. J., G. T. Horn and H. A. Erlich (1986). "Direct cloning and sequence analysis of enzymatically amplified genomic sequences." Science **233**(4768): 1076-1078.

Scherrer-Crosbie, M. and H. B. Thibault (2008). "Echocardiography in translational research: of mice and men." J Am Soc Echocardiogr **21**(10): 1083-1092.

Schinkel, S., R. Bauer, R. Bekeredjian, R. Stucka, D. Rutschow, H. Lochmuller, J. A. Kleinschmidt, H. A. Katus and O. J. Muller (2012). "Long-term preservation of cardiac structure and function after adeno-associated virus serotype 9-mediated microdystrophin gene transfer in mdx mice." Hum Gene Ther **23**(6): 566-575.

Schmidtke, G., R. Kraft, S. Kostka, P. Henklein, C. Frommel, J. Lowe, R. Huber, P. M. Kloetzel and M. Schmidt (1996). "Analysis of mammalian 20S proteasome biogenesis: the maturation of beta-subunits is an ordered two-step mechanism involving autocatalysis." EMBO J **15**(24): 6887-6898.

Schutzer, W. E. and S. L. Mader (2003). "Age-related changes in vascular adrenergic signaling: clinical and mechanistic implications." Ageing Res Rev **2**(2): 169-190.

Scruggs, S. B., N. C. Zong, D. Wang, E. Stefani and P. Ping (2012). "Post-translational modification of cardiac proteasomes: functional delineation enabled by proteomics." Am J Physiol Heart Circ Physiol **303**(1): H9-18.

Senyo, S. E., M. L. Steinhauser, C. L. Pizzimenti, V. K. Yang, L. Cai, M. Wang, T. D. Wu, J. L. Guerquin-Kern, C. P. Lechene and R. T. Lee (2013). "Mammalian heart renewal by pre-existing cardiomyocytes." Nature **493**(7432): 433-436.

Shan, J., M. J. Betzenhauser, A. Kushnir, S. Reiken, A. C. Meli, A. Wronska, M. Dura, B. X. Chen and A. R. Marks (2010). "Role of chronic ryanodine receptor phosphorylation in heart failure and beta-adrenergic receptor blockade in mice." J Clin Invest **120**(12): 4375-4387.

Shimpo, M., U. Ikeda, Y. Maeda, M. Takahashi, H. Miyashita, H. Mizukami, M. Urabe, A. Kume, T. Takizawa, M. Shibuya, K. Ozawa and K. Shimada (2002). "AAV-mediated VEGF gene transfer into skeletal muscle stimulates angiogenesis and improves blood flow in a rat hindlimb ischemia model." Cardiovasc Res **53**(4): 993-1001.

Shiojima, I., K. Sato, Y. Izumiya, S. Schiekofer, M. Ito, R. Liao, W. S. Colucci and K. Walsh (2005). "Disruption of coordinated cardiac hypertrophy and angiogenesis contributes to the transition to heart failure." J Clin Invest **115**(8): 2108-2118.

Shringarpure, R., T. Grune and K. J. Davies (2001). "Protein oxidation and 20S proteasome-dependent proteolysis in mammalian cells." Cell Mol Life Sci **58**(10): 1442-1450.

Shringarpure, R., T. Grune, J. Mehlhase and K. J. Davies (2003). "Ubiquitin conjugation is not required for the degradation of oxidized proteins by proteasome." J Biol Chem **278**(1): 311-318.

Smith, D. M., S. C. Chang, S. Park, D. Finley, Y. Cheng and A. L. Goldberg (2007). "Docking of the proteasomal ATPases' carboxyl termini in the 20S proteasome's alpha ring opens the gate for substrate entry." Mol Cell **27**(5): 731-744.

Solomon, V. and A. L. Goldberg (1996). "Importance of the ATP-ubiquitin-proteasome pathway in the degradation of soluble and myofibrillar proteins in rabbit muscle extracts." J Biol Chem **271**(43): 26690-26697.

Spaich, S., R. D. Will, S. Just, S. Spaich, C. Kuhn, D. Frank, I. M. Berger, S. Wiemann, B. Korn, M. Koegl, J. Backs, H. A. Katus, W. Rottbauer and N. Frey (2012). "F-box and leucine-rich repeat protein 22 is a cardiac-enriched F-box protein that regulates sarcomeric protein turnover and is essential for maintenance of contractile function in vivo." Circ Res **111**(12): 1504-1516.

Stansfield, W. E., R. H. Tang, N. C. Moss, A. S. Baldwin, M. S. Willis and C. H. Selzman (2008). "Proteasome inhibition promotes regression of left ventricular hypertrophy." Am J Physiol Heart Circ Physiol **294**(2): H645-650.

Strait, J. B. and E. G. Lakatta (2012). "Aging-associated cardiovascular changes and their relationship to heart failure." Heart Fail Clin **8**(1): 143-164.

Stypmann, J. (2007). "Doppler ultrasound in mice." Echocardiography **24**(1): 97-112.

Sundstrom, J., L. Lind, J. Arnlov, B. Zethelius, B. Andren and H. O. Lithell (2001). "Echocardiographic and electrocardiographic diagnoses of left ventricular hypertrophy predict mortality independently of each other in a population of elderly men." Circulation **103**(19): 2346-2351.

Takimoto, E., D. G. Soergel, P. M. Janssen, L. B. Stull, D. A. Kass and A. M. Murphy (2004). "Frequency- and afterload-dependent cardiac modulation in vivo by troponin I with constitutively active protein kinase A phosphorylation sites." Circ Res **94**(4): 496-504.

Tanahashi, N., Y. Murakami, Y. Minami, N. Shimbara, K. B. Hendil and K. Tanaka (2000). "Hybrid proteasomes. Induction by interferon-gamma and contribution to ATP-dependent proteolysis." J Biol Chem **275**(19): 14336-14345.

Triposkiadis, F., G. Karayannis, G. Giamouzis, J. Skoularigis, G. Louridas and J. Butler (2009). "The sympathetic nervous system in heart failure physiology, pathophysiology, and clinical implications." J Am Coll Cardiol **54**(19): 1747-1762.

Tsukamoto, O., T. Minamino, K. Okada, Y. Shintani, S. Takashima, H. Kato, Y. Liao, H. Okazaki, M. Asai, A. Hirata, M. Fujita, Y. Asano, S. Yamazaki, H. Asanuma, M. Hori and M. Kitakaze (2006). "Depression of proteasome activities during the progression of cardiac dysfunction in pressure-overloaded heart of mice." Biochem Biophys Res Commun **340**(4): 1125-1133.

Van Kaer, L., P. G. Ashton-Rickardt, M. Eichelberger, M. Gaczynska, K. Nagashima, K. L. Rock, A. L. Goldberg, P. C. Doherty and S. Tonegawa (1994). "Altered peptidase and viral-specific T cell response in LMP2 mutant mice." Immunity **1**(7): 533-541.

Vasan, R. S., M. G. Larson, E. J. Benjamin, J. C. Evans, C. K. Reiss and D. Levy (1999). "Congestive heart failure in subjects with normal versus reduced left ventricular ejection fraction: prevalence and mortality in a population-based cohort." J Am Coll Cardiol **33**(7): 1948-1955.

Verdoes, M., B. I. Florea, V. Menendez-Benito, C. J. Maynard, M. D. Witte, W. A. van der Linden, A. M. van den Nieuwendijk, T. Hofmann, C. R. Berkers, F. W. van Leeuwen, T. A. Groothuis, M. A. Leeuwenburgh, H. Ovaa, J. J. Neefjes, D. V. Filippov, G. A. van der Marel, N. P. Dantuma and H. S. Overkleeft (2006). "A fluorescent broad-spectrum proteasome inhibitor for labeling proteasomes in vitro and in vivo." Chem Biol **13**(11): 1217-1226.

Verdoes, M., L. I. Willems, W. A. van der Linden, B. A. Duivenvoorden, G. A. van der Marel, B. I. Florea, A. F. Kisselev and H. S. Overkleeft (2010). "A panel of subunit-selective activity-based proteasome probes." Org Biomol Chem **8**(12): 2719-2727.

Vernace, V. A., T. Schmidt-Glenewinkel and M. E. Figueiredo-Pereira (2007). "Aging and regulated protein degradation: who has the UPPer hand?" Aging Cell **6**(5): 599-606.

Vidal, M., T. Wieland, M. J. Lohse and K. Lorenz (2012). "beta-Adrenergic receptor stimulation causes cardiac hypertrophy via a Gbetagamma/Erk-dependent pathway." Cardiovasc Res **96**(2): 255-264.

Voges, D., P. Zwickl and W. Baumeister (1999). "The 26S proteasome: a molecular machine designed for controlled proteolysis." Annu Rev Biochem **68**: 1015-1068.

Wahr, P. A., D. E. Michele and J. M. Metzger (2000). "Effects of aging on single cardiac myocyte function in Fischer 344 x Brown Norway rats." Am J Physiol Heart Circ Physiol **279**(2): H559-565.

Wang, B., Q. Yang, W. W. Bai, Y. F. Xing, X. T. Lu, Y. Y. Sun and Y. X. Zhao (2014). "Tongxinluo protects against pressure overload-induced heart failure in mice involving VEGF/Akt/eNOS pathway activation." PLoS One **9**(6): e98047.

Wang, Z. and D. R. Storm (2006). "Extraction of DNA from mouse tails." Biotechniques **41**(4): 410, 412.

Wang, Z. V. and J. A. Hill (2015). "Protein Quality Control and Metabolism: Bidirectional Control in the Heart." Cell Metab **21**(2): 215-226.

Weber, C., I. Neacsu, B. Krautz, P. Schlegel, S. Sauer, P. Raake, J. Ritterhoff, A. Jungmann, A. B. Remppis, M. Stangassinger, W. J. Koch, H. A. Katus, O. J. Muller, P. Most and S. T. Pleger (2014). "Therapeutic safety of high myocardial expression levels of the molecular inotrope S100A1 in a preclinical heart failure model." Gene Ther **21**(2): 131-138.

Whitby, F. G., E. I. Masters, L. Kramer, J. R. Knowlton, Y. Yao, C. C. Wang and C. P. Hill (2000). "Structural basis for the activation of 20S proteasomes by 11S regulators." Nature **408**(6808): 115-120.

Willis, M. S., W. H. Townley-Tilson, E. Y. Kang, J. W. Homeister and C. Patterson (2010). "Sent to destroy: the ubiquitin proteasome system regulates cell signaling and protein quality control in cardiovascular development and disease." Circ Res **106**(3): 463-478.

Witt, S. H., H. Granzier, C. C. Witt and S. Labeit (2005). "MURF-1 and MURF-2 target a specific subset of myofibrillar proteins redundantly: towards understanding MURF-dependent muscle ubiquitination." J Mol Biol **350**(4): 713-722.

Wong, M., G. Johnson, R. Shabetai, V. Hughes, G. Bhat, B. Lopez and J. N. Cohn (1993). "Echocardiographic variables as prognostic indicators and therapeutic monitors in chronic congestive heart failure. Veterans Affairs cooperative studies V-HeFT I and II. V-HeFT VA Cooperative Studies Group." Circulation **87**(6 Suppl): VI65-70.

Wong, M., L. Staszewsky, R. Latini, S. Barlera, R. Glazer, N. Aknay, A. Hester, I. Anand and J. N. Cohn (2004). "Severity of left ventricular remodeling defines outcomes and response to therapy in heart failure: Valsartan heart failure trial (Val-HeFT) echocardiographic data." J Am Coll Cardiol **43**(11): 2022-2027.

Wu, S., Q. Li, M. Du, S. Y. Li and J. Ren (2007). "Cardiac-specific overexpression of catalase prolongs lifespan and attenuates ageing-induced cardiomyocyte contractile dysfunction and protein damage." Clin Exp Pharmacol Physiol **34**(1-2): 81-87.

Ye, X., H. M. Zhang, Y. Qiu, P. J. Hanson, M. G. Hemida, W. Wei, P. A. Hoodless, F. Chu and D. Yang (2014). "Coxsackievirus-induced miR-21 disrupts cardiomyocyte interactions via the downregulation of intercalated disk components." PLoS Pathog **10**(4): e1004070.

Zaiss, D. M., S. Standera, H. Holzhutter, P. Kloetzel and A. J. Sijts (1999). "The proteasome inhibitor PI31 competes with PA28 for binding to 20S proteasomes." FEBS Lett **457**(3): 333-338.

Zhang, R., J. Zhao, A. Mandveno and J. D. Potter (1995). "Cardiac troponin I phosphorylation increases the rate of cardiac muscle relaxation." Circ Res **76**(6): 1028-1035.

Zile, M. R., W. H. Gaasch, J. D. Carroll, M. D. Feldman, G. P. Aurigemma, G. L. Schaer, J. K. Ghali and P. R. Liebson (2001). "Heart failure with a normal ejection fraction: is measurement of diastolic function necessary to make the diagnosis of diastolic heart failure?" Circulation **104**(7): 779-782.

Appendix - Sequence of the AAV CMV/MLC0.26 βi1 vector

```
   1  ctgcgcgctc gctcgctcac tgaggccgcc cgggcaaagc ccgggcgtcg ggcgaccttt
  61  ggtcgcccgg cctcagtgag cgagcgagcg cgcagagagg gagtggaatt cacgcgtcgg
 121  cggccgcttc gagctcgccc gacattgatt attgactagt tattaatagt aatcaattac
 181  ggggtcatta gttcatagcc catatatgga gttccgcgtt acataactta cggtaaatgg
 241  cccgcctggc tgaccgccca acgacccccg cccattgacg tcaataatga cgtatgttcc
 301  catagtaacg ccaatagggа ctttccattg acgtcaatgg gtggagtatt tacggtaaac
 361  tgcccacttg gcagtacatc aagtgtatca tatgccaagt acgcccccta ttgacgtcaa
 421  tgacggtaaa tggcccgcct ggcattatgc ccagtacatg accttatggg actttcctac
 481  ttggcagtac atctacgtat tagtcatcgc tattaccatg gtgatgcggt tttggcagta
 541  catcaatggg cgtggatagc ggtttgactc acggggattt ccaagtctcc accccattga
 601  cgtcaatggg agtttgtttt ggcaccaaaa tcaacgggac tttccaaaat gtcgtaacaa
 661  ctccgcccca tgcggccgct ctaggaccca gagcacagag catcgttccc aggccaggcc
 721  ccagccactg tctctttaac cttgaaggca tttttgggtc tcacgtgtcc acccaggcgg
 781  gtgtcggact ttgaacggct cttacttcag aagaacggca tggggtgggg gggcttaggt
 841  ggcctctgcc tcacctacaa ctgccaaaag tggtcatggg gttatttta accccaggga
 901  agaggtattt attgttccac agcaggggcc ggccagcagg ctccttgccc aagctttatt
 961  gcggtagttt atcacagtta aattgctaac gcagtcagtg cttctgacac aacagtctcg
1021  aacttaagct gcagaagttg gtcgtgaggc actgggcagg taagtatcaa ggttacaaga
1081  caggtttaag gagaccaata gaaactgggc ttgtcgagac agagaagact cttgcgtttc
1141  tgataggcac ctattggtct tactgacatc cactttgcct ttctctccac aggtgtccac
1201  tcccagttca attacagctc ttaaggctag agtacttaat acgactcact ataggctagc
1261  ctcgacggta ccgcgggccc gggatccacc ggtgccacca tgctgcgggc aggagcacct
1321  accgccggct cgttccggac ggaagaagtc cacaccggga caaccatcat ggcagtggag
1381  tttgacgggg gtgtcgtggt gggctctgat tcccgggtgt cagcgggaac agcagtggtg
1441  aaccgcgtgt tcgacaagct ctcccctctg caccagcaca tcttctgtgc cctctcaggt
1501  tccgctgctg atgcccaagc catagctgac atggccgcct accagctgga gctacacggg
1561  ttggagctgg aggagccgcc cctcgttctg gctgctgcaa acgtggtgaa gaacatctcc
1621  tacaagtacc gtgaggactt gttagcgcat ctcatagtag ctggctggga ccaatgtgag
1681  gggggacagg tatatggaac catgggaggg atgctaattc gacagccctt taccatcggc
1741  ggttccggaa gctcctacat ttatggttat gtggacgcag cttataagcc aggcatgacc
1801  cctgaggagt gccggcgttt caccacagat gccatcactc tggccatgaa ccgagatggc
1861  tctagtgggg gtgtcatcta cctggtcacc atcacagctg ctggtgtgga ccatcgagtc
1921  atcctgggag atgagctgcc aaaattctac gatgagtgat gtacaagtaa agcggccgcg
1981  actctagatc ataatcagcc ataccacatt tgtagaggtt ttacttgctt taaaaaacct
2041  cccacacctc cccctgaacc tgaaacataa aatgaatgca attgttgttg ttaacttgtt
2101  tattgcagct tataatggtt acaaataaag caatagcatc acaaatttca caaataaagc
2161  attttttca ctgcattcta gttgtggttt gtccaaactc atcaatgtat cttaaggcgg
2221  gaattgatct aggaacccct agtgatggag ttggccactc cctctctgcg cgctcgctcg
2281  ctcactgagg ccgcccgggc aaagcccggg cgtcgggcga cctttggtcg cccggcctca
2341  gtgagcgagc gagcgcgcag agagggagtg gccaa
```

Figure 43. Sequence of the AAV CMV/MLC0.26 β1i vector within the inverted terminal repeats (ITR) (2375 bp of 5990 bp).

The ITR (5' ITR and 3' ITR) (yellow), the genetically engineered promotor consisting of parts of the viral cytomegalovirus (CMV_{enh}) immediate-early promotor (light purple) and a fragment of the tissue-specific myosin light chain promotor (MLC0.26) (dark purple), the β1i gene (green) and the Simian virus 40 polyadenylation signal (SV40 polyA) (blue) are highlighted within the sequence. Sequenced area of the AAV CMV/MLC0.26 β1i vector is in bold.

Danksagung

Ich möchte mich zunächst bei Herrn Prof. Markus Hecker für die Möglichkeit bedanken dieses interessante Dissertationsthema bearbeiten zu dürfen, sowie auch für die anregenden wissenschaftlichen Diskussionen und die konstruktive Kritik zu meiner Arbeit.

Mein besonderer Dank für die kontinuierliche Unterstützung gilt meinem Betreuer und Arbeitsgruppenleiter Dr. Oliver Drews. Diese Arbeit wurde mit finanzieller Unterstützung einer Marie-Curie-Maßnahme der Europäischen Kommission (CIG294213 an Dr. O. Drews) durchgeführt

Weiterhin möchte ich mich bei Herrn Prof. Thomas Wieland für die Erstellung des Gutachtens meiner Arbeit, sowie bei Herrn Prof. Johannes Backs und Herrn PD Dr. Ralf Bischoff für die Teilnahme an der Prüfungskommission bedanken. Ich danke Ihnen für Ihre Zeit und Ihr Interesse sich mit meiner Arbeit auseinanderzusetzen.

Ich möchte mich ebenfalls bei meinen Kooperationspartnern, insbesondere Frau PD Dr. Petra Kleinbongard, für die gute Zusammenarbeit bedanken, die es mir ermöglicht hat die Proteasomregulation in einem anderen Zusammenhang zu untersuchen.

Mein besonderer Dank gilt ebenfalls Herrn Prof. Oliver Müller und seiner Arbeitsgruppe, insbesondere Dr. Andreas Jungmann, für die Produktion der AAV, ohne die die Durchführung meiner Arbeit nicht möglich gewesen wäre.

Ich danke auch dem Team der Interfakultären Biomedizinischen Forschungseinrichtung, insbesondere Bianca Heil, für die Durchführung der i. v. Injektionen und die Betreuung während der versuchtierkundlichen Arbeiten.

Weiterhin möchte ich mich bei Herrn PD Dr. Emmanuel Chorianopoulos und Herrn PD Dr. Philipp Raake und deren Mitarbeitern, insbesondere bei Susann Werkmeister, Henrike Tscheschner und Julia Reinkober, für die Hilfe bei der Etablierung der NRCM-Präparation in unserem Labor bedanken.

Mein Dank gilt auch Herrn Dr. Bogdan Florea für die Bereitstellung und die Hilfe bei der Etablierung des active site Labeling in unserem Labor.

Insbesondere möchte ich mich bei den Mitgliedern der Arbeitsgruppe Drews für die gute Zusammenarbeit und die Unterstützung bedanken: Lidia Gaal, Anita Kühner, Mathilde Lorenz, Felix Trogisch, Synie Wieber.

Weiterhin danke ich auch den anderen Arbeitsgruppenleitern unseres Institutes, PD. Dr. Thomas Korff, Dr. Nina Ulrich und PD Dr. Andreas Wagner, für die konstruktive Kritik zu meiner Arbeit.

Mein besonderer Dank gilt Cordula Rumig für anregende wissenschaftliche, aber vor allem auch nicht-wissenschaftliche Gespräche und ihre Freundschaft, als auch Franziska Fitzer, Nadine Scholz, Jan Simon und Tanja Wiedenmann für die angenehmen Mittagspausen, nach denen man motiviert zur Arbeit zurückkehren konnte.

Ich danke auch den technischen Mitarbeiterinnen und Mitarbeitern, die mit ihrer langjährigen Erfahrung den Doktoranden immer hilfreich zur Seite standen: Renate Cattaruzza, Felicia Feiler, Yvonne Haag, Maria Harlacher, Manuela Höfer, Gudrun Scheib, Ender Serbest. Weiterhin möchte ich mich bei Barbara Richards bedanken, die sich weit über ihre Zuständigkeiten engagiert hat.

Bedanken möchte ich mich ebenfalls für die gute Zusammenarbeit bei allen anderen Doktoranden, die noch dabei sind oder den Weg bereits erfolgreich abgeschlossen haben: Oliver Adolph, Caroline Arnold, Andrea Bireckoven, Jennifer Braun, Eda Demirel, Julia Eldrod, Johannes Eschrich, Anja Feldner, Subhajit Ghosh, Maximilian Heiß, Maren Hödebeck, Fan Jiang, Ivelina Kadiyska, Branislav Kollar, Hanna Kuk, Hui Liu, Sebastian Lont, Kerstin Möller, Taslima Nahar, Larissa Pfisterer, Anca Remes, Clemens Scherer, Florian Schnitter, Hannes Schröder, Cheryl Sultan, Sibgha Tahir.

Mein größter Dank gilt jedoch meiner Familie, die mich bereits mein Leben lang begleitet und unterstützen haben: meinen wunderbaren Eltern und meiner Schwester Carolin. Ich danke euch, dass ihr nie an mir gezweifelt habt und mir den Rückhalt gegeben habt, durch den ich diesen Weg erst gehen konnte.